Springer Theses
Recognizing Outstanding Ph.D. Research

Jonas Hannestad

Fluorescence in Bio-inspired Nanotechnology

First as Probe, Then as Function

Springer

Springer Theses

Recognizing Outstanding Ph.D. Research

For further volumes:
http://www.springer.com/series/8790

Aims and Scope

The series “Springer Theses” brings together a selection of the very best Ph.D. theses from around the world and across the physical sciences. Nominated and endorsed by two recognized specialists, each published volume has been selected for its scientific excellence and the high impact of its contents for the pertinent field of research. For greater accessibility to non-specialists, the published versions include an extended introduction, as well as a foreword by the student's supervisor explaining the special relevance of the work for the field. As a whole, the series will provide a valuable resource both for newcomers to the research fields described, and for other scientists seeking detailed background information on special questions. Finally, it provides an accredited documentation of the valuable contributions made by today’s younger generation of scientists.

Theses are accepted into the series by invited nomination only and must fulfill all of the following criteria

- They must be written in good English.
- The topic should fall within the confines of Chemistry, Physics, Earth Sciences, Engineering and related interdisciplinary fields such as Materials, Nanoscience, Chemical Engineering, Complex Systems and Biophysics.
- The work reported in the thesis must represent a significant scientific advance.
- If the thesis includes previously published material, permission to reproduce this must be gained from the respective copyright holder.
- They must have been examined and passed during the 12 months prior to nomination.
- Each thesis should include a foreword by the supervisor outlining the significance of its content.
- The theses should have a clearly defined structure including an introduction accessible to scientists not expert in that particular field.

Jonas Hannestad

Fluorescence in Bio-inspired Nanotechnology

First as Probe, Then as Function

Doctoral Thesis accepted by
Chalmers University of Technology, Gothenburg, Sweden

Springer

Author
Dr. Jonas Hannestad
Department of Chemical and Biological Engineering
Chalmers University of Technology
Gothenburg
Sweden

Supervisor
Prof. Dr. Bo Albinsson
Department of Chemical and Biological Engineering
Chalmers University of Technology
Gothenburg
Sweden

ISSN 2190-5053 ISSN 2190-5061 (electronic)
ISBN 978-3-319-01067-0 ISBN 978-3-319-01068-7 (eBook)
DOI 10.1007/978-3-319-01068-7
Springer Cham Heidelberg New York Dordrecht London

Library of Congress Control Number: 2013942148

Printed on acid-free paper

Springer is part of Springer Science+Business Media (www.springer.com)

Parts of this thesis have been published in the following journal articles

I. **Self-Assembled DNA Photonic Wire for Long-Range Energy Transfer**
Jonas K. Hannestad, Peter Sandin, Bo Albinsson*
Journal of the American Chemical Society (2008), 130 (47), 15889−15895.

II. **Self-Assembled DNA-Based Fluorescence Waveguide with Selectable Output**
Jonas K. Hannestad, Simon R. Gerrard, Tom Brown, Bo Albinsson*
Small (2011), 7 (22), 3178−3185.

III. **Self-Assembled Nanoscale DNA-Porphyrin Complex for Artificial Light-Harvesting**
Jakob G. Woller, Jonas K. Hannestad, and Bo Albinsson*
Journal of the American Chemical Society (2013), 135 (7), 2759–2768.

IV. **Platform for Controlled Supramolecular Nanoassembly**
Ilja Czolkos†, Jonas K. Hannestad†, Aldo Jesorka, Ravindra Kumar, Tom Brown, Bo Albinsson, Owe Orwar*
Nano Letters (2009), 9 (6), 2482−2486.
† Both authors contributed equally to this work

V. **Kinetics of Diffusion-Controlled DNA Hybridization in Lipid Monolayer Films Determined by Single Molecule Fluorescence Spectroscopy**
Jonas K. Hannestad, Ralf Brune, Ilja Czolkos, Aldo Jesorka, Afaf H. El-Sagheer, Tom Brown, Bo Albinsson, and Owe Orwar*
ACS Nano (2013), 7 (1), 308–315.

Supervisor's Foreword

DNA Nanotechnology, in which bottom-up construction of 10–200 nm sized objects with single nm precision is developed, is the focus of this Ph.D. thesis. In his thesis, "Fluorescence in Bio-inspired Nanotechnology: First as Probe, Then as Function", Jonas Hannestad describes this evolving field in a lucid and easily accessible way. In particular, applications based on fluorescence resonance energy transfer (FRET) are highlighted. Here, the directional energy transfer through arrays of self-assembled chromophores and light harvesting in biomimetic antenna complexes are two beautiful experimental demonstrations of the unique properties of functional DNA nanotechnology. Another important contribution is the development of a lipid monolayer platform for the stepwise assembly of DNA nanoconstructs.

DNA is a remarkable molecule whose high-fidelity recognition power and rigid structure allows both linear information readout with extremely high throughput and the ability to be patterned in many different ways at the nanometer scale. In his thesis, Jonas Hannestad has pioneered a simple yet very flexible method for the self-assembly of photonic wires and nanoscale light harvesting systems. Starting with a simple wire construct based on linear DNA, he shows how the DNA scaffold could be used to efficiently transport excitation energy from one end of the DNA molecule to the other. The mechanism of energy transfer between identical chromophores (homo-FRET) is central for the function of the self-assembled wire. In a slightly more elaborate branched DNA construct the same transport mechanism is used to direct excitation energy to either of two spatially and spectrally distinct readout positions, thus showing how a pre-determined DNA pattern is used to switch the energy flow within the construct. Both linear and branched DNA-constructs are also shown to work as self-assembled nanoscale light harvesting antennas; in these constructs a redox active porphyrin acts as the terminal energy acceptor, thereby mimicking the functions of the natural photosynthetic light harvesting systems.

By using DNA as a scaffold for chromophores capable of energy and electron transfer reactions a number of attractive features become accessible. Compared to synthetic systems based on covalent organic synthesis the DNA-based systems are easily scaled to sizes bridging lithographical patterns (20–100 nm). This might

enable hybrid molecular solid-state devices for the future development of molecular scale electronics or aid in the nanostructuring of light harvesting and electron transporting components in molecular photovoltaics. In addition, again comparing to synthetic organic multifunctional molecular complexes, the self-assembled functionalized DNA structures are to a large degree "self-healing" as they are based on equilibrium structures, in which photo damaged chromophores are dynamically replaced. As a logical extension of Dr. Hannestad's thesis work even larger nanostructured DNA constructs, such as DNA origami, is now being investigated. Here, further development of light harvesting, spatially controlled photoinduced redox reactions, and surface binding will be explored for eventual use in the different applications mentioned above.

Bo Albinsson

Acknowledgments

I would like to thank the following people: My supervisor Bo—thank you for inspiring me to try my own solutions and to seek out new paths and challenges. My co-supervisor Owe—thank you for making me a part of your group and for revealing new worlds and ideas to me. It is always nice to find someone who shares my interest in weird music. A big thank you to all my co-workers. Peter, Ilja, Aldo, Ralf and Jakob at Chalmers and Ravindra, Simon and Afaf in Tom Brown's group in Southampton. To everyone who accompanied me on conferences, thank you for the great times. I will especially remember Japan, thank you Erik, Fredrik, Joakim, John, Karl, Marcus and Pär. To all colleagues at Physical Chemistry, those who are, those who were and those who will be there after I'm gone, thank you for the great atmosphere. Joanna, although we might not share esthetic preferences, I greatly value your friendship. Thank you for all the good times in the office (I'm sorry I didn't take better care of your plants). John, thank you for being a great friend and an amazing source of inspiration. Erik, being it science, politics, food or culture—your knowledge and commitment has really pushed me to reach further. Maria, your encouragement and critique during the writing of this thesis have been invaluable. I especially appreciate our discussions of the values, both scientific and otherwise, that lie beyond the everyday work. That, and the coffee. Karl, I have really enjoyed working with you on the nano-societies projects. Thank you for helping me expanding my horizons. To all my friends outside academia—thank you for all the good time during the years. All my love and thanks goes to my family, especially Jenny, Hjalmar and Hedvig.

Contents

Chapter 1
Introduction

> Empathy, evidently, existed only within the human community, whereas intelligence to some degree could be found throughout every phylum and order including the arachnida. For one thing, the emphatic faculty probably required an unimpaired group instinct; a solitary organism, such as a spider, would have no use for it; in fact it would tend to abort a spider's ability to survive. It would make him conscious of the desire to live on the part of his prey. (p. 26)

> 'Empathy,' he said.

> 'Something like that. Identification; there goes I. My god; maybe that's what'll happen. In the confusion you'll retire me, not her. And she can go back to Seattle and live my life. I never felt like this before. We are machines, stamped out like bottle caps. It's an illusion that I—I personally—really exist; I'm just representative of a type.' She shuddered. (p. 164)

The above passages come from the novel "Do Androids Dream of Electric Sheep", written by Philip K. Dick in 1968 [1]. The novel asks the question what -in a society where the creation of intelligent humanoid robots, androids, is possible—is definably human. The question is a question of boundaries, where does the biological entity, the human, end and where does the technological entity, the android, begin? When the androids become more and more like humans, to the point that they are almost indistinguishable, these boundaries are blurred.

This fictional story in many ways represents the scientific development in biology and nanotechnology. The expansion of molecular biology during the 20th century has challenged many of the boundaries between living and non-living objects and between biology and technology. The understanding of biology on a molecular level decodes life packing its functions into discrete (albeit interacting) units. From a different perspective, biology is defined as technology through the development of transgenic species, functioning as production units or disease models. These hybrid beings are both autonomous biological entities and technological objects.

Nanotechnology is a field of science dealing with objects with one dimension in the length scale of 1–100 nm. The reasons for creating technology at this length scale are many. By making smaller devices, we can fit more functionalities

J. Hannestad, *Fluorescence in Bio-inspired Nanotechnology*, Springer Theses,
DOI: 10.1007/978-3-319-01068-7_1,

in a smaller space, opening up for the creation of new technologies in areas where size previously has been a limiting factor. Creating technology on a smaller scale also potentially means that fewer resources are needed in the production. Because of this, nanotechnology can be beneficial from an environmental point of view. However, what makes this size range really stand out is that it corresponds to the size of many biological macro- and supramolecules. This way, biological molecules and structures are turned into objects of technology. Thus, what molecular biology has done to organisms, nanotechnology does to the bio-molecules themselves.

It is not only the biological molecules that are of technological interest. Also the way biological structures are assembled can be utilized in the creation of novel technology. Conventional technology, including much of today's nanotechnology, relies on top-down techniques such as lithography where the created object is etched from a bulk material according to a predetermined pattern. Biological structures on the other hand assemble from the bottom up. Based on simple building blocks, systems with complex emergent properties can form, guided by the mutual interaction of the constituting parts. In Chap. 2, I discuss these questions further, exploring how biological processes enter into technology, thereby creating hybrid systems.

The main focus of this thesis is on three biological fundaments, being either molecules or molecular assemblies whose structures or functions have potential as technology. The first system, covered in Chap. 3, is DNA. In biology, the information bearing properties of DNA is utilized to code for genes and gene regulatory patterns. However, the capacity of molecular recognition can also be used to build physical structures to be used as scaffolds or functional devices in nanoscale technology. This constitutes a high-resolution template for designed structures on the nanometer scale.

In Chap. 5 the light-harvesting complexes of photosynthetic bacteria are presented. In these remarkable examples of nano-scale architecture, excitation energy is transported in multiple steps through ring-shaped assemblies to the reaction center where all redox-chemistry occurs. By arranging light-harvesting in this fashion, photosynthetic organisms can both cover a wider range of the solar spectrum and increase the turnover rate of the reaction center. Just as gathering of excitation energy is utilized in photosynthesis to drive reactions, it can also be applied in chemical devices. Photonic functionalities are desirable, not only in nanotechnology, but in many applications since they can carry information in a form that is easily translated between systems and offer noninvasive means of control. By wiring of excitation energy transfer through a molecular meshwork, in a way mimicking the light-harvesting complexes, reactions circuits could be constructed on the nanometer scale. Several examples where these principles are adopted in the design of novel technology are discussed in Chap. 5, including photonic wires and artificial antenna devices.

The final bio-molecular fundament, covered in Chap. 6, is lipids; or rather their assembled state as lipid vesicles or lipid mono- or bilayers. In water solution, certain lipids have the tendency to self-assemble into membrane enclosed compartments capturing some of the water inside. It is this assembled membrane bubble

that constitutes the fundamental structure of every biological cell. Without compartmentalization, assembly of autopoietic[1] systems combining metabolism and Darwinian evolution would not be possible. Hence, compartmentalization is a prerequisite for life. Lipid structures and membranes are not only physical boundaries; they are also highly dynamic being both bendable and having two-dimensional fluidity. This is reflected in the morphological and functional diversity of lipid membrane systems. Both the capability for compartmentalization and the structural dynamics of lipid systems make them interesting from a device perspective. In Chap. 6 several examples are provided where ultra-small containers for molecular detection or interaction are created from liposomes. Further, the dynamic nature of lipid membrane is used to create two-dimensional flow cells with controlled mixing of components.

To summarize, one might state that the three bio-molecular fundaments can be said to represent three different structural/functional aspects. DNA is the static structure that has a defined and rigid one, two or three-dimensional form, functioning more or less as a molecular scaffold. The light harvesting complexes on the other hand, are photonic structures, offering infrastructure for information transfer and control of functions on a nanometer scale. Finally, lipids are dynamic structures functioning to promote interactions by superpositioning molecular flows. In this thesis I describe how these systems are combined to create assemblies to introduce new functionalities. A common theme in the presented work is the use of fluorescence to study the constructed systems. Conventionally, fluorescence-based techniques utilize fluorescence as a probe or marker for some other functionality. In the presented work, fluorescence is recurringly being used in this way. However, a core element in this thesis is also to use fluorescence as a function in itself, in a way similar to the natural light-harvesting complexes.

In Chap. 8, where the papers which this thesis is based on are presented, these supramolecular structures come together in various forms. The actual papers are no included in the thesis, but can be found through the references on page III. In papers I-III, DNA-based structures that facilitates the assembly of multi-chromophoric systems are created. In papers I and II, the purpose is to assemble systems that enable directional excitation energy transfer from a defined starting position to one or two target fluorophores in one or two dimensions, respectively. Energy transfer between input and output proceeds in multiple steps and requires diffusive energy migration through a mediator part consisting of intercalated YO-PRO-1 molecules. In paper III, the purpose is different. Here, multiple donor molecules, again YO-PRO-1, are associated to a DNA scaffold. To the scaffold, a porphyrin is covalently attached, linking the entire structure to a lipid membrane. The intercalated fluorophores enhance *the excitation of the* porphyrin through resonance energy transfer, acting as a light-harvesting antenna. Finally in paper IV and V, phospholipid monolayer films created on patterned and homogeneous hydrophobic surfaces are utilized to facilitate mixing and hybridization of membrane anchored

[1] Autopoietic means self-creating.

DNA molecules. This represents a platform for dynamic supramolecular assembly on surfaces. The process is followed using fluorescence microscopy with single molecule sensitivity.

Through the incorporation of fluorescence as a component in nanometer scale devices inspired by biological assemblies, the work presented here represent a use fluorescence not only as an indirect probe, but also as a function in itself. This way, fluorescence appears, first as probe, then as function.

Reference

1. Dick PK (1968) Do androids dream of electric sheep?. Gollancz, London

Chapter 2
Being Bioinspired

As outlined in the introduction, an important part of the work in this thesis deals with the integration of biological systems and processes in technology. In order to understand what the implications of this are, and what it means on a practical level, it is of interest to discuss what the intermingling of biology and technology consists of. In this chapter, I will try to present some aspects of how nanotechnology brings biology into the realm of technology, in ways that to a certain extent are different from the bioscience of the late 20th century. I will also discuss how this interrelation disrupts the dualistic relationship between nature and technology, creating a world of hybrid entities. The purpose of this is to provide a better understanding of the ontological status of the different systems and assembly processes presented in this thesis. An important aspect of this is the notion that technological research is not descriptive, but performative. We, as researchers are not just studying the world, we are also creating it.

To illustrate the merging of nature and technology, I will discuss two different examples approaching each other from opposite directions. In 2010 Craig J. Venter and co-workers presented a bacterial cell controlled entirely by a synthesized genome [1]. Aside from the aspect of wanting to study e.g., gene function in a controlled way, an important goal within synthetic biology is the creation of minimal cells for engineering purposes. This would then constitute a purely technological entity with a designed constitution in the form of a living cell. The other perspective is represented by protocells, constructed membrane compartments having cell-like properties. Protocells are technological entities designed to perform certain functions where their life-likeness is part of the function [2]. Here, we see transitions were biological objects are designed to become more like technical devices, and vice versa.

Both these phenomena are clearly effects of the development of molecular biology, which offers access to biological system on the level of individual molecules. This access is associated with a certain merging of biology and technology. In "Modest_ Witness@Second_Millennium." Donna J. Haraway argues that biotechnology replaces the previously dominating conception of "Nature", characterized

J. Hannestad, *Fluorescence in Bio-inspired Nanotechnology*, Springer Theses,
DOI: 10.1007/978-3-319-01068-7_2,

by whole organisms, with the conception of "Life", materialized as information in the form of genes [3]. While whole organisms encompass life, genes are inanimate objects acting as a constituent for life. Genes also have transferable properties at a completely different scale than a complete organism has. These things together allow genes, and the living organism that host them, to become a technological entity. Of course, living organisms have been part of the technological domain before the advent of bioscience (breeding of livestock and crops in agriculture is perhaps the most striking example). However, this relation has been an external relation between living and non-living objects rather than a relation that transgresses the boundaries of the individual organism. The genetic material of an organism is both an internal and an external materiality (see schematic is Fig. 2.1).

Haraway writes:

> Transgressive border-crossing pollutes lineages-in a transgenic organism's case, the lineages of nature itself-transforming nature into its binary opposite, culture. […] The revolutionary continuities between natural kinds instaurated by the theory of biological evolution seem flaccid compared to the rigorous couplings across taxonomic kingdoms. (p. 60)

The transitory process when an object becomes a technological entity has close ties to the question of patentability. Haraway writes that, as late as 1980, is was possible to patent biotechnical processes but not the microorganisms themselves. In 1980 however, a patent was approved for a bacterium that breaks down petroleum. The bacterium was ruled to be a patentable composition of matter and a product of human ingenuity.

Although much of this development occurs in the latter part of the 20th century, it should be noted however, that the conception of living organisms as machines is older than contemporary bioscience. The poster "Der Mensch als Industriepalast" by Fritz Kahn from 1929 depicts a cross-section of a human being (Fig. 2.2). Instead of having internal organs, the body is filled with connected industrial facilities performing all bodily functions. The poster works only on the level of metaphors but is still a striking representation of how the human bodily processes are incorporated into industrial logic and structure. Further, it is worth noting that the poster is produced during a period of great expansion of the German chemical industry.

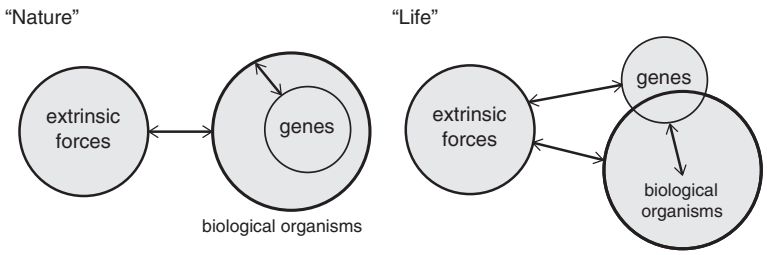

Fig. 2.1 Interrelation patterns for the organism-centered "nature" and the gene-centered "life" ontologies. The extrinsic forces can be any living or non-living entity acting upon the specified organism and its genome

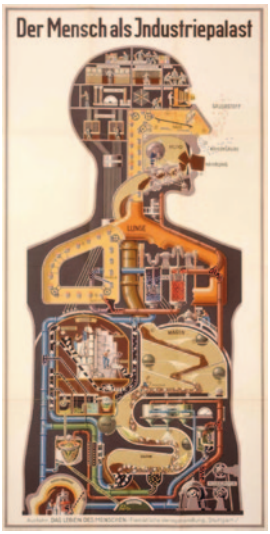

Fig. 2.2 "Der Mensch als Industriepalast" Fritz Kahn 1929. Courtesy of the National Library of Medicine

How does this all fit in with nanotechnology? While biotechnology more or less hijacks biological organisms to serve a specific purpose, nanotechnology completely removes systems and processes from their biological context. Nanotechnology has been defined as structures with dimension in the size range of 1–100 nm. This size range contain both the upper limit for synthetic structures and the lower limit for lithographic structures, as shown e.g., by Whitesides et al. in 1991 [4]. Moreover, this size range encompasses a wide variety of molecular structures, making them ideal candidates as bridging units between the molecular and lithographic domains. Sarikaya et al. describe techniques based on proteins with affinity to inorganic surfaces which could function as a biomimetic bridge between the macroscopic-technological realm and the molecular one [5].

2.1 Self-Assembly

For many bio-inspired technological systems, there is one process that is continuously reoccurring: self-assembly. Self-assembly is the process where a number of disordered entities spontaneously come together to form a system with higher order, often with emergent properties. This process is driven by the interaction of the constituting objects, and not by any external force acting on the system. The concept of self-assembly can be applied to a wide range of systems, acting on different levels. Self-assembly is not only a process found on the molecular scale, several macroscopic physical phenomena such as galaxies, weather patterns and schools of fish are characterized by self-assembly [6]. Even human

societies carry aspects of self-assembly. How is self-assembly within these different domains related? Here, it can be useful to turn to Alfred N. Whitehead's conception of society. Michael Halewood writes in "A. N. Whitehead and Social Theory" [7].

> for Whitehead, societies refer to the achievement of groups of entities, of any kind, in managing to cohere and endure and thus to constitute some kind of unity. The term social refers to the manner and milieu in which such endurance is gained. Rocks, stones, amoeba, books can, thus, be considered to be societies. (p. 85)

According to Whitehead, societies are systems of interrelation between entities of any kind. Since self-assembly as a process is based solely on the interaction between the comprising entities, self-assembled systems are societies in themselves. This does not mean that all self-assembled systems are identical or that something which applies within one system necessarily holds for all. However, many of the fundamental aspects are transferable and it is reasonable to analyze different self-assembled systems using similar theoretical frameworks.

In this text, I will discuss self-assembly from a molecular and supramolecular perspective, outlining some of the key features of self-assembled systems. Where applicable, I will try to draw parallels to other, non-molecular systems, highlighting similarities and differences. Self-assembly within chemistry has been studied extensively by Whitesides [4, 5, 8]. He has also made a great effort to try to define what self-assembly in chemistry actually is. In order to distinguish self-assembly from other formation processes, he has put up five criteria that is defining for systems characterized by self-assembly [8]. The first criterion (1) deals with the self-assembling components. As previously stated, objects that undergo self-assembly are initially in a state of disorder. This disordered state can be e.g., molecules freely moving in solution or polymer subunits in random coil conformation. Nomadic populations of early human history can be seen as a type of disordered state since they lack physical structure, e.g., in the form of a localized settlement. Entities that undergo self-assembly need to have properties that facilitate interactions that lead to a more high-ordered state. Further, (2) interactions between components consist of a balance between attractive and repulsive forces and are generally of weak nature, e.g., hydrogen bonds and van der Waal forces. The dependence of weak interactions is associated with another important characteristics of self-assembled systems: reversibility (3). Since molecules move randomly by diffusion, they probe all reaction pathways available to them. For complex assemblies to spontaneously form, the process needs to be guided through a series of states of increasing stability allowing continuous rearrangements. For this to be possible, the strength of the bonds has to be of the same order as the thermal fluctuations of the system, hence the requirement for weak interactions.

Arranging large numbers of individual components into complex assemblies equals a large decrease in system disorder. Following the second law of thermodynamics, this decrease in disorder comes with an energetic cost. The driving

force for self-assembly is provided through the change in interaction between the self-assembling components and their environment (4). If the components have properties that force the molecules in the environment to assume a highly ordered conformation, the formation of the assembled structure can lead to an overall decrease in order if it leads to a release of the environment molecules from this unfavorable conformation. The final point is perhaps obvious: the components must be mobile (5). This is a natural consequence of the dependence on diffusion for formation. The combination of weak and reversible interactions and mobile interacting objects is akin to the rise of cities. Following the reasoning of Manuel De Landa, cities are intensification of material flows in crystallized form [9]. One of the earliest processes leading to formation of cities was the cultivation of plants. Plants, in turn, are essentially stored energy from sunlight. Thus, cultivation of plants represents intensification of energy. Through the interaction of the many individuals in a city, material flows can change and transform.

It is of interest to take a closer look at how the interaction between individual subunits can lead to the self-assembly of complex, defined systems. Self-assembly is different from aggregation in the sense that in an aggregated system, the interaction between components is unspecific and the formed structure is disordered. In a self-assembled system, a defined structure is formed through specific interactions between the comprising entities. This specific interaction is called molecular recognition and consists of patterns of non-covalent bonds. Examples of molecular recognition are duplex formation between two complementary DNA strands or folding of proteins through the creation of specific patterns of hydrogen bonds. By design of patterns of molecular recognition, the structure of self-assembled systems can be controlled. This controlled formation is called supramolecular chemistry, a term coined by Jean-Marie Lehn. Supramolecular chemistry is a wide field ranging from biology to physics, where the focus is not on the formation of covalent bonds, but on non-covalent bonds [10–12]. Lehn writes [11]:

> Supramolecular chemistry, the chemistry beyond the molecule, is the designed chemistry of the intermolecular bond, just as molecular chemistry is that of the covalent bond. (p. 1304)

Supramolecular chemistry takes processes that are ubiquitous in biology, where components assemble from the bottom up rather than top down, and applies them in chemistry. The benefit of supramolecular chemistry is that it facilitates the creation of structures that are very difficult, or even impossible, to synthesize using conventional chemistry. This is particularly true for DNA nanotechnology, where molecular recognition patterns are designed to create a plethora of structures on the nanometer scale. In the combination of supramolecular chemistry and self-assembly, we find perhaps the most obvious example of how bio-inspired nanotechnology is qualitatively different from conventional technology. It is also through processes such as self-assembly which nanotechnology can widen our conception of what technology can be.

References

1. Gibson DG, Glass JI, Lartigue C, Noskov VN, Chuang RY, Algire MA, Benders GA, Montague MG, Ma L, Moodie MM, Merryman C, Vashee S, Krishnakumar R, Assad-Garcia N, Andrews-Pfannkoch C, Denisova EA, Young L, Qi ZQ, Segall-Shapiro TH, Calvey CH, Parmar PP, Hutchison CA, Smith HO, Venter JC (2010) Creation of a bacterial cell controlled by a chemically synthesized genome. Science 329:52–56
2. Pohorille A, Deamer D (2002) Artificial cells: prospects for biotechnology. Trends Biotechnol 20:123–128
3. Haraway DJ (1997) Modest_Witness@Second_Millennium.Femaleman©_Meets_ Oncomouse™. Routledge, New York
4. Whitesides GM, Mathias JP, Seto CT (1991) Molecular self-assembly and nanochemistry—a chemical strategy for the synthesis of nanostructures. Science 254:1312–1319
5. Sarikaya M, Tamerler C, Jen AKY, Schulten K, Baneyx F (2003) Molecular biomimetics: nanotechnology through biology. Nature Mater 2:577–585
6. Whitesides GM, Grzybowski B (2002) Self-assembly at all scales. Science 295:2418–2421
7. Halewood M (2011) A.N. Whitehead and social theory: tracing a culture of thought. Anthem Press, London
8. Whitesides GM, Boncheva M (2002) Beyond molecules: self-assembly of mesoscopic and macroscopic components. Proc Natl Acad Sci USA 99:4769–4774
9. De Landa M (1997) A thousand years of nonlinear history. Zone Books, Brooklyn
10. Lehn JM (1988) Supramolecular chemistry—scope and perspectives molecules, supermolecules, and molecular devices. Angew Chem Int Ed 27:89–112
11. Lehn JM (1990) Perspectives in supramolecular chemistry—from molecular recognition towards molecular information-processing and self-organization. Angew Chem Int Ed 29:1304–1319
12. Lehn JM (2002) Toward self-organization and complex matter. Science 295:2400–2403

Chapter 3
DNA: Molecular Recognition and Information Storage

There is no better symbol for the development of biology during the last 100 years than the double helix of DNA. Discovered in 1953 by James D. Watson and Francis Crick [1, 2], it stands as one of the great discoveries of the 20th century. Their description of the molecular structure of DNA, and how it enables storage of genetic information is one of the cornerstones of an understanding of biology at a molecular level.

DNA is a polymer built from nucleotide units. Each nucleotide consists of three parts: a 2-deoxyribose sugar, a phosphate group and a base. By linking the phosphate sugar on one nucleotide with the phosphate group of another nucleotide through a phosphodiester bond the backbone of DNA is created, consisting of an alternating pattern of sugar and phosphate groups. The coding part of DNA is the sequence of bases that is formed when the polymer is created from the nucleotide monomers. There are four different bases used in DNA: adenine (A), guanine (G), cytosine (C) and thymine (T). They are all depicted in Fig. 3.1, connected through the phosphodiester backbone. The bases are nitrogen-containing aromatic compounds comprised of either a one-ring or two-ring system. The pyrimidines C and T are one-ring systems and the purines A and G are two-ring systems. A central feature of DNA is its ability to form a duplex consisting of two individual DNA strands. This property comes from the bases' ability to form hydrogen bonds with each other in a specific manner; A forms two hydrogen bonds with T and G forms three hydrogen bonds with C (see Fig. 3.2). These particular associations between two bases are called Watson and Crick base pairs. Because of this hydrogen-bonding pattern, every strand of DNA has another strand that has a complementary base sequence. Because the DNA backbone is asymmetric, DNA strands have directionality. The ribose sugar of nucleotide unit n is connected to the $n - 1$ unit through the $5'$ carbon and to the $n + 1$ unit through the $3'$ carbon. Therefore, DNA sequences are (by convention) written in the $5'$ to $3'$ direction. When two complementary strands form a duplex, they do so in an anti-parallel fashion, i.e. the $5'$ end of one strand binds to the $3'$ end of the other.

J. Hannestad, *Fluorescence in Bio-inspired Nanotechnology*, Springer Theses,
DOI: 10.1007/978-3-319-01068-7_3, © Springer International Publishing Switzerland 2013

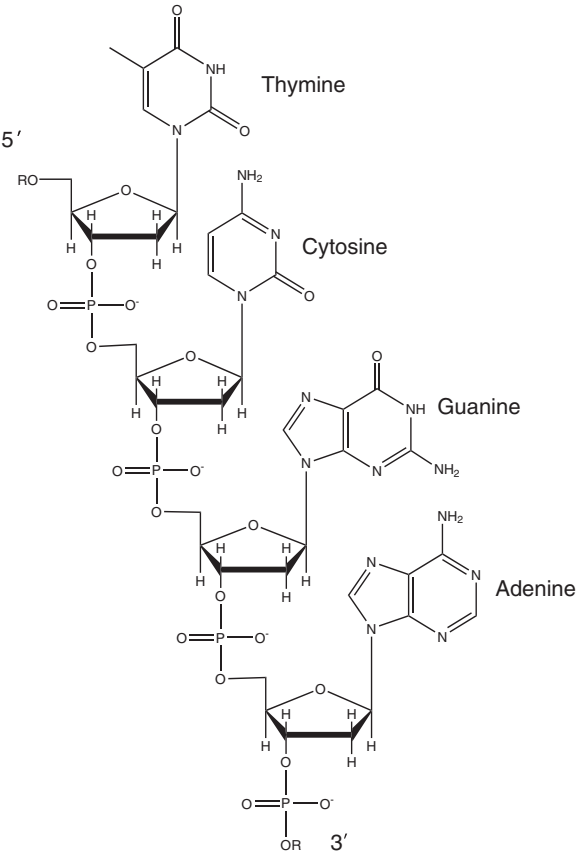

Fig. 3.1 The four DNA bases thymine, cytosine, guanine and adenine connected through the phosphodiester backbone

Single-stranded DNA is a highly flexible polymer, commonly modelled as a random coil. By contrast, the DNA duplex is very rigid, with a persistence length of 50 nm.[1] The driving force to go from the disordered random coil of the unpaired DNA to the highly ordered duplex is provided by a combination of the hydrogen bonds between the base pairs and the hydrophobic core that is created when the bases stack on top of each other in the duplex. Under physiological conditions, the DNA duplex form a right handed helix with a helical pitch of 10 base pairs. This form is called B-DNA. There are two other known forms of DNA, A-DNA and Z-DNA. However, the biological relevance of these forms is disputed. The width of the DNA duplex is 22 Å and the base pair-to-base pair distance is 3.4 Å. Another prominent feature of the DNA duplex is the two grooves in the

[1] Persistence length is a measure of the stiffness of a polymer and defines the length over which directional correlation in the polymer is lost.

helix, which are regions along the double helix where the bases are not shielded by the backbone making them accessible from the DNA exterior. These two voids are of unequal size and are denoted major and minor groove. Because the bases are exposed in the grooves, they play an important role in the interaction between DNA and many molecules, e.g. DNA binding proteins.

3.1 DNA Nanotechnology

DNA nanotechnology is the term used for the non-biological use of DNA aimed at creating nanoscale assemblies[2] with certain structural or functional characteristics. In all work presented in this thesis, DNA is used in a non-biological fashion, either as a scaffolding material to coordinate functions (papers I-III) and to provide molecular recognition in self-assembled systems (I–V). Here, I will discuss the development of the field of DNA nanotechnology which took off during the 1990s and figuratively exploded during the 2000s [3, 4].

What does the statement that DNA nanotechnology is a non-biological use of DNA mean? What properties of DNA are utilized? DNA is essentially a molecular container for storage of information. In a biological organism, DNA stores genetic information, which is a blueprint for the inner workings of the organism. The genetic information is copied through replication and is, when the organism reproduces, passed on to its progeny. However, DNA is not limited to storage of genetic information. Essentially any information can be stored in DNA e.g. texts and even whole books complete with images [5].

What DNA nanotechnology does is that it explores the ability of DNA to store structural information on an aggregate level. With this I mean that the "blueprint" for the assembled structure lies, not in the individual sequence, but in the specific interaction of multiple (semi) complementary sequences (or in different parts of a single sequence, if dealing with hairpin[3] structures). Here, different, partly complementary strands self-assemble into a specific structure defined by the base-pairing pattern of the constituting strands. Therefore, it is possible to write the structure into the sequence of the DNA strands used to build it.

Already in the early 1980s Nadrian C. Seeman discussed the potential of immobilized DNA junctions to function as novel material [6, 7]. Inspiration for these immobilized structures comes from Holliday junctions, a phenomenon first discovered in fungi [8]. Holliday junctions are complex DNA structures consisting of four different strands, A, B, A′ and B′. The assembly is created when the strands exchange base-pairing partners, i.e. AB change to AB′ and vice versa (Fig. 3.3).

[2] The term is also used for larger, crystalline lattices with internal geometries on the nanometer scale.

[3] Hairpin are intramolecular structures formed when two complementary regions of the same molecule base pair.

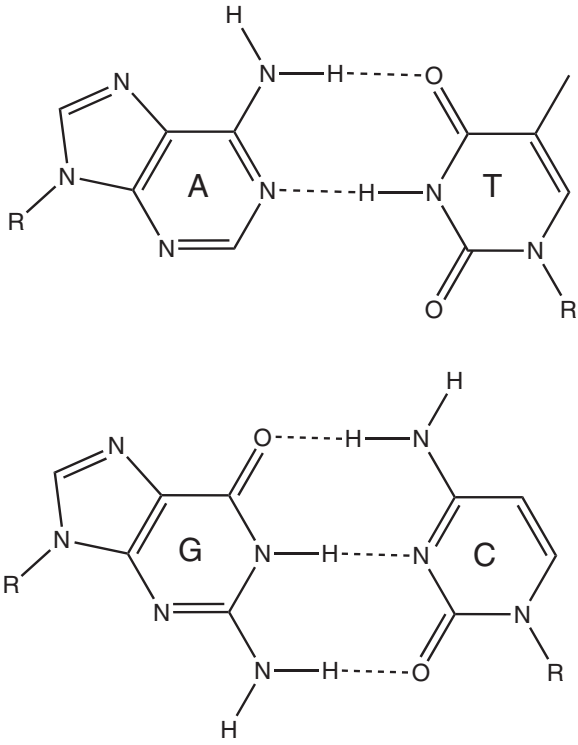

Fig. 3.2 Watson-Crick base pairing. A pairs with T and G pairs with C

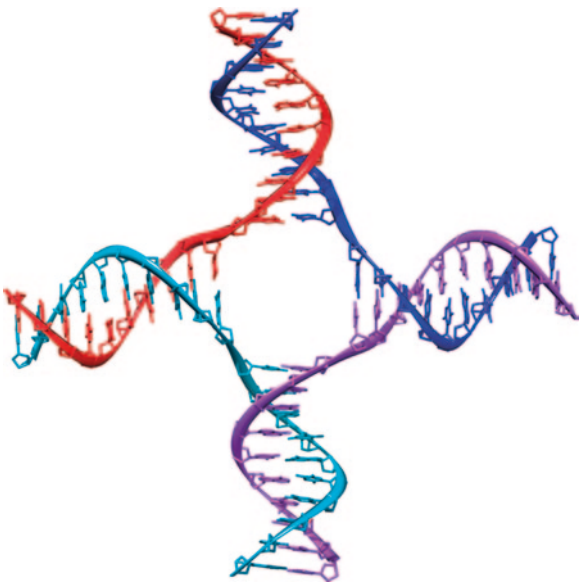

Fig. 3.3 Holiday junction. Each strand is denoted by a specific color

For this to occur the strands need to have regions with identical sequences, i.e. they need to be homologous. The problem with the structures from a technological perspective is that the Holliday junctions are able to migrate along the region with sequence identity. What Seeman and co-workers did was to create a similar structure that did not have regions of sequence identity. Instead, sequences A, B, C and D were used. The only way for these strands to create complete duplex structures was to create a junction structure with only one possible cross-over position. Seeman et al. [9] developed this principle further by creating the double cross-over (DX) motif (Fig. 3.4). The DX motif features two junction structures in close vicinity and with one common cross-over strand creating a structure that is more stable and rigid than the single junction. Following the double cross-over motif, more complex structures have been created such as the triple-cross over (TX) [10] or the paranemic (PX) [11] cross-over structures. These motifs can be applied in a wide variety of ways and we will see them reoccurring quite frequently in the work presented in this chapter.

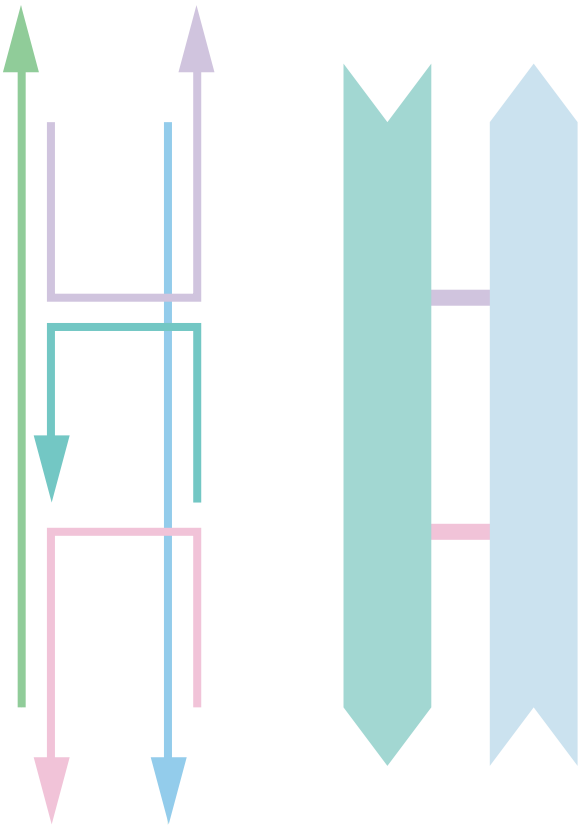

Fig. 3.4 Two different schematic representations of the DX motif. Each *arrow* in the image to the *left* represents a DNA strand. The structure contains two sites where base strands cross-link

3.1.1 Structural DNA Nanotechnology

One branch of DNA nanotechnology concerns DNA-based assemblies whose primary feature is their physical form. The motivation can e.g. be to create a DNA-based material or to use DNA to scaffold some other molecule thereby controlling its positioning using the nanostructured DNA. The structural DNA nanotechnology can in turn be divided into two categories, namely repetitive and non-repetitive structures. The repetitive structures are pseudo-crystalline and have a total size that is on the order of micrometers. They do, however, have internal geometry on the nanometer scale. The non-repetitive objects have true nanoscale geometry.

In 1998 Seeman et al. [12] presented a two-dimensional pseudo-crystalline lattice. This was the first example of how DNA could be designed to form a large-scale structure such as a lattice. The assembled structure was built using repeated DX motifs. In the years following this, a wide variety of structures were created. Yan et al. [13] constructed a nano-grid capable of organizing proteins on a surface using a square building block. Another example comes from Mao et al. [14], who constructed a two-dimensional array using three-way nodes resulting in a lattice consisting of hexagons. About the same time, the same group also presented work that deviates from the rigid arrays already discussed. Instead of the rigid lattices, they created triangle-shaped structures with four-strand junctions in each corner [15]. The design of the triangles is based on the structural concept of tensegrity, meaning a combination of tension and compression forces. In a tensegrity structure, rigid bars are placed in a net of tension created by cables that join the bars together. When the forces balance, a simple but very stable structure is created. In the case of the DNA triangle, the duplexes in the triangle sides constitute the bars of the tensegrity structure and the flexible four-strand junction the joining cables (Fig. 3.5). Multiple triangles can be joined together to create e.g. two-dimensional sheets or one-dimensional arrays.

So far, I have mostly been focusing on two-dimensional objects. However, DNA has also been used to create repetitive structures in three dimensions. In

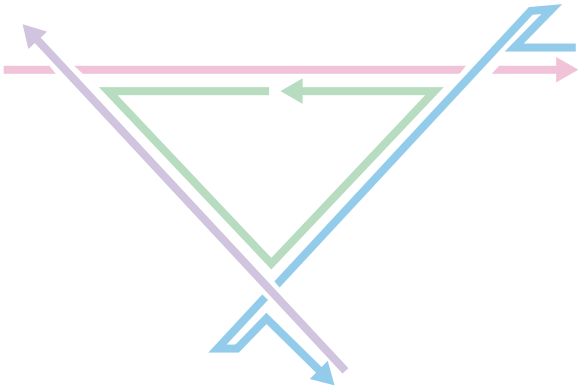

Fig. 3.5 Tensegrity triangle consisting of four DNA strands. Adapted from Liu et al. [15]

2009, Seeman et al. [16] created a three-dimensional crystal based on the tensegrity triangle. In this work, the triangles were assembled into rhombohedral lattices and formed crystals with dimensions exceeding 250 μm. The internal cavities were, for some structures, on the order of 1,000 nm^3. With cavities of this size, these or similar assemblages could be used as scaffolds for bio-molecules, e.g. for protein crystallography studies. Another type of three-dimensional structure comes in the form of tubes. The formation of DNA nanotubes was first observed by Yan et al. [13] in a design based on tiles of four-way junctions. Interestingly, nanotube formation was favored in a design where there was an even number of helical half-turns in between adjacent junction centers, meaning that all junctions face the same direction. Contrastingly, lattice formation was favored in the design where the direction of the junction alternated with every unit. LaBean et al. [17] refined, the nanotube concept by basing the design on TX motifs, resulting in a more uniform tube morphology compared to the previous design. Moreover, both Winfree et al. [18] as well as Turberfield et al. [19] have presented nanotube designs based on the DX motif. Seeman et al. [20] introduced a further refinement of the nanotube concept by creating a tube based on a six-helix bundle. Compared to the previous examples which where essentially rolled up lattices, the six-helix bundle is designed only to fold as a tube. The six helices that make up the tube form a ring with a hollow center and each helix is connected to its neighbor by two DX motifs. The hole in center of the helix ring is large enough to fit an additional DNA duplex, something that was later demonstrated in the creation of a seven-helix bundle [21].

The second direction in structural DNA nanotechnology has to a large extent been focused at creating different geometrical shapes on the nanometer scale. Again, one of the early examples was presented by Seeman et al. [22] in the form of a truncated octahedron. Following this, a range of different structures has been created, such as tetrahedrons [23–25], bi-pyramids [26], octahedrons [27] and buckyballs [28]. The same three-way junction motif that was utilized in the assembly of the buckyballs can be used to create a wide variety of shapes [29] and was also used in the creation of the hexagonal two-dimensional lattices previously discussed [14].

In an effort to create a non-repetitive lattice platform with high resolution addressability, Nordén et al. [30] constructed a hexagonal building block with a 10 base pair side length. Two versions of the hexagonal structure were created, one consisting of linear DNA molecules with flexible TT-hinges[4] in the corners of the structure and one built from custom made three-way DNA molecule (Fig. 3.6a). In both assembled structures, every side is unique making them individually addressable. Lundberg et al. [31] improved the TT-hinged hexagonal structure by introducing covalent cross-linking of the different strands using click chemistry. The three-way node used to build the latter of the structures is constructed using a

[4] TT-hinges are two adjacent T bases that are left unpaired, creating a region of flexibility in a structure.

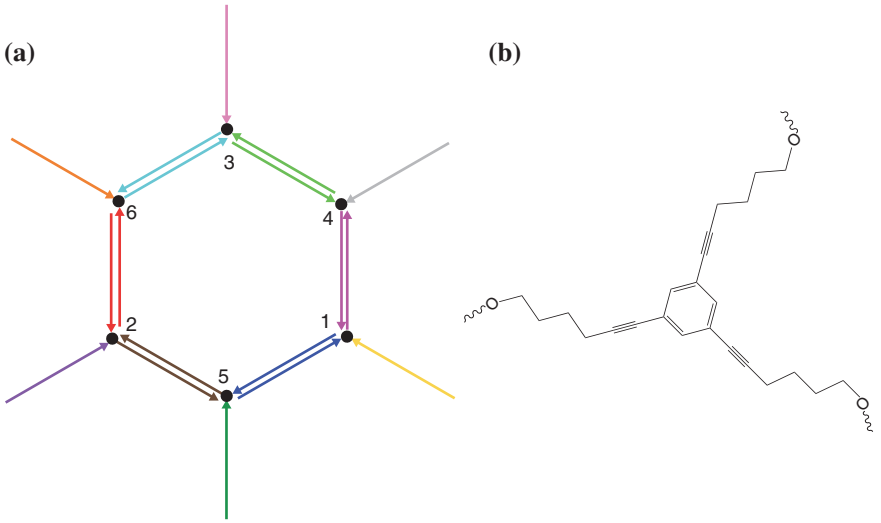

Fig. 3.6 **a** Hexagonal DNA structure built from three-way oligomers. **b** Three-way node. Figure adapted from Tumpane et al. [30]

1,3,5-tri-substituted benzene connecting three different single-stranded DNA moieties (Fig. 3.6b). When the three-way nodes assemble into a hexagon, single stranded 10-mer arms extend from its corners. This makes it possible to attach additional hexagons, thereby building a larger network. The branched hexagon is used in paper II in this thesis to create a photonic network [32]. Tumpane et al. [33] demonstrated the addressability of the system by binding a triplex strand to one of the sides of a bi-cyclic assembly. Triplex binding is verified by means of resonance energy transfer between a fluorophore on the triplex strand and one on the assembled structure.[5] Furthermore, triplex binding was turned on and off using pH changes making the system switchable. In 2011, Lundberg et al. [34] presented a four ring assembly using the three-way nodes, which is the largest structure to date using this method. This study demonstrated one of the issues with constructing large and complex DNA-based structures: there is a drastic decrease in the structure yield with growing structure size. This effect is likely especially important in assemblies requiring equimolar addition of the building block and in structures with complex topologies with high flexibility requiring sequential formation of DNA duplexes.

The structure that has perhaps been most widely used is the tetrahedron created by Turberfield et al. [24] (Fig. 3.7). The tetrahedron is a fairly robust structure with sides that are either 20 or 30 base pairs, creating a structure with dimension of approximately 10 nm. Some of the reasons behind its popularity are the simplistic

[5] For a description of energy transfer see Sect. 4.2.

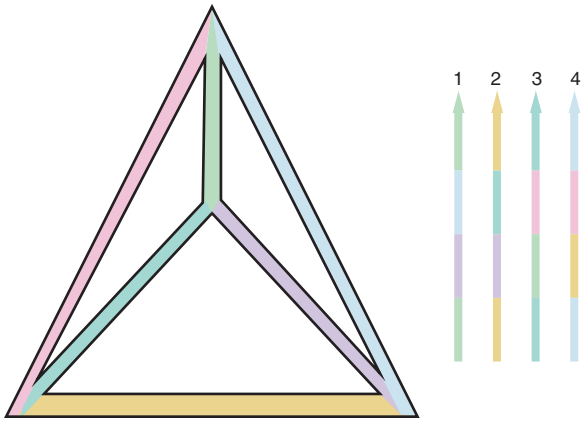

Fig. 3.7 Assembled DNA tetrahedron shown together with the constituent strands. Coloring of the strands correspond to their region in the tetrahedron. Adapted from Goodman et al. [23]

one step-assembly and a high structure yield of approximately 95 %. One application of the DNA tetrahedron is presented by Armitage et al. [35] who created a supramolecular multi-fluorophore assembly. This work will be discussed more in detail in the chapter focused on nanoscale photonic devices (Chap. 5). Another example comes from Alivisatos et al. [36] who assembled clusters of gold nanoparticles using the Turberfield tetrahedron.

3.1.2 DNA Origami

In principle part of the structural DNA-nanotechnolgy, DNA origami also represents something of a thematic shift in the research field making it justifiable to discuss it in a separate section. The term DNA origami was coined by Paul Rothemund who introduced the technique in 2006 [37]. DNA origami is based on the folding of the single-stranded 7.3 kilobase genome of the M13mp18 bacteriophage into various shapes and patterns using more than 200 unique short staple strands. The staple strands crosslink two or more regions of the template strands thereby folding it into the desired shape (Fig. 3.8). When creating a structure using this technique, staple strands are added in excess (at least tenfold, in many cases more). This in order to make sure that the final structure is produced with sufficient yield. Recently, Lundberg et al. [34] discussed the formation yield as a function of structure size calling for more in depth investigation of the reliance on addition of staple strands in great excess. There are few mechanistic insights into the formation process of DNA origami assemblies. For instance, what is the error tolerance of the structures? How many of the staple strands can be removed whilst still retaining the same shape? Bearing this in mind, it is important to note the DNA origami has a number of strengths contributing to the popularity of the design concept. One of them is the versatility of the fundamental design. With only small changes in the staple sequences it is possible to vary the geometry of the

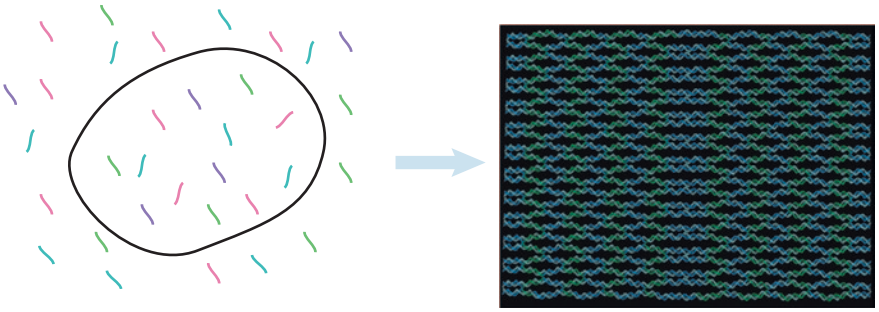

Fig. 3.8 Assembly of DNA origami rectangle. The single-stranded genome of M13mp18 (*black*) is mixed with short staple strands (*colored*). The staple strands force the virus strand to fold into the designed shape by crosslinking separate regions of the scaffold strand

formed structure almost indefinitely. In the original paper, Rothemund presented a wide range of two-dimensional structures with the 70 × 100 nm [2] rectangle perhaps being the simplest one. Another two-dimensional assembly was presented by Kjems et al. [38] who created a nanoscale shape in the form of a dolphin.

Although Rothemund is credited with the invention of DNA origami, the principle of folding a long single stranded DNA into a defined shape using shorter strands had previously been implemented by Shih et al. [27] in the design of a nanoscale octahedron. Shih has since then continued to use DNA origami to create a plethora of three-dimensional structures with every conceivable shape [39]. These three-dimensional assemblies are created by folding sheets of helices on top of each other. The helices in one layer are slightly shifted with respect to the helices in the layers above and below. This gives the structures a honeycomb-like cross section.

Another strength of DNA origami is that it is fairly easily functionalized. Since the structures are held together by relatively short oligomers (usually ~32-mers) which can easily be modified, there are plenty of potential functionalization targets. Furthermore, as the staple strands are usually designed to be unique, the structures are also addressable. One example of this comes from Gothelf et al. [40] who created a platform for localized chemical reactions on a DNA origami rectangle. In this work, certain staple strands were fitted with biotin moieties connected to the oligomer via either a cleavable or an un-cleavable linker. When the origami rectangle had formed streptavidin was added to the sample. The presence of staple strands decorated with biotin enabled streptavidin to bind to the structure, this way producing a pattern that could be detected with AFM.[6] The biotin moieties can than be removed from the strands with cleavable linkers thereby changing the labeling pattern. Gothelf and co-workers also show that it is possible to covalently couple new groups to the already formed structure using both click chemistry and NHS ester conjugation. Single reaction events were detected in real time by Simmel et al. [41]. Using a staple strand with a single stranded overhang, they

[6] Atomic Force Microscopy.

were able to fish complementary, fluorescently labeled oligomers from solution whilst detecting the binding and unbinding events using single molecule fluorescence spectroscopy.

There are also a few examples where DNA origami assemblies are created to function as hosts for other molecules. In 2009, Kjems et al. [42] created a rectangular box with a lid that could be opened using a set of "key" oligonucleotides. In contrast with the three-dimensional origami objects designed by Shih and co-workers, the box has an internal void. This makes the box a potential carrier of payload molecules. A similar idea is presented by Douglas et al. [43] who have designed a barrel-like structure capable of carrying antibody fragments. The barrel is constructed from two origami sheets which are joined in one end by single-stranded scaffold hinges. The sheets can be non-covalently connected in the other end using an aptamer-based lock mechanism.[7] The lock mechanism is designed to function as a logic AND gate, requiring the simultaneous recognition of two antigens to be opened. When the structure is assembled it forms the opened state, allowing the payload molecules to be incorporated. However, in this state the lock components are held far apart. Since the spontaneous folding to the closed state is highly improbable, guiding strands were added to facilitate this process.

Before moving on to other subjects I just want to mention two studies that concerns the influence of DNA origami on larger scale systems, either by producing macroscopic effects or by interacting with macroscopic objects. Recently, Liedl et al. [44] constructed a DNA nanorod that is decorated with gold particles. The gold particles create a helical shape with either a right handed or a left handed twist. The assemblies show substantial circular dichroism and optical rotary dispersion. These effects are attributed to the collective plasmon–plasmon interactions of the gold nanoparticles. The spectral properties of the nanoparticles could also be tuned by growing silver on the gold particles, this way producing a spectral blue-shift. In another study Wallraff et al. [45] showed that it is possible to make controlled deposition of DNA origami structures on surfaces patterned with e-beam lithography.

3.1.3 Nanomechanical Devices and DNA Computation

So far, my focus has been on more or less static structures. This section will instead discuss DNA-based assemblies where molecular dynamics is part of the core functionality. The assemblies that fall into this category are usually described by words such as nanomechnical devices or nanorobotics. However, I will also investigate dynamic DNA constructs that process information.

Like before, we start off with an example from Seeman and co-workers. In 1999 they presented a structure consisting of two DX motifs held together by a linking strand that is 4.5 turns long. The linking strand contains a $d(CG)_{10}$

[7] Aptamers are nucleic acid or peptide molecules capable of binding to target molecules.

sequence which can be converted from B-form to Z-form under high ionic strength and by doing so, twisting the two DX motifs in relation to each other [46]. Conceptually similar to the B/Z-switch, variations in the microenvironment around DNA can be utilized to drive conformational changes. One example of such is the G-quadruplex structures which are found both in biology and in synthetic assemblies [47]. Formation of these structures depends on the presence of a cation template. Similarily there are complex structures whose assembly is pH dependent. Just as guanine-rich sequence can form G-quadruples, cytosine-rich sequences are also capable of forming tetraplex structure, termed I-motifs [48]. I-motifs rely of $C–C^+$ base pairing, i.e. one cytosine has to be protonated in order for it to form. Because of this, the process is pH dependent. Liedl et al. [49, 50], have constructed an I-motif-based assembly that is coupled to a chemical oscillator producing pH changes. This way the structure continuously cycles through its different conformations following the chemical oscillations.

Another approach towards nanodevices was adopted by Yurke et al. [51] who presented a DNA-based molecular "tweezers" whose underlying design principle has become defining for almost all DNA-based nanomechanical devices that have followed. Instead of using an extrinsic driving force such as changes in pH or ionic strength to promote changes in the device, Yurke et al. used DNA itself as fuel. Just as the free energy associated with the duplex formation of two complementary strands can be utilized to build the highly ordered structures discussed in the previous sections, it can also drive mechanical work. In its open state, the tweezers consists of three partially complementary DNA strands, creating a structure with two duplex regions, a small hinge and two longer single-stranded overhangs (Fig. 3.9). The single-stranded overhangs enable a fuel strand (F) to hybridize with the tweezers thereby creating the closed structure. In order for the

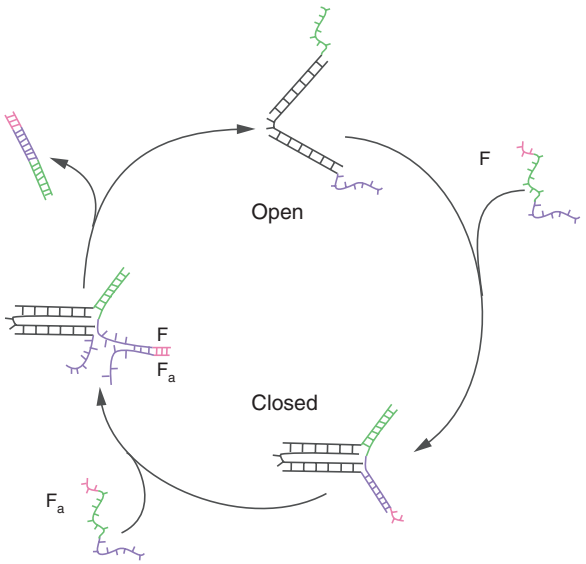

Fig. 3.9 DNA tweezers switching between an open and a closed state using a combination of fuel and anti-fuel strands. Yurke et al. [51]

assembly to be able to cycle between open and closed states, the fuel strand is also equipped with a short single stranded overhang, called toehold. This toehold is the key to the device mechanism because it enables the fuel strand to be displaced by an anti-fuel strand offering full complementarity. The combination of fuel and anti-fuel strands is denoted as waste strand, and repeated switching between device states entices a continuous generation of these waste strands. Following this, Seeman et al. [52] have presented a larger, more complex, nanomachine where a series of fuel and anti-fuel strands are used to cycle the device between different DX motifs creating conformational changes. Another example of toehold devices demonstrates how mechanical assemblies can be combined with structural ones using location-specific association of the switching device [53].

By constructing a series of DNA-based "footholds" it is possible to convert the back-and-forth toehold device into a walker structure that moves unidirectionally along a programmed path. In 2004, Seeman et al. [54] presented a bipedal walking device, capable of following a foothold track. The construction has single stranded overhangs on both feet as well as on all footholds. In order for the foot to attach to the foothold, a fuel strand complementary to both overhangs is added. This strand can later be removed using an anti-fuel strand, releasing the foot. By attaching one foot whilst releasing the other, it is possible to create a progressive motion. Simultaneously, a similar device was constructed by Turberfield et al. [55]. Following this the unidirectional walker concept has been developed further through e.g. increased leg coordination [56] and additional functionalities [57].

DNA-based walking devices can also be constructed by make use of the action of deoxyribozymes. Deoxyribozymes are nucleic acids with catalytic activity, capable of cleaving the phosphodiester backbone of DNA. One such device was constructed by Stojanovic et al. [58] in the form of a multipedal DNA walker or DNA spider. The spider walks on top of a DNA substrate through a multi-leg version of random walk. When the spiders move through the matrix they catalyze the cleavage of the DNA substrate this way directing the spider toward new, uncleaved regions of the DNA matrix. The same group developed the spider concept further by introducing a DNA origami landscape with cleavable and non-cleavable regions [59]. This way they are able to direct the movement of the spider to a specific path with both start and stop positions. Turberfield et al. [60] have constructed a similar system of path-dependent motion, capable of selective motion along four different tracks. However, in this assembly, propagation is driven by strand displacement. A goal for many of the walker designs is to create nanoscale platforms for reaction control where molecular recognition provided by DNA can be utilized to coordinate chemical reactions [61]. In 2010 Seeman et al. [62] presented a DNA-based assembly line combining a range of different DNA nanoconstructs. In this design, a DNA origami rectangle was used as a scaffold for a series of DX-based, two-state cargo containers. Finally, the system featured a walker based on the tensegrity triangle designed by Mao et al. [15]. The walker moves in a directed path along the DNA origami substrate picking up cargo using the arms of the triangle at the different loading stations.

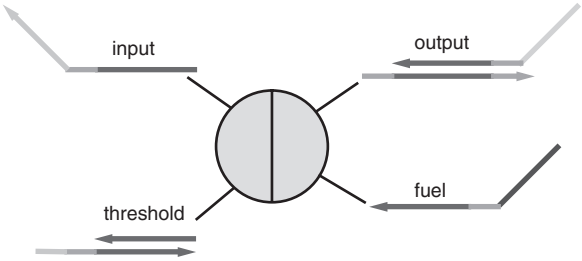

Fig. 3.10 Principal layout of the seesaw gate. Adapted from Qian et al. [65]

In a way related to the nanomechanical devices, DNA can also be utilized for computational purposes. DNA-based computation was demonstrated as early as 1994 by Leonard Aldeman [63]. However, here I will focus on more recent work by Eric Winfree, providing a brief overview of his research [64–66]. In a first example, which is essentially a method for the assembly of DNA-based structures, a DNA origami seed, capable of promoting algorithmic self-assembly is presented [64]. The seed allows attachment of smaller DNA tiles in a programmable manner enabling the creation of complex DNA-based crystals. This is not computation per se. However, it represents a perspective on DNA and DNA-based structures as pieces of information fitting in computational algorithms. Furthermore, the self-assembly method implies a long-range order beyond the direct molecular recognition. It also enables, using different techniques, the generation of complex patterns [67, 68]. One example where the computational function have been more direct is DNA-based logic circuits. There are a number of examples of groups who have constructed logic circuits of varying complexity, but all relying on advanced DNA structure designs [57, 69, 70]. Using toehold-based assemblies, Qian and Winfree [65] created a series of DNA-based logic circuits using fluorescence as a reporter function. Toehold designs are well suited for computational applications because they enable the creation of selection-functions with high simplicity and low number of incorporated DNA strands. In the center of the design is a simple "seesaw" gate-motif. Seesawing is an assemblage of reversible strand displacement reactions that exchanges the activity of DNA functions. The design features an input strand, output and threshold duplexes, both with single-stranded overhangs and a fuel strand (Fig. 3.10). These gate motifs can be combined with each other to create more complex operations including a four-bit square root circuit and even an artificial neural network model [66].

3.1.4 Challenges for DNA Nanotechnology

In a recent review published in *Nature Nanotechnology*, Pinheiro et al. [71] call for shift to a more function-oriented focus of the field of DNA nanotechnology. In the paper they conclude that since the advent of DNA-nanotechnology, from the first proposals approximately 30 years ago to today, there have been a tremendous

growth in both structure variety and complexity. However, a number of challenges are associated with future development of the field. For one, how much more complex can the structures become? Pinheiro et al. writes [71]:

> It is instructive to note that the number of transistors per integrated circuit has doubled every two years for the past four decades—roughly a one-million-fold increase between 1971 and 2011. Such an increase in complexity underlies the difference between a modern-day smart phone and a simple pocket calculator: a comparable example from biology would be the difference between a cell and an individual macromolecular complex (for example, a ribosome). (p. 765)

For a similar development in DNA nanotechnology to occur, a number of challenges must be overcome. The large structure size that would be needed creates a demand for new assembly strategies, combining many smaller structures into a larger whole. Further, there is a distinctive lack of quality control measures in many of today's designs (see the discussion regarding structure yields in Lundberg et al. [34]). In order for more complex, combination designs to be successful, there has to be methods in place to ensure that defect-free assemblies can be produced with high yields. There is also a price issue; for DNA structures with even more complex designs to be reasonable affordable, the price of DNA synthesis has to be substantially lower.

Another challenge lies in the combination of complex structures and actual functions. What type of functionalities can be introduced in DNA-based devices? How do these devices interact with larger scale technology? These questions are at the core of what I want to address in this thesis, both when it comes to novel DNA-based photonic devices and surface incorporation of DNA.

References

1. Watson JD, Crick FHC (1953) Molecular structure of nucleic acids—a structure for deoxyribose nucleic acid. Nature 171:737–738
2. Watson JD, Crick FHC (1953) Genetical implications of the structure of deoxyribonucleic acid. Nature 171:964–967
3. Seeman NC (2003) DNA in a material world. Nature 421:427–431
4. Seeman NC (2010) Structural DNA nanotechnology: growing along with nano letters. Nano Lett 10:1971–1978
5. Church GM, Gao Y, Kosuri S (2012) Next-generation digital information storage in DNA. Science 337:1628
6. Seeman NC (1982) Nucleic-acid junctions and lattices. J Theor Biol 99:237–247
7. Kallenbach NR, Ma RI, Seeman NC (1983) An immobile nucleic-acid junction constructed from oligonucleotides. Nature 305:829–831
8. Holliday R (1964) Mechanism for gene conversion in fungi. Genet Res 5:282
9. Fu TJ, Seeman NC (1993) DNA double-crossover molecules. Biochemistry 32:3211–3220
10. LaBean TH, Yan H, Kopatsch J, Liu FR, Winfree E, Reif JH, Seeman NC (2000) Construction, analysis, ligation, and self-assembly of DNA triple crossover complexes. J Am Chem Soc 122:1848–1860
11. Shen ZY, Yan H, Wang T, Seeman NC (2004) Paranemic crossover DNA: a generalized holliday structure with applications in nanotechnology. J Am Chem Soc 126:1666–1674

12. Winfree E, Liu FR, Wenzler LA, Seeman NC (1998) Design and self-assembly of two-dimensional DNA crystals. Nature 394:539–544
13. Yan H, Park SH, Finkelstein G, Reif JH, LaBean TH (2003) DNA-templated self-assembly of protein arrays and highly conductive nanowires. Science 301:1882–1884
14. He Y, Chen Y, Liu HP, Ribbe AE, Mao CD (2005) Self-assembly of hexagonal DNA two-dimensional (2d) arrays. J Am Chem Soc 127:12202–12203
15. Liu D, Wang MS, Deng ZX, Walulu R, Mao CD (2004) Tensegrity: construction of rigid DNA triangles with flexible four-arm DNA junctions. J Am Chem Soc 126:2324–2325
16. Zheng J, Birktoft JJ, Chen Y, Wang T, Sha R, Constantinou PE, Ginell SL, Mao C, Seeman NC (2009) From molecular to macroscopic via the rational design of a self-assembled 3d DNA crystal. Nature 461:74–77
17. Liu D, Park SH, Reif JH, LaBean TH (2004) DNA nanotubes self-assembled from triple-crossover tiles as templates for conductive nanowires. Proc Natl Acad Sci USA 101:717–722
18. Rothemund PW, Ekani-Nkodo A, Papadakis N, Kumar A, Fygenson DK, Winfree E (2004) Design and characterization of programmable DNA nanotubes. J Am Chem Soc 126:16344–16352
19. Mitchell JC, Harris JR, Malo J, Bath J, Turberfield AJ (2004) Self-assembly of chiral DNA nanotubes. J Am Chem Soc 126:16342–16343
20. Mathieu F, Liao SP, Kopatscht J, Wang T, Mao CD, Seeman NC (2005) Six-helix bundles designed from DNA. Nano Lett 5:661–665
21. Wang R, Liu W, Seeman NC (2009) Prototyping nanorod control: A DNA double helix sheathed within a DNA six-helix bundle. Chem Biol 16:862–867
22. Zhang YW, Seeman NC (1994) Construction of a DNA-truncated octahedron. J Am Chem Soc 116:1661–1669
23. Goodman RP, Berry RM, Turberfield AJ (2004) The single-step synthesis of a DNA tetrahedron. Chem Comm 12:1372–1373
24. Goodman RP, Schaap IAT, Tardin CF, Erben CM, Berry RM, Schmidt CF, Turberfield AJ (2005) Rapid chiral assembly of rigid DNA building blocks for molecular nanofabrication. Science 310:1661–1665
25. Goodman RP, Heilemann M, Doose S, Erben CM, Kapanidis AN, Turberfield AJ (2008) Reconfigurable, braced, three-dimensional DNA nanostructures. Nat Nanotechnol 3:93–96
26. Erben CM, Goodman RP, Turberfield AJ (2007) A self-assembled DNA bipyramid. J Am Chem Soc 129:6992–6993
27. Shih WM, Quispe JD, Joyce GF (2004) A 1.7-kilobase single-stranded DNA that folds into a nanoscale octahedron. Nature 427:618–621
28. He Y, Ye T, Su M, Zhang C, Ribbe AE, Jiang W, Mao CD (2008) Hierarchical self-assembly of DNA into symmetric supramolecular polyhedra. Nature 452:198–202
29. Zhang C, Su M, He Y, Zhao X, Fang PA, Ribbe AE, Jiang W, Mao CD (2008) Conformational flexibility facilitates self-assembly of complex DNA nanostructures. Proc Natl Acad Sci USA 105:10665–10669
30. Tumpane J, Sandin P, Kumar R, Powers VEC, Lundberg EP, Gale N, Baglioni P, Lehn JM, Albinsson B, Lincoln P, Wilhelmsson LM, Brown T, Nordén B (2007) Addressable high-information-density DNA nanostructures. Chem Phys Lett 440:125–129
31. Lundberg EP, El-Sagheer AH, Kocalka P, Wilhelmsson LM, Brown T, Norden B (2010) A new fixation strategy for addressable nano-network building blocks. Chem Commun 46:3714–3716
32. Hannestad JK, Gerrard SR, Brown T, Albinsson B (2011) Self-assembled DNA-based fluorescence waveguide with selectable output. Small 7:3178–3185
33. Tumpane J, Kumar R, Lundberg EP, Sandin P, Gale N, Nandhakumar IS, Albinsson B, Lincoln P, Wilhelmsson LM, Brown T, Nordén B (2007) Triplex addressability as a basis for functional DNA nanostructures. Nano Lett 7:3832–3839
34. Lundberg EP, Plesa C, Wilhelmsson LM, Lincoln P, Brown T, Nordén B (2011) Nanofabrication yields. Hybridization and click-fixation of polycyclic DNA nanoassemblies. ACS Nano 5:7565–7575

35. Özhalıcı-Ünal H, Armitage BA (2009) Fluorescent DNA nanotags based on a self-assembled DNA tetrahedron. ACS Nano 3:425–433
36. Mastroianni AJ, Claridge SA, Alivisatos AP (2009) Pyramidal and chiral groupings of gold nanocrystals assembled using DNA scaffolds. J Am Chem Soc 131:8455–8459
37. Rothemund PWK (2006) Folding DNA to create nanoscale shapes and patterns. Nature 440:297–302
38. Andersen ES, Dong M, Nielsen MM, Jahn K, Lind-Thomsen A, Mamdouh W, Gothelf KV, Besenbacher F, Kjems J (2008) dna origami design of dolphin-shaped structures with flexible tails. ACS Nano 2:1213–1218
39. Douglas SM, Dietz H, Liedl T, Hogberg B, Graf F, Shih WM (2009) Self-assembly of DNA into nanoscale three-dimensional shapes. Nature 459:414–418
40. Voigt NV, Torring T, Rotaru A, Jacobsen MF, Ravnsbaek JB, Subramani R, Mamdouh W, Kjems J, Mokhir A, Besenbacher F, Gothelf KV (2010) Single-molecule chemical reactions on DNA origami. Nat Nanotechnol 5:200–203
41. Jungmann R, Steinhauer C, Scheible M, Kuzyk A, Tinnefeld P, Simmel FC (2010) Single-molecule kinetics and super-resolution microscopy by fluorescence imaging of transient binding on DNA origami. Nano Lett 10:4756–4761
42. Andersen ES, Dong M, Nielsen MM, Jahn K, Subramani R, Mamdouh W, Golas MM, Sander B, Stark H, Oliveira CLP, Pedersen JS, Birkedal V, Besenbacher F, Gothelf KV, Kjems J (2009) Self-assembly of a nanoscale DNA box with a controllable lid. Nature 459:73–76
43. Douglas SM, Bachelet I, Church GM (2012) A logic-gated nanorobot for targeted transport of molecular payloads. Science 335:831–834
44. Kuzyk A, Schreiber R, Fan ZY, Pardatscher G, Roller EM, Hogele A, Simmel FC, Govorov AO, Liedl T (2012) DNA-based self-assembly of chiral plasmonic nanostructures with tailored optical response. Nature 483:311–314
45. Kershner RJ, Bozano LD, Micheel CM, Hung AM, Fornof AR, Cha JN, Rettner CT, Bersani M, Frommer J, Rothemund PWK, Wallraff GM (2009) Placement and orientation of individual DNA shapes on lithographically patterned surfaces. Nat Nanotechnol 4:557–561
46. Mao CD, Sun WQ, Shen ZY, Seeman NC (1999) A nanomechanical device based on the B–Z transition of DNA. Nature 397:144–146
47. Davis JT (2004) G-quartets 40 Years later: from 5 '-Gmp to molecular biology and supramolecular chemistry. Angew Chem Int Ed 43:668–698
48. Gehring K, Leroy JL, Gueron M (1993) A tetrameric DNA-structure with protonated cytosine–cytosine base-pairs. Nature 363:561–565
49. Liedl T, Simmel FC (2005) Switching the cConformation of a DNA molecule with a chemical oscillator. Nano Lett 5:1894–1898
50. Liedl T, Olapinski M, Simmel FC (2006) A surface-bound DNA switch driven by a chemical oscillator. Angew Chem Int Ed 45:5007–5010
51. Yurke B, Turberfield AJ, Mills AP, Simmel FC, Neumann JL (2000) A DNA-fuelled molecular machine made of DNA. Nature 406:605–608
52. Yan H, Zhang XP, Shen ZY, Seeman NC (2002) A robust DNA mechanical device controlled by hybridization topology. Nature 415:62–65
53. Ding B, Seeman NC (2006) Operation of a DNA robot arm inserted into a 2d DNA crystalline substrate. Science 314:1583–1585
54. Sherman WB, Seeman NC (2004) A precisely controlled DNA biped walking device. Nano Lett 4:1203–1207
55. Yin P, Yan H, Daniell XG, Turberfield AJ, Reif JH (2004) A unidirectional DNA walker that moves autonomously along a track. Angew Chem Int Ed 43:4906–4911
56. Omabegho T, Sha R, Seeman NC (2009) A bipedal DNA brownian motor with coordinated legs. Science 324:67–71
57. Yin P, Choi HMT, Calvert CR, Pierce NA (2008) Programming biomolecular self-assembly pathways. Nature 451:318–322
58. Pei R, Taylor SK, Stefanovic D, Rudchenko S, Mitchell TE, Stojanovic MN (2006) Behavior of polycatalytic assemblies in a substrate-displaying matrix. J Am Chem Soc 128:12693–12699

59. Lund K, Manzo AJ, Dabby N, Michelotti N, Johnson-Buck A, Nangreave J, Taylor S, Pei R, Stojanovic MN, Walter NG, Winfree E, Yan H (2010) Molecular robots guided by prescriptive landscapes. Nature 465:206–210
60. Wickham SFJ, Bath J, Katsuda Y, Endo M, Hidaka K, Sugiyama H, Turberfield AJ (2012) A DNA-based molecular motor that can navigate a network of tracks. Nat Nanotechnol 7:169–173
61. Li XY, Liu DR (2004) DNA-templated organic synthesis: nature's strategy for controlling chemical reactivity applied to synthetic molecules. Angew Chem Int Ed 43:4848–4870
62. Gu HZ, Chao J, Xiao SJ, Seeman NC (2010) A proximity-based programmable dna nanoscale assembly line. Nature 465:202–206
63. Adleman LM (1994) Molecular computation of solutions to combinatorial problems. Science 266:1021–1024
64. Barish RD, Schulman R, Rothemund PWK, Winfree E (2009) An information-bearing seed for nucleating algorithmic self-assembly. Proc Natl Acad Sci USA 106:6054–6059
65. Qian L, Winfree E (2011) Scaling up digital circuit computation with DNA strand displacement cascades. Science 332:1196–1201
66. Qian L, Winfree E, Bruck J (2011) Neural network computation with DNA strand displacement cascades. Nature 475:368–372
67. Turing AM (1937) On computable numbers, with an application to the entscheidungsproblem. Proc London Math Soc 42:230–265
68. Wang H (1961) Proving theorems by pattern recognition. Bell Syst Tech J 40:1–40
69. Seelig G, Soloveichik D, Zhang DY, Winfree E (2006) Enzyme-free nucleic acid logic circuits. Science 314:1585–1588
70. Zhang DY, Turberfield AJ, Yurke B, Winfree E (2007) Engineering entropy-driven reactions and networks catalyzed by DNA. Science 318:1121–1125
71. Pinheiro AV, Han D, Shih WM, Yan H (2011) Challenges and opportunities for structural DNA nanotechnology. Nat Nanotechnol 6:763–772

Chapter 4
Photophysics

Photophysics is the physics of light, especially in dealing with its interaction with matter. In order to describe this interaction, light has to be treated both as a wave and as a particle. The wave nature of light, described as electromagnetic radiation, consists of two components, one electric and one magnetic. These two components form two separate waves of perpendicular orientation. However, light energy is not continuous. Instead, it comes in discrete energy packages, photons, behaving as particles. The energy of a photon is proportional to the frequency of the electromagnetic wave according to Eq. 4.1.

$$E = hv \tag{4.1}$$

In this expression, E is the photon energy, v is the frequency of the electromagnetic wave and h is Planck's constant. Since light has an electrical component and molecules consist of charged particles, it is not surprising that light interacts with matter. When a molecule interacts with a photon, this results in a perturbation of the electric field of the molecule. However, in order for the interaction to occur, the energy difference between the initial state (1) and the final state (2) of the molecule must correspond to the energy of the photon. This requirement is called the Bohr frequency condition and is expressed in Eq. 4.2.

$$\Delta E = E_2 - E_1 = hv \tag{4.2}$$

4.1 Excited State Processes

When a molecule absorbs a photon, it moves from the ground state to an electronically excited state. Between the electronic states there are also a large number of closely spaced vibrational states. Figure 4.1 shows a Jabłonski diagram outlining the different electronic and vibrational states of a generalized molecule, as well as the different pathways between them. Following absorption the molecule is usually put in one of the upper vibronic levels of the same multiplicity, i.e. the same number of unpaired electrons, as the ground state. For most molecules this is the

J. Hannestad, *Fluorescence in Bio-inspired Nanotechnology*, Springer Theses,
DOI: 10.1007/978-3-319-01068-7_4,

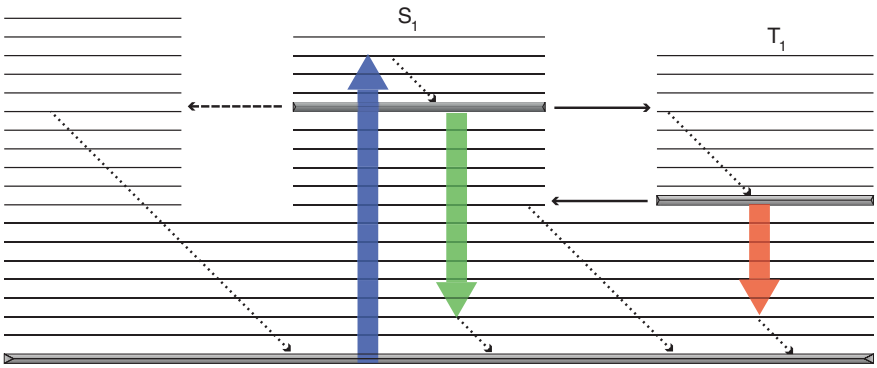

Fig. 4.1 Jablonski diagram describing different photophysical processes. *Colored arrows* represent the radiative transitions absorption (*blue*), fluorescence (*green*) and phosphorescence (*red*). *Dotted arrows* represent vibrational relaxation, *dashed* internal conversion and the filled line is inter-system crossing

singlet state, i.e. the electron spins are paired. This is followed by rapid relaxation to the lowest vibrational level of the first excited state, S_1. Here, there are several possible fates for the molecule. Molecules can decay to the ground state non-radiatively through internal conversion to excited vibrational levels of the ground state. From here, vibrational relaxation back to the ground state is fast. Another pathway is through inter-system crossing to an excited triplet state (T_1). The triplet state is generally lower in energy than the singlet state which means that the electron is first transferred to an excited vibrational state before it relaxes to the T_1 state. The inter-system crossing changes the multiplicity of the molecule and involves a quantum-mechanically forbidden spin flip. That a process is forbidden does not mean that is does not occur. Rather, the associated probability is low, resulting in a low rate for the process. Apart from the non-radiative decay processes the molecule can also decay to the ground state with the emission of a photon. Emission from the S_1 state is called fluorescence and emission from T_1 is called phosphorescence. Since phosphorescence involves a transition between triplet and singlet states, it requires a change in spin. Phosphorescence therefore occurs at a lower rate than fluorescence. For most molecules, emission occurs from a state that is lower in energy than the absorbing state. Therefore, emission from a molecule is observed at longer wavelengths than absorption. This spectral difference between absorption band and emission band is called Stokes shift. Since non-radiative decay is often faster than radiative decay, molecules are in general non-emissive.

Every deactivation process is associated with a specific rate constant, k_i. Processes with a high rate constant will dominate over those with a low rate constant. The quantum yield for a certain deactivation pathway is given by the rate constant for that process over all other rate constants for processes originating in the excited state.

$$\phi_i = \frac{k_i}{\sum_j k_j} \tag{4.3}$$

The lifetime of a certain state is given by the inverse of the sum of the decay rates from that state. In the case of fluorescence, the rate constant can be described by the fluorescence quantum yield and the fluorescence lifetime, τ_f.

$$k_i = \frac{\phi_i}{\tau_f} \tag{4.4}$$

The fluorescence lifetime is useful to describe the fluorescence intensity decay of an ensemble of molecules over time,

$$I(t) = I_0 \exp\left(-t/\tau_f\right) \tag{4.5}$$

where I_0 is the intensity at $t = 0$. Equation 4.5 describes the fluorescence decay for one emitting species. For an ensemble of emitting species the expression becomes a sum of exponentials. Experimental observations of fluorescence decays are further discussed in the section covering time correlated single photon counting (Sect. 7.2.2)

4.2 FRET Fundamentals

Apart from being deactivated through vibrational relaxation, excited molecules can also return to the ground state through the interaction with other proximal molecules. Such processes are called quenching. There are several different mechanisms behind fluorescence quenching including excited state reactions, electron transfer and molecular rearrangement. The result is an introduction of an additional decay rate, k_Q, resulting in a shorter fluorescence lifetime. Fluorescence resonance energy transfer (FRET) is one type of quenching that involves the transfer of excitation energy from the quenched molecule (the donor) to the quenching molecule (the acceptor). Here, a brief overview of FRET fundamentals is provided. A more extensive coverage is provided by e.g. Joseph R. Lakowicz in "Principles of Fluorescence Spectroscopy" [1]. An important difference between resonance energy transfer and ordinary quenching is that FRET is a through-space phenomenon. Fluorescence resonance energy transfer occurs through a dipole–dipole interaction between the two molecules and does not, in spite of its name, involve transfer of photons. Because of this fluorescence is often exchanged to Förster in the abbreviation FRE0T—this after Theodor Förster who discovered the effect [2]. As for all other photophysical and photochemical processes, there is a rate constant associated with FRET. Resonance energy transfer competes with all the other deactivation pathways and the rate constant, k_T, determines the transfer efficiency.

$$k_T(r) = \frac{1}{\tau_D}\left(\frac{R_0}{r}\right)^6 \tag{4.6}$$

In this expression, τ_D is the fluorescence lifetime of the unquenched donor and r is the donor–acceptor distance. Because of the inverse sixth-power distance dependence, FRET is a very useful tool to study interaction dynamics in the supramolecular regime. The term denoted R_0 is the Förster distance which is the distance where half the donors decay through energy transfer and half by all other radiative and non-radiative processes. We can express the energy transfer efficiency by dividing the rate constant k_T with the sum of all rates according to Eq. 4.7.

$$E = \frac{k_T}{k_T + \tau_D^{-1}} \tag{4.7}$$

We see that when the half the molecules in a population undergo excitation energy transfer, i.e. when $k_T = t_D^{-1}$, the energy transfer efficiency is 50 %. Thus R_0 correspond to the donor–acceptor distance where energy transfer efficiency is 50 %. Combining Eqs. 4.6 and 4.7 we can express the energy transfer efficiency as Eq. 4.8.

$$E = \frac{R_0^6}{R_0^6 + r^6} \tag{4.8}$$

The Förster distance can be calculated from the donor and acceptor properties according to Eq. 4.9.

$$R^6 = \frac{9000\,(\ln 10)\,\kappa^2 \phi_D}{128\pi^5 N n^4} \int F_D\,(\lambda)\,\varepsilon_A\,(\lambda)\,\lambda^4 d\lambda \tag{4.9}$$

In this expression, ϕ_D is the fluorescence quantum yield of the donor, n the refractive index of the medium and N is Avogadro's number. The integral describes the spectral overlap between the normalized donor emission (F_D) and the acceptor molar absorption (ε_A) and finally κ^2 describes the orientation of the donor and acceptor transition dipoles in relation to each other.

The orientation factor κ^2 can be described through a number of geometrical parameters

$$\kappa^2 = (\cos\theta_T - 3\cos\theta_D \cos_A)^2 \tag{4.10a}$$

$$\kappa^2 = (\sin\theta_D \sin\theta_A \cos\phi - 2\cos\theta_D \cos\theta_A)^2 \tag{4.10b}$$

In these two equations θ_T is the angle between the donor emission and acceptor absorption transition dipoles, θ_D and θ_A are the angles between the dipoles and the vector joining them, and ϕ is the angle between the planes. A graphic explanation of these terms is given in Fig. 4.2. From the equation it can be seen that the orientation resulting in maximum energy transfer is when the two transition dipoles are oriented colinear. Here, κ^2 is 4. A parallel orientation yields a κ^2 of 1 while perpendicular transition dipoles makes energy transfer impossible ($\kappa^2 = 0$). If the orientation of the donor and acceptor are not known κ^2 is usually assumed to be

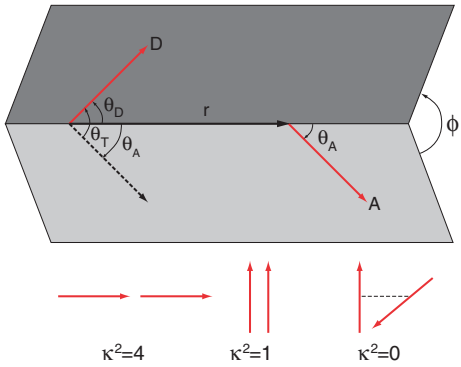

Fig. 4.2 The orientational factor κ^2 varies between 4 for a head-to-tail orientation to 0 for a perpendicular orientation of the donor and acceptor. Figure adapted from Lakowicz [1]

2/3. This is the averaged value over all possible directions and represents freely rotating chromophores.

When a fluorescence resonance energy transfer experiment is performed, the most common parameter to monitor is the quenching of the donor fluorescence. The fluorescence intensity or lifetime is measured at a wavelength where there is only donor emission. By measuring both in absence and presence of acceptor a transfer efficiency can be determined according to Eq. 4.11.

$$E = 1 - \frac{F_{DA}}{F_D} = 1 - \frac{\tau_{DA}}{\tau_D} \tag{4.11}$$

Here, F_{DA} and F_D are the fluorescence intensities in the presence and absence of acceptor, respectively. In the same way τ_{DA} and τ_D are the fluorescence lifetimes in presence and absence of the acceptor, respectively. Knowing the Förster distance an intermolecular distance can be determined. When measuring donor quenching as a measure for donor–acceptor distance it is important to have complete labeling of the studied system (e.g. a macromolecule such as protein or DNA) with the acceptor. If the labeling is incomplete the result will be an apparent lower efficiency which results in an overestimation of the inter-chromophore distance. It is also possible to determine energy transfer efficiency by measuring sensitized acceptor fluorescence. One way to do this is to compare the number of photons absorbed by the donor with the number of photons emitted by the acceptor. This method is e.g. used to estimate system efficiency in paper I and II.

4.3 Multi-Step FRET

FRET is not only possible between a single donor and a single acceptor chromophore. Rather, the one-step FRET process should be considered as an idealized case of multi-chromophoric FRET. Conveniently, multi-chromophoric FRET more or less follows the same principles as common one-step FRET. In a way, it can be treated as two (or more) separate FRET processes having (at least) one

chromophore in common, acting as both donor and acceptor. However, how to actually describe multi-step FRET will be dictated by the choice of fluorophores. It is handy to speak of two different regimes: hetero-FRET and homo-FRET. Hetero-FRET can be treated as ordinary two-chromophoric FRET and is the form that is most commonly used. Homo-FRET, on the other hand, is based on energy transfer between identical fluorophore units with sufficiently small Stokes shift. Since the energy transfer occurs between identical molecules there is no directionality in a homo-FRET system. Furthermore it is not possible to selectively excite individual fluorophores in the pure homo-FRET system. Figure 4.3 shows a schematic energy level diagram and illustrates the key difference between hetero-FRET and homo-FRET. It is important to note that the figure shows one possible energy pathway for each case. In a multi-chromophoric FRET system, multiple energy transfer as well as other de-excitation pathways are always present.

4.3.1 Hetero-FRET

In a multi-chromophoric hetero-FRET system consisting of fluorophores A, B and C, the fluorescence band of fluorophore A overlaps with the absorption band of B, whose fluorescence band, in turn, overlaps with the absorption band of C. This facilitates the transfer of excitation energy from A, via B, and further on to C in a cascade of decreasing excitation energy. This cascade can be further extended by adding more fluorophores with absorption and fluorescence of lower energy than C. The limitation is instead practical; with a large number of donor–acceptor pairs the electromagnetic spectrum becomes more and more crammed. In addition, when the spectral difference between fluorophores is small it becomes increasingly difficult to avoid crosstalk in the system. Because of this, in multi-chromophoric FRET, it is not only important to minimize direct excitation of the acceptor,

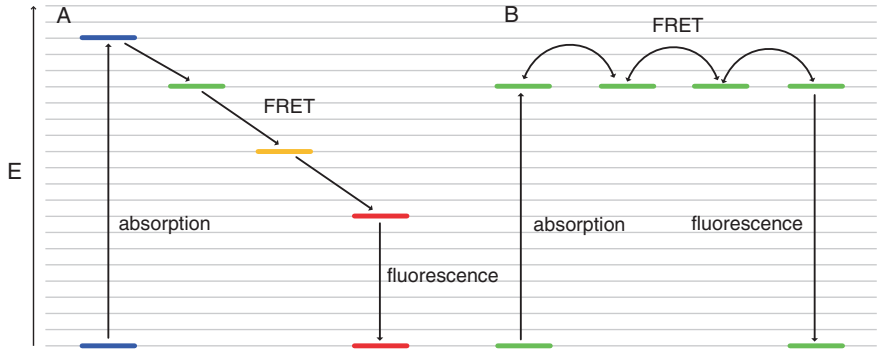

Fig. 4.3 Schematic energy level diagram showing examples of multi-step hetero-FRET (**a**) and homo-FRET (**b**). *Arrows* indicate one of many potential energy pathways from the initial absorption at a donor fluorophore to the emission from the final acceptor

it is also important to consider energy transfer pathways other than the one going through all the steps. In the simple three-chromophoric FRET (A-B–C), the cases that need consideration are A to C transfer, direct excitation of B (with subsequent transfer to C) and direct excitation of C (Fig. 4.4).

The crosstalk present in multi-chromophoric FRET can be utilized to gain information on the spatial organization of the fluorophores in the studied system. Consider the set of fluorophores A, B and C, where FRET is possible between A and C both as A–B–C, but also directly as A–C. Thus the resulting output from the system following excitation of A will depend on three separate distances; A–B, B–C and A–C.

By combining these different distances it is possible to obtain an estimate of the chromophore positions in three dimensions. A detailed description on how to design two-step FRET measurements was provided by Barkley and co-workers [3]. In this model the integrated excited state lifetimes of the three fluorophores, following excitation of the initial donor, can be described as a function of the energy transfer processes in the system according to Eq. 4.12a, b,

$$I_A = {}^{1}/_{(k_A + k_{AB} + k_{AC})} \tag{4.12a}$$

$$I_B = [k_{AB}/\,(k_A + k_{AB} + k_{AC})]\,.\,[1/\,(k_B + k_{BC})] \tag{4.12b}$$

$$I_C = \left[\left(\frac{k_{AB}}{k_A + k_{AB} + k_{AC}}\right)\left(\frac{k_{BC}}{k_B + k_{BC}}\right) + \frac{k_{AC}}{k_A + k_{AB} + k_{AC}}\right]\left(\frac{1}{k_C}\right) \tag{4.12c}$$

where I_i, k_i and k_{ij} denote the integrated excited state lifetime in presence of FRET, the sum of radiative and non-radiative decay from fluorophore i, and energy

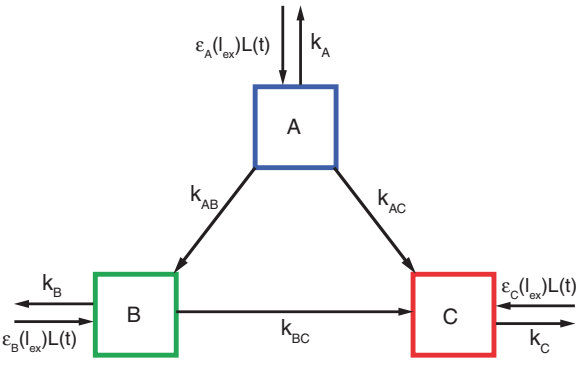

Fig. 4.4 Excitation energy pathways in a three-chromophoric FRET cascade going from A, through B, to C. Radiative and non-radiative decay from any fluorophore i is represented by k_i and energy transfer between fluorophores i and j by k_{ij}. Direct excitation of fluorophore i is denoted by $\varepsilon_i(\lambda_{ex})L(t)$. Adapted from Watrob et al. [3]

transfer between i and j, respectively (where i and j can be either A, B or C). To determine the different energy transfer rates, corresponding to different donor acceptor distances, multiple intensity measurements are needed. The quenching efficiency for fluorophore A depends on energy transfer to both B and C, as stated in Eq. 4.13,

$$E_{A,tot} = E_{AB} + E_{AC} = 1 - I_A/\tau_A \tag{4.13}$$

where τ_A is the excited state lifetime of A in the absence of FRET. In order to determine the individual energy transfer efficiencies it is possible to measure the sensitized emission of B in the presence of energy transfer to C (Eq. 4.14),

$$E'_{AB} = I_B/\tau'_B \tag{4.14}$$

where I_B is the fluorescence lifetime as described in Eq. 4.12b and τ'_B is the fluorescence lifetime of B in presence of the acceptor C. Finally, the sensitized emission from fluorophore C can be described as a function of energy transfer in both one and two steps.

$$E_{tot} = I_C/\tau_C = E'_{AB} \times E_{BC} + E'_{AC} \tag{4.15}$$

In Eq. 4.15 E_{tot} denotes the total energy transfer to fluorophore C, both through the two-step process (A–B–C) and directly from A to C. Combining Eqs. 4.13–4.15 it is possible to extract all inter-chromophoric distances by measuring the quenching of donor A, the sensitized emission of B as well as the sensitized emission of C. However, care must be taken to correct for direct excitation of both fluorophores B and C at the wavelength employed to excite fluorophore A. Additionally, the same limitations that apply to ordinary FRET are of course also valid when determining distances with multistep FRET. The measured donor quenching is an average value and the actual donor separation relies on the dynamics of the studied system. In addition, the linking of the fluorophores to the studied system has to be considered in the same way as for one-step FRET. The ideal case is when the fluorophores are all rigid parts of the studied molecule. However, in many cases, especially when dealing with fluorescently labeled biomolecules, fluorophores are attached by flexible linkers reducing the precision of distance measurements from FRET.

Aside from the conventional methods to detect multi-chromophoric FRET using bulk steady-state or time resolved fluoresce techniques, the vast development of single molecule fluorescence spectroscopy has led to many new ways of measuring excitation energy transfer [4]. In order to fully investigate a multi-chromophoric energy transfer system, all constituting FRET pairs need to be probed. One of the strengths inherent in single-molecule techniques is the capacity to probe individual molecular assemblies one at a time. This makes estimation of the distribution of different parameters, e.g. intermolecular distance, possible. For a multi-FRET system, this means that all the donor–acceptor pairs have to be probed for every investigated assembly. One way this has been realized is through the technique alternating-laser excitation (ALEX). The term ALEX was coined by

Weiss and co-worker and describes a technique based on single molecule fluorescence microscopy that relies on the combination of multiple, spectrally distinct, detection channels with a switching between multiple excitation wavelengths [5]. For a two-color FRET experiment, emission from all constituting fluorophores is detected simultaneously at the same time as the excitation is varied between donor only and donor and acceptor excitation. The strength in this approach is that it is possible to distinguish between cases where low FRET efficiency is due to large donor acceptor distance and those due to incomplete labeling resulting in donor-only assemblies.

Following the initial development of the ALEX technique its use has been extended to include more than a single pair of donor and acceptor. This requires that the experimental setup has the capability to switch the excitation wavelength between all the used fluorophores and enough detectors to be able to differentiate emissions from the different donors from each other. Using ALEX in a multi-chromophoric FRET system it is possible to probe all the inter-chromophoric distances simultaneously [6]. Additionally, the multi-color ALEX approach allows determination of labeling stoichiometry as well as dissection of ensemble heterogeneities.

However, as more fluorophores are added, great care must be taken to carefully select excitation and emission bandwidths to reduce effects from crosstalk. This crosstalk involves leakage of emission into the detection channels of other fluorophores, direct excitation of acceptors and energy transfer to multiple, different, acceptors. In order to accurately characterize the studied system, the extent of this crosstalk needs to be determined and compensated for. With an increasing number of FRET pairs this correction becomes both more important and experimentally complicated.

4.3.2 Homo-FRET

In contrast to the cascade in the hetero-FRET case, energy transfer following homo-FRET is not unidirectional. The name homo-FRET comes from the fact that, instead of being based on unique donors and acceptors, the process usually relies on one single molecular species. The term homo-FRET is a little bit misleading since it is not the use of identical fluorophores that is the defining criterion. Rather, the principle relies on dyes where the energy difference between the absorption and fluorescence is very small, allowing energy to go both ways. This reasoning can be extended to include more than one fluorophore species given that it fulfills the stated criterion.

In cases when the coupled fluorophores are very closely spaced, energy transfer is so efficient that it is difficult to talk about individual chromophores. Instead, the excitation can be considered to be delocalized in the entire system, as a coupled exciton. Such strong coupling generally leads to perturbed electronic states, which can manifest as altered absorption spectra.

In complex multi-chromophoric systems, energy migration can sometimes be characterized by a combination of strong, delocalized, coupling and through-space dipole–dipole coupling. Elisabetta Collini and Gregory D. Scholes studied this intermediate regime using the conjugated polymer poly[2-metoxy,5-(2′-ethyl-hexoxy)-1,4-phenylene-vinylene] (MEH-PP) [7]. Energy migration processes were studied in the polymer systems in two different conformations: one in chloroform promoting extended chain conformations, and the other in aqueous solution where individual polymer chain collapses to form nanoparticles. In the collapsed state, segments of the polymer, not directly linked to each other through covalent bonds are close together in space, compared to the extended conformations where only the neighboring segments are adjacent. Because of this, it is likely that the dense nanoparticles will display substantial through-space energy migration between non-linked segments, whereas energy migration in the extended polymer chain in chloroform will predominantly be of the coherent and strongly coupled type between adjacent segments. In order to measure the two different migratory processes two-time anisotropy decay (TTAD) experiments were performed. The anisotropy decay is recorded as a function of two time delays, τ and T. The time delay, T, is the population time, during which excited state dynamics, such as excitation energy transfer, occurs. The second time lag, τ, scans a time period when the system is in coherence between ground and excited electronic states. The experiments show that the anisotropy decays more rapidly during T for the nanoparticles, than for the extended polymer chain. This can be explained by the interchain energy transfer, made possible by the compact structure of the nanoparticles. In contrast, only the extended MEH-PPV in chloroform showed anisotropy decay during τ. Thus, in a complex system, excitation energy can migrate through several conceptually different processes due to variation in structural conformation.

Calculating the energy transfer efficiencies in a homo-FRET system is somewhat different compared to the hetero-FRET case because of the multi-directionality of the energy transfer. Figure 4.5 shows a homo-FRET system consisting of four identical fluorophores. Because all fluorophores have the same spectral properties, it is not possible to selectively excite individual fluorophores in a pure homo-FRET system.

The energy transfer scheme presented in Fig. 4.5 is not limited to the case with just four fluorophores. Equation 4.16 describes the change in excitation energy at any given fluorophore, n, in a general homo-FRET system with the total number of m fluorophores.

$$\frac{dI_n}{dt} = \varepsilon_n(\lambda_{ex})\, L(t) + \sum_{i \neq n}^{m} \left(k_{in} I_i - (k_n + k_{ni})\, I_n\right) \tag{4.16}$$

In this expression, the excitation concentration of n depends on radiative and non-radiative decay rates (k_n), excitation power ($\varepsilon_n(\lambda_{ex})L(t)$) as well as ingoing and outgoing excitation energy transfer (k_{in}, k_{ni}). As can be seen from Eq. 4.16, in a pure homo-FRET system the energy transfer has no directionality as the rate is

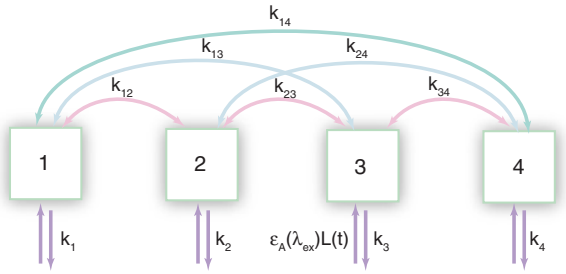

Fig. 4.5 A homo-FRET system consisting of four identical fluorophores with indicated absorption, emission and energy transfer pathways. Because of the homo- FRET conditions, all possible energy transfer pathways are bi-directional

equal in both directions between each "donor" and "acceptor". It is also not possible to investigate homo-FRET efficiencies using e.g. donor quenching since both donors and acceptors are spectroscopically identical. However, information from fluorescence anisotropy can be utilized to gain information on homo-FRET processes in multi-chromophoric systems. As FRET has a depolarizing effect on the emission, the degree of anisotropy can be used to measure the extent of energy transfer in a system, which, in turn, is related to the number of participating fluorophores within energy transfer range, and thus a measure for the compactness of the multi-chromophoric system. Kaminski, and co-workers, show in a review article how homo-FRET can be used in conjunction with fluorescence anisotropy imaging (FAIM) to study assembly and aggregation of macro- or supramolecular structures [8]. Examples where this technique has been put to use include studies on amyloid aggregation [9], lipid rafts [10–12] and protein clusters [13, 14].

One fluorophore with substantial capability for homo-FRET is the DNA binding fluorophore YO (Fig. 4.6) [15–17]. YO is virtually non-fluorescent in solution, but in the presence of DNA, the fluorescence quantum yield increases by about a thousand fold. YO has been shown to bind to DNA through intercalation between the base pairs. This is true for fluorophore/base pair ratios up to 0.2. At higher YO concentrations, other modes of binding become apparent [15]. An effort to quantify the fluorescence depolarization caused by homo-FRET in a system with non-covalent DNA binders, such as YO, PO and DAPI, was made by Albinsson and co-workers [17]. In this work, fluorescence depolarization was described by a semi-empirical Markov chain model where the degree of fluorescence depolarization was investigated as a function of the intercalator density. The depolarization caused by energy transfer is dependent on the relative orientation of the donor and acceptor emission and absorption transition dipoles, respectively. This is, in turn, determined by the relative positions of the donor and acceptor in the DNA strand (i.e. the number of base pairs separating them). For a given random distribution of intercalated YO molecules, there is a set of energy transfer and emission probabilities for each fluorophore in the system. These probabilities define the energy migration pathway and thus the fluorescence depolarization. The simulation algorithm is constructed in steps where excitation energy located at any of the

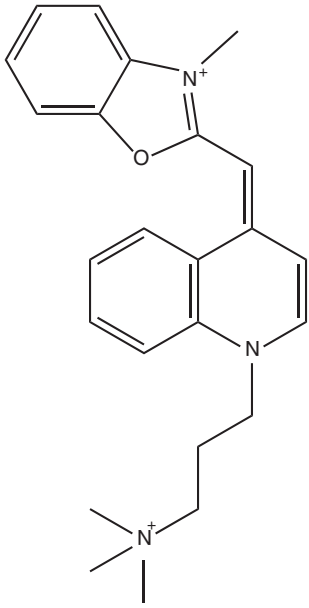

Fig. 4.6 The DNA intercalator dye YO-PRO-1

fluorophores can either be emitted or transferred to any of the other fluorophores in the system. In this way, the distribution of excitation energy at any given step, $\mathbf{v}_n$, is defined as a product of the excitation energy distribution in the previous step, $\mathbf{v}_{n-1}$, and the complete set of emission and energy transfer probabilities, $\mathbf{M}$. By repeating this recursive calculation it is possible to express the excitation energy distribution at any point as a function of the initial excitation energy distribution, $\mathbf{v_0}$, according to Eq. 4.17

$$\mathbf{v}_n = \mathbf{v}_{n-1} \cdot \mathbf{M} = \ldots = \mathbf{v}_0 \cdot \mathbf{M}^n \tag{4.17}$$

The steady state product, $\mathbf{v}_\infty$, is obtained by letting the number of steps approach infinity, as shown in Eq. 4.18.

$$\mathbf{v}_\infty = \mathbf{v}_0 \lim_{n\to\infty} \mathbf{M}^n \tag{4.18}$$

Thus, the resulting depolarization is obtained as a product of all the energy transfer steps leading up to the eventual emission of a photon, and the removal of the excitation energy from the system. As stated, the matrix $\mathbf{M}$ gathers emission and energy transfer probabilities according to Eq. 4.19.

$$\mathbf{M} = \begin{bmatrix} \mathbf{A} & \mathbf{D} \\ \mathbf{0} & \mathbf{I} \end{bmatrix} \tag{4.19}$$

In this expression $\mathbf{A}$ is a matrix with 0 diagonal and all other elements being p_{ij} corresponding the energy transfer probabilities between chromophores i and j.

D, on the other hand has elements p_i on the diagonal with all other elements being zero. This corresponds to the probability of emission when the excitation is position on chromophore *i*. By forming $\mathbf{M}^{\mathrm{n}}$ and letting n go to infinity, the expression in Eq. 4.20 is obtained.

$$\lim_{n\to\infty} \mathbf{M}^n = \begin{bmatrix} \mathbf{0} & (\mathbf{I}-\mathbf{A})^{-1}\,\mathbf{D} \\ \mathbf{0} & \mathbf{I} \end{bmatrix} \tag{4.20}$$

The simulations show an expected decrease in emission polarization with increasing dye concentration. The steepness of the decrease is dependent on the Förster radius for homo-FRET between the intercalated dyes. For systems with $R_0 = 10$ Å, there is a linear dependence of the degree of depolarization on the dye-to-base pair ratio. For FRET pairs with larger Förster radius, $R_0 \geq 29$ Å, the expected limiting depolarization value, 0.25 or $r = 0.1$, is reached around 0.2 intercalators per base pair. This model can be extended to accommodate any dye bound to any linear scaffolding molecule. However, care must be taken to accurately describe both the angle between the dye transition moment and the long axis of the scaffold molecule, as well as the relative orientation of the dyes as function of their linear separation. This model is used extensively in Papers I-III where it is used to determine energy transfer efficiencies in multi-chromophoric FRET assemblies.

References

1. Lakowicz JR (2006) Principles of fluorescence spectroscopy. Springer, New York
2. Förster T (1948) Zwischenmolekulare Energiewanderung Und Fluoreszenz. Ann Phys 2:55–75
3. Watrob HM, Pan CP, Barkley MD (2003) Two-step fret as a structural tool. J Am Chem Soc 125:7336–7343
4. Tinnefeld P, Sauer M (2005) Branching out of single-molecule fluorescence spectroscopy: challenges for chemistry and influence on biology. Angew Chem Int Ed 44:2642–2671
5. Kapanidis AN, Lee NK, Laurence TA, Doose S, Margeat E, Weiss S (2004) Fluorescence-aided molecule sorting: analysis of structure and interactions by alternating-laser excitation of single molecules. Proc Natl Acad Sci USA 101:8936–8941
6. Lee NK, Kapanidis AN, Koh HR, Korlann Y, Ho SO, Kim Y, Gassman N, Kim SK, Weiss S (2007) Three-color alternating-laser excitation of single molecules: monitoring multiple interactions and distances. Biophys J 92:303–312
7. Collini E, Scholes GD (2009) Coherent intrachain energy migration in a conjugated polymer at room temperature. Science 323:369–373
8. Chan FTS, Kaminski CF, Kaminski Schierle GS (2010) Homofret fluorescence anisotropy imaging as a tool to study molecular self-assembly in live cells. Chem Phys Chem 12:500–509
9. van Ham TJ, Esposito A, Kumita JR, Hsu STD, Kaminski Schierle GS, Kaminski CF, Dobson CM, Nollen EAA, Bertoncini CW (2010) Towards multiparametric fluorescent imaging of amyloid formation: studies of a Yfp model of [Alpha]-Synuclein aggregation. J Mol Biol 395:627–642
10. Varma R, Mayor S (1998) Gpi-anchored proteins are organized in submicron domains at the cell surface. Nature 394:798–801

11. Jacobson K, Mouritsen OG, Anderson RGW (2007) Lipid rafts: at a crossroad between cell biology and physics. Nat Cell Biol 9:7–14
12. Sharma P, Varma R, Sarasij RC, Gousset K, Krishnamoorthy G, Rao M, Mayor S (2004) Nanoscale organization of multiple GPI-anchored proteins in living cell membranes. Cell 116:577–589
13. Bader AN, Hofman EG, Henegouwen P, Gerritsen HC (2007) Imaging of protein cluster sizes by means of confocal time-gated fluorescence anisotropy microscopy. Opt Express 15:6934–6945
14. Bader AN, Hofman EG, Voortman J, van Bergen en Henegouwen PMP, Gerritsen HC (2009) Homo-fret imaging enables quantification of protein cluster sizes with subcellular resolution. Biophys J 97:2613–2622
15. Larsson A, Carlsson C, Jonsson M, Albinsson B (1994) Characterization of the binding of the fluorescent dyes Yo and Yoyo to DNA by polarized-light spectroscopy. J Am Chem Soc 116:8459–8465
16. Carlsson C, Larsson A, Jonsson M, Albinsson B, Nordén B (1994) Optical and photophysical properties of the oxazole yellow DNA probes Yo and Yoyo. J Phys Chem 98:10313–10321
17. Carlsson CLA, Björkman M, Jonsson M, Albinsson B (1997) Experimental and simulated fluorescence depolarization due to energy transfer as tools to study DNA-dye interactions. Biopolymers 41:481–494

Chapter 5
Nanoscale Photonic Devices

Photonics is a subject area dealing with the emission, transmission, modulation, processing and sensing of light signals. A photonic device is an entity, constructed with the purpose to facilitate any or all of the above processes. This definition can be made almost indefinitely broad, requiring a much wider scope than this thesis for sufficient coverage. The inclusion of nanoscale in the heading narrows things down a bit to devices that fit into the size regime of 1–100 nm. I will go even further, by restricting the discussion to assemblies based on Förster type energy transfer and whose main functionalities are to transmit and modulate excitation energy. This way, the chapter creates a logic transition to the work presented in papers 1–3. Since one-step FRET between a single donor and a single acceptor is fairly limited when it comes to designing devices where photonic processes are the main functionalities, the designs featured in this chapter will almost exclusively rely on energy transfer between multiple fluorophores in multiple steps. Since many of the devices rely on excitation energy transfer through multiple fluorophores, it is logical to start the discussion with the light-harvesting complexes of photosynthetic bacteria. These advanced self-assembled systems rely on energy transfer in multiple steps to deliver excitation energy to the bacterial reaction center and has served as inspiration for the design of many of the devices discussed in this chapter.

5.1 Natural Light-Harvesting

Photosynthetic organisms have developed an intricate set of chromophoric arrangements to gather the energy from sunlight. Here, I will exemplify this by describing how photosynthetic bacteria use a remarkable example of nanoscale engineering to feed the reaction center with excitation energy. This text should not be read as a complete review of the function of the bacterial light-harvesting complexes. Instead, I want to provide a brief overview, largely because the light-harvesting complexes have had an important role to inspire many of the nanoscale

J. Hannestad, *Fluorescence in Bio-inspired Nanotechnology*, Springer Theses,
DOI: 10.1007/978-3-319-01068-7_5, © Springer International Publishing Switzerland 2013

photonic assemblies that is presented in this thesis. This text is, to a large extent, based on the work by Klaus Schulten and co-workers [1–3].

In bacterial photosynthesis, a closely spaced pair of bactreriochlorophylls, called the special pair, is responsible for an excited state electron transfer reaction that leads to polarization of the cell membrane. Instead of letting the sunlight just excite the special pair in the reaction centre directly; photosynthetic bacteria arrange a large number of circular light harvesting complexes around the reaction center. These complexes channel the excitation energy to the reaction center in multiple steps. The pigment molecules, mostly bacteriochlorophylls, responsible for channeling the excitation energy, vastly outnumber the reaction center complexes; often the ratio is in the order of hundreds to thousands pigment molecules per reaction center.

Why do the photosynthetic bacteria organize the gathering of light energy by having a large number of light harvesting protein complexes delivering excitation energy to a small number of reaction centers (RC) instead of just having more reaction centers? There are multiple reasons for this. One is the turnover rate of the reaction center. The reaction center is capable of undergoing the electron transfer reaction at a rate of 1,000 Hz. However, the chlorophylls of the RC that feeds the reaction with energy only absorb at 10 Hz in direct sunlight and 0.1 Hz in dim light. Thus, the reaction center is not capable of functioning at maximum turnover on its own. Instead, the light harvesting complexes helps the reaction center to reach maximum turnover by feeding it with excitation energy. Another reason is that the light harvesting complexes absorb light at different wavelengths than the reaction center making it possible for the bacterium to make more use of the sunlight. Additionally, the light harvesting complexes are smaller and less complex than the reaction center and therefore require less energy from the organism's metabolic system to synthesize.

In the bacterial photosynthesis there are two different ring-shaped protein complexes responsible for directing excitation energy to the reaction center, named LH-I and LH-II (Fig. 5.1). LH-I consists of 16 identical building blocks called αβ-heterodimers arranged in a circle around the reaction center. The αβ-heterodimer is a complex that consists of one α-apoprotein, one β-apoprotein, three BChls and one carotenoid. The α-apoprotein and the β-apoprotein are both α-helices of 56 and 45 amino acids, respectively. The constituent responsible for channeling the excitation energy to the reaction center is a ring-shaped assemblage of the 48 bacteriochlorophylls. This ring, LH-I, is formed around the reaction center to which LH-I is strongly associated.

The LH-II ring is slightly smaller than LH-I, about 14 nm in diameter, and is positioned in multiple copies in between the RC-LH-I assemblies. LH-II consists of 8 ab-heterodimers, compared to the 16 of LH-I. The proteins scaffold 24 bacteriochlorophylls (BChls) and 8 carotenoids. Sixteen of the BChls form a ring-shaped aggregate known as B850. The remaining 8 BChls form a second ring which is looser, denoted B800. The eight carotenoids span the distance between the BChls, each touching 2 separate bacteriochlorophylls.

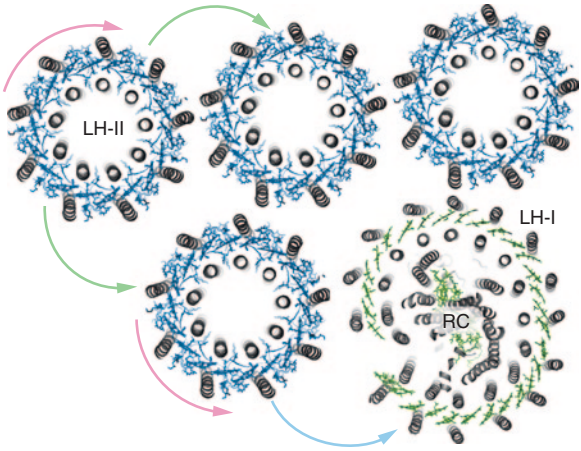

Fig. 5.1 Bacterial photosynthetic assembly comprising Light-harvesting complex I and II and the reaction center

The energy transfer cascade starts in the LH-II complexes. LH-II has the ability to absorb light at both 850 nm through the bacteriochlorophyll ring and at 800 nm though the carotenoid-associated bacteriochlorophylls. Excitation energy absorbed by the B800 BChls can be transferred to the B850 by FRET. In the B850 ring, photons are absorbed only by 2 of the 16 possible exciton states, the second and third energetically lowest. As the lowest excited state is optically forbidden, the B850 ring acts as an energy storage unit, preserving excitation energy until it can be forwarded further in the cascade toward the RC. LH-I absorbs at lower energies than LH-II (875 nm). This makes it possible to funnel excitation energy from multiple LH-II through LH-I to the RC. The photoactive component in all these assemblies is the BChl-a unit. Since the absorptivity of monomeric BChl-a peaks at 772 nm, the 800 and 850 nm absorption of the two LH-II rings as well as the 875 nm absorption of LH-I are results of the spatial organization of the fluorophores. Suggested explanations for this are excitonic interactions as well as BChl-protein interactions. The energy transfer from LH-II, via LH-I, to RC occurs within 100 ps at 95 % efficiency. Beside the high efficiency and the high rate, one remarkable feature is the number of potential pathways leading to the reaction center. One possible pathway, using excitation at 800 nm, involves 4 sequential steps. Starting with initial excitation of B800, excitation energy is transferred to the B850 ring in the same LH-II assembly. Excitation energy is then, in turn, transferred to the B850 ring of the next LH-II. This is the followed by energy transfer to LH-I, which finally transfers the excitation energy to the reaction center.

The fascinating features of the bacterial light harvesting systems show how spatial organization and precise tuning of absorption and emission properties can be used to construct systems for efficient excitation energy transfer with high spatial precision. How these principles can be applied in nanoscale devices will be discussed in the next section.

5.2 Photonic Wires

One of the most basic examples of the use of multi-step FRET in nanotechnology is the creation of so called photonic wires. This can be compared to an optical waveguide where light energy is transported linearly from one end to the other. In the case of the FRET-based photonic wires, fluorophores are arranged in a linear fashion to achieve directional energy transfer from one end of the wire to the other. Either the wire can be constructed directly out of the coupled fluorophores or, some kind of molecular scaffold can be used to arrange the fluorophores in a wire-like fashion. The perhaps most prominent example of the former category are arrays of linked porphyrin molecules [4–6]. In 1994 Lindsey and co-workers presented the first example of the concept of a molecular photonic wire, drawing inspiration from natural light harvesting complexes [4]. In this work, a supramolecular assembly consisting of a boron-dipyrromethene (BODIPY) input unit, three zinc porphyrins and a free-base porphyrin covalently connected through diarylethyne linkers was presented (Fig. 5.2). In this assembly, emission was predominately observed from the free-base porphyrin following excitation of BODIPY showing that excitation energy had been transferred along the constructed wire. The energy flow in the porphyrin-based wire was shown to be characterized by a combination of Dexter-type through bond super exchange-mediated interactions and FRET [7].

One of the simplest examples of what could be considered as a photonic wire is the perylene trimer studied by Hernando et al. which consists of three identical tetra phenoxy-perylene diimide chromophoric units covalently linked together [8]. The rigid structure of the trimers holds the chromophoric units locked in a perpendicular conformation thus preventing full extension of the conjugated p-system. This, in combination with a short inter-chromophoric distance of only 1.3 nm, results in strong exciton coupling leading to a delocalization of the excitation over the entire multichromophoric system. The strong coupling enables propagation of excitation energy in the system without the presence of a strong driving force in the form of a steep energetic gradient. With the addition of a high energy dye at one extreme of the wire and a low energy dye at the other a highly efficient end-to-end transfer could be achieved. However, because of the short inter-chromophoric distance in the perylene arrays, their usefulness as wires in nanoscale systems is fairly limited. The limited size is a drawback common to most chromophoric arrays based on covalently linked chromophores.

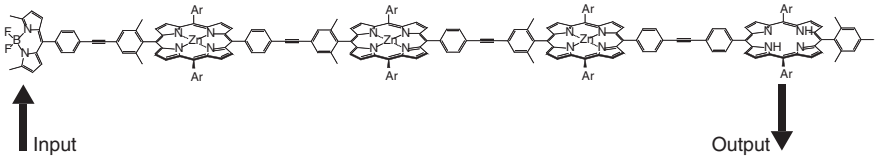

Fig. 5.2 Molecular photonic wire consisting of a BODIPY input unit, three zinc porphyrin and a free-base porphyrin. Adapted from Wagner et al. [4]

When the designed structures become larger and more complex, the required synthesis becomes increasingly difficult. To create assemblies that have potential to function as nanoscale devices, it is therefore of interest to adopt self-assembly strategies in order to organize chromophores in the form of a wire.

This brings us to the second approach to wire assembly, which is to use some kind of scaffolding molecule, e.g. DNA, for arranging the fluorophores. The fluorophores have to be selected so that there is an energetic gradient going from one end to the other. This makes it possible to excite the edge-fluorophore in the high-energy end and obtain multi-step energy transfer all the way to the other end. An early example of multi-step FRET coupled to DNA comes from the work of Turro [9]. Here, three fluorophores, 6-carboxyfluorescein (F), N,N,N′,N′-tetramethyl-6-carboxyrhodamine (R) and Cy5 (C) were coupled to a 26 bases long single-stranded DNA molecule.

This multi-chromophoric assembly is not designed to function as a wire, conveying excitation energy between two spatially separate points. Rather, the fluorophores function together to form a nanoscale dye with a "Stokes shift" of 182 nm. The quenching of the initial donor, F, is 99 % and the assembly has an overall fluorescence quantum yield of 0.13. Even before this, Uchimaru and co-workers had introduced a sequential arrangement of donor and acceptor dyes in double stranded DNA [10]. The fluorophore 6-Carboxyfluorescein (F) was coupled to a 25-mer scaffold strand. This fluorophore acts as the initial donor in a three-dye system. The other two fluorophores, 4,7,2′,4′,5′,7′-hexachloro-6-carboxyfluorescein (H) and 6-carboxy-X-rhodamine (R) are coupled to a 15-mer and a 10-mer oligonucleotide, respectively, which both bind to the 25-mer scaffold. The total end-to-end distance is approximately 80 Å, which is within the range than can be covered by single step FRET. The assembly is not labeled as a "photonic wire"; instead the intermediate step is used as an enhancer of the FRET process between the fluorophores at each end of the DNA strand. The intermediate fluorophore was shown to enhance FRET between the end dyes by 360 %. These results provide a basis for the use of DNA-based FRET over even longer distances, something that came to be referred to as molecular photonic wires or DNA-based photonic wires.

The concept of the DNA-based photonic wire was first introduced by Sauer and coworkers [11]. Here, DNA was used a scaffold for a series of fluorophores creating a photonic wire based on the cascade principle [11, 12]. In conjunction to this, it is also appropriate to mention the work by Ohya et al. [13]. Although, the term "wire" is not mentioned in the paper, the work carries many of the characteristics associated with the term. Yuichi Ohya's take on the DNA-based molecular wire is discussed more in depth later in this section.

Because of the increase in the number of high quality (high molar absorptivity and high quantum yield) fluorophores for nucleic acid labeling there are a large number of donor–acceptor combinations available that can be used in a multi-step energy transfer cascade. In the work by Sauer and co-workers a 60-mer single stranded DNA molecule is used as a template strand [11, 12, 14, 15]. To this strand, complementary 20-mer DNA strands are hybridized. The design, featuring a long scaffold strand for a number of short functionalized strands is similar to that

of Uchimaru and co-workers. The 20 base pair oligomers are labeled with fluorophores which, when all strands hybridize with the template, form a chain of energy transfer donor acceptors (Fig. 5.3). Here, the sequence specificity of the base pairing of the labeled strands with the template strand is used to assure that the fluorophores arrange in the correct order to achieve end-to-end energy transfer in the wire. The dyes are placed so that, when all strands assemble, there is a 10 base pair separation between them. The choice to use a 10 base pair separation between the fluorophores in the FRET cascade is not by chance; as 10 base pairs corresponds to one turn of the B-DNA helix all fluorophores will be positioned on the same side of the DNA duplex. This increases the potential efficiency of the wire since all excitation energy propagation is along the wire axis instead of both along and across the duplex, which would be the case if the fluorophores were positioned on opposite sides of the DNA duplex. In addition, a 3.4 nm separation (corresponding to 10 base pairs) between the fluorophores in the cascade will result in one-step FRET efficiencies of 91–98.7 % for donor acceptor-pairs with Förster distances of 50 and 70 Å, respectively. Thus, these dyes provide a potential for high overall wire efficiency. However, multiple studies on photonic wires of this type have shown lower experimental end-to-end energy transfer efficiencies than what could be expected from the Förster distances of the individual donor–acceptor pairs [14, 15]. Using the same principal design, Sauer and co-workers have created variations of the original wire by altering the fluorophore composition. In one wire, the fluorophore combination rhodamine green (RhG), tetramethylrhodamine (TMR), ATTO 590, Light Cycler Red (LCR) and ATTO 680 was used [11, 12].

In a second wire, LCR was replaced by ATTO 620 [14, 15]. In both cases, the fluorophores were placed with 10 base pairs separation, which would correspond to individual FRET efficiencies above 90 %. This should, in turn, yield overall efficiency of at least 70 %. Instead, the observed overall efficiency was on the order of 15–30 % Using single molecule measurements Sauer and co-workers revealed subpopulations of wires in which approximately 90 % of the emission was detected in the channel corresponding to the most low-energy dye. End-to-end energy migration was further studied by sequentially bleaching the wires that

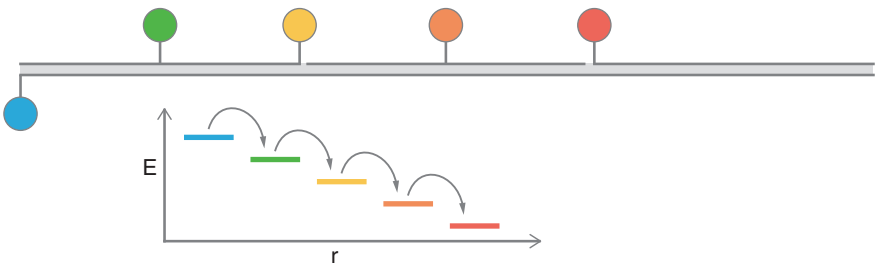

Fig. 5.3 Hetero-FRET based photonic wire consisting of five different fluorophores positioned along a 60 base pair long DNA strand. The distance from the donor to the final acceptor corresponds to 40 bp. Adapted from Heilemann et al. [11]

emitted in the red channel. These experiments showed that the terminal acceptor is bleached first, followed by the more high-energy dyes in order, with the initial donor bleaching last. The emission intensity profile also revealed that emission from the wires were, at any time, dominated by one single fluorophore, i.e. energy transfer is efficient up to the last available dye in the cascade [11].

In an effort to explain the observed heterogeneity of the photonic wires, Sauer and co-workers investigated the assembly process of the wires using single-molecule fluorescence spectroscopy [14, 15]. Although all wire components had been added to the sample there is a large fraction of the wires that showed predominant emission from one of the linking fluorophores. The prevalent explanation for this is focused on the assembly of the DNA duplex. Because of the arrangement with the different dyes covalently linked to short oligomers that bind to a longer template strand the, assembly of the wire requires not only for two single stranded DNA molecules to form a duplex, but for several of these events to occur. This, more complex, assembly procedure puts high demands on the conformational freedom of the constituting strands in the assembly process. By using a surface attachment that allows the DNA strands to reorient, the heterogeneity can be drastically reduced. Another factor that impedes the wire functionality is incomplete labeling. Since the wire requires that excitation energy passes all fluorophores between the input and output dye, loss of one or more dyes can be detrimental to the functioning of the wire.

In the photonic wire there are two principle loss terms. Firstly, the directionality implies a decrease in excitation energy by going from one end of the wire to the other. This red shift means that there is less energy to use for driving photochemical reactions at the output of the wire. Secondly, excitation energy can be lost due to photo physical processes other than FRET, e.g. emission from one of the linking dyes or internal conversion. The wire can be said to have a specific quantum yield for end-to-end transfer that depends on the number of constituting fluorophores and how they couple. These two parameters have to be balanced against each other in the design of the wire system. The red shift is minimized by limiting the number of different fluorophores in the system, since every new donor–acceptor pair leads to lower excitation energy. However, a high quantum yield is obtained by having strong coupling between the fluorophores, i.e. short donor–acceptor distances. However, short distances mean that many donor–acceptor pairs are needed to extend the wire, thus increasing the red shift. Carefully choosing the fluorophores and their relative positions can strongly influence the efficiency of the wire. For instance, it is unnecessary to place donors and acceptors closer than roughly 50 % of R_0 since that distance corresponds to an excitation energy transfer efficiency of 98 %. There is therefore very little to gain by moving the fluorophores even closer.

The red shift problem can also be tackled in another way. Instead of building the wire through an energy transfer cascade with a stepwise red-shift with every dye, the middle part of the wire can be constructed from a sequence of fluorophores capable of homo-FRET. In this mediating homo-FRET part of the wire, the energy transfer proceeds in a way that can be described by one-dimensional

statistical diffusion. If the fluorophores are separated by an equal distance there is no net driving force for energy transfer in either direction of the wire. Instead, directionality is achieved by flanking the homo-FRET dyes with a higher energy dye (injector) on one side and a lower energy dye (detector) on the other side. In this way, it is possible to direct the flow of excitation energy without the associated red-shifts of energy transfer cascades.

Already in 2003, Ohya and co-workers presented a photonic wire where homo-FRET was used to achieve end-to-end energy transfer [13]. In this work, a template oligomer (20, 30 or 40-mer) is combined with shorter, dye-labeled, 10-mer strands to generate the photonic wire. The wire consists of the three fluorophores eosin (Eo), TexasRed (TR) and tetramethylrhodamine (Rho), each covalently attached to a 10-mer DNA complementary to the longer template strand. The strands assemble in an order that creates an energy transfer cascade going from one end of the wire to the other. For the 30 and 40-mer wires, the Rho unit is present in one and two copies, respectively. When there are two Rho units present in the wire, as is the case for the 40-mer wire, part of the energy transfer is mediated through homo-FRET between the identical Rho units. Fluorescence measurements showed no energy transfer between eosin and Texas Red in the absence of tetramethylrhodamine, both for the 30-mer and for the 40-mer wires. When DNA strands with Rho attached in the 5′ end was added to the system a 23.7 and 21.6 % energy transfer efficiency was detected for the 30-mer and for the 40-mer, respectively. Ohya and co-workers use the formula presented in Eq. 5.1 to calculate the energy transfer efficiency,

$$T_{app}(\%) = A_{(X)}/A_{(100)} \times 100 = \{\varphi_D F_D/\varphi_A F_A(1-T)+T\} \times 100 \quad (5.1)$$

where T_{app} is the apparent energy transfer efficiency, $A_{(100)}$ and $A_{(x)}$ are the integrated emission and excitation spectra, respectively. The terms φ and F represent the quantum yield and fluorescence intensity, respectively, for both donor (D) and acceptor (A) fluorophores. T is the actual energy transfer efficiency. The equation is adapted from Imanishi and co-workers [16] and compensates for the spectral overlap between donor and acceptor emission. A weakness of this model is that it does not account for the fraction of the acceptor emission that is due to direct excitation of the mediator dyes rather than the original donor, something that is relevant in the case of multi-chromophoric FRET. In many systems this effect is pronounced, especially if the wire contains many mediator dyes.

Quake and co-workers present another example of a DNA-based photonic wire utilizing homo-FRET to facilitate end-to-end energy transfer. The photonic wire is built using the fluorophores 6-carboxyfluorescein (6-FAM), 6-tetramethylrhodamine 5(6)-carboxamide (TAMRA) and Cy5 [17]. In this work dyes are covalently attached to either one of the two equally long DNA strands forming the final duplex (Fig. 5.4). Note that in this case, the strategy of allowing multiple singly labeled short strands assemble into a wire is not used. Instead, equally long strands with multiple covalent modifications are used. The fluorophores are positioned with a separation of ten base pairs putting them either on the same side or the opposite side of the duplex depending on whether they attached to the same

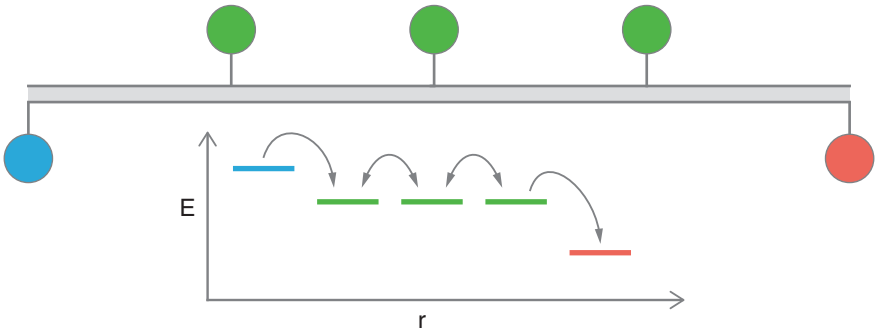

Fig. 5.4 Three-chromophoric photonic wire having a central mediating part consisting of three homo-FRET dyes. Adapted from Vyawahare et al. [17]

or to different DNA strands. The fluorophore TAMRA functions as a mediating unit connecting 6-FAM and Cy5. The number of attached TAMRA units depends on the length of the wire. For the wire based on a 20-mer DNA strand, only one TAMRA fluorophore is used to bridge the gap between injector and detector dyes. Since only one mediating unit is present in the assembled wire, there is no homo-FRET occurring. Instead, end-to-end transfer occurs primarily through the two-step 6-FAM-TAMRA-Cy5 FRET (there is also a slight contribution of direct 6-FAM to Cy3 FRET to the end-to-end transfer). An extension of the wire to a 40-mer DNA means inclusion of two more TAMRA units to a total of three. Here, substantial homo-FRET between the mediating TAMRA fluorophores is required for energy to be transferred from the injector to the detector end of the wire. The amount of end-to-end transfer in the longer wire is dependent on the number of mediating units. Removal of the middle of the three TAMRA units results in a decrease in the Cy5 fluorescence together with an increase in the 6-FAM fluorescence. However, there is still successful end-to-end energy transfer in the system.

The concept of linking functionalities on the nanometer scale using multi-step FRET can be expanded from the simple one-dimensional wire to include more complex structures in two and (potentially) three dimensions. Multidimensional structures provide an opportunity to incorporate several functional units located within the range for multi-step FRET. Here, the positional precision of energy transfer becomes even more important since there is a need to distinguish between different energy transfer targets.

The development of DNA origami has allowed the creation of a wide variety of DNA structures in two and three dimensions (see the discussion on Sect. 3.1.2). DNA origami does not only allow the construction of different geometrical shapes, but is also readily functionalized. This is utilized by Tinnefeld and co-workers to construct a two-way photonic wire assembled in a DNA-origami rectangle [18]. Here, an input dye is placed at a central position in between two different output dyes, as shown in the schematic illustration in Fig. 5.5. Energy transfer from the donor to the acceptor is controlled using a jumper dye that functions as an

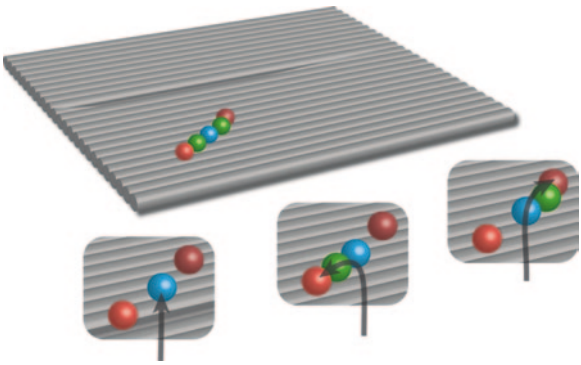

Fig. 5.5 Two-way photonic wire in a DNA origami matrix. The positioning of the *green* jumper dye determines the directionality of the excitation energy transfer. Adapted from Stein et al. [18]

intermediate station in the energy transfer cascade between the donor and both acceptor dyes. Directional control is obtained by attaching the jumper dye to different staple strands at either positions between the donor and the two acceptor dyes. In the design, the fluorophore

ATTO 488 was used as the donor dye, the fluorophores ATTO 647N and Alexa 750 were used as the two different output dyes and ATTO 565 was used as the jumper dye. The modified staple strands are positioned diagonally across the origami rectangle with the fluorophores protruding from the same side of the fl at structure. The structure is designed to give an average inter-fluorophore distance of roughly 9 nm. Theoretically, this gives a low efficiency for direct donor acceptor FRET in the absence of the jumper dye but a high efficiency for the two-step process in the presence of the jumper dye.

The performance of the wire is studied using single molecule fluorescence spectroscopy with alternating laser excitation. Without any of the two jumper dyes, the system is dominated by fluorescence from the donor dye with only a small fraction of the excitation energy being transferred to the output dyes. When either of the jumper dyes is added, the excitation energy distribution is shifted towards the output dye on the side where the strand with the jumper dye binds. This way, using the binding of a sequence specific jumper strand, it is possible to control the directionality of the energy transfer. When the green jumper dye is positioned between the donor dye and the red output dye, the energy transfer efficiency, determined as the fraction of photon counts in the output channel divided by the sum of photon counts in the input and output channels, is 0.34. When the jumper dye is instead positioned between the donor and the IR output the energy transfer efficiency is centered at 0.27. When both the jumper dyes are used simultaneously the resulting energy transfer efficiencies are 0.36 and 0.27 for energy transfer to the red and IR outputs, respectively. Interestingly, the two energy transfer pathways do not seem to compete with each other, as indicated by the fact that the energy transfer efficiency is roughly the same for both paths whether one or two jumper strands are present. Instead the added FRET comes from increased quenching of the donor dye.

For all the constructs, the FRET efficiency distributions are quite broad. Whether this heterogeneity is due to actual dynamics of the DNA-origami structure, or if it is caused by the photo physical properties of the fluorophores and the fluorescence detection, is difficult to answer. In order to evaluate the readout reliability of the system, an output ratio measure was defined as the photon counts from the red output channel divided by the sum of the red and IR outputs. When the jumper dye is located on the side of the red output, the output ratio is centered on 1, and when the jumper dye is located on the side of the side of the IR output the output ratio is centered on 0, with little overlap between the two cases. Finally, when both jumper dyes are present, the output ratio is centered on 0.5. This shows that it is possible to differentiate between the different cases from the obtained signals. The key element in this work is, in principle, two combined photonic wires with a common input, where selection is achieved by the addition of either jumper strand. In addition to this, the work also illustrates how multiple chromophoric units can be combined in a complex matrix to perform a function. The binding of the fluorophore labeled staple strands to the M13mp18 genome are separate from each other, but when the origami-structure is folded, they are organized in a way that facilitates the energy transfer from input to output.

5.3 Artificial Antennas

In addition to transferring energy from one specific point in space to another (as in the case with the photonic wire) there are also examples were multi-chromophoric FRET has been employed to convey excitation energy from a large number of fluorophores to few or single acceptors. The inspiration comes again from the light harvesting complexes in photosynthetic organisms. The approach that is used in the artificial light harvesting devices resembles in a way a funnel for excitation energy, as excitation energy at any donor fluorophore is directed towards the acceptor or acceptors in a way schematically depicted in Fig. 5.6. This type of funnel, or antenna assembly, can be created in numerous ways and can function in one [19], two [20] or three dimensions [21]. The molecular foundation of the antenna complexes has varied greatly and examples include cyclodextrins [22], dendritic [23, 24] or ring-shaped [24–29] arrangements of porphyrins, and pyrene-perrylene assemblies [30, 31] The assemblies rely either on scaffolding of chromophores around some kind of molecular framework or on the ability of the chromophores themselves to arrange into an antenna complex. Especially the ring-shaped porphyrin assemblies closely mimic the arrangement found in the bacterial light harvesting complexes LH-I and LH-II. Furthermore, Ana Moore, Thomas Moore and Devens Gust have perhaps more than anyone else, created systems that closely mimic photosynthetic functions, including light harvesting, redox reactions and proton gradient generation [32–36]. All these examples can be discussed in length. However, the focus of this section is primarily on antenna assemblies relying on self-assembly of bio-molecules, such as DNA or proteins, into scaffolds

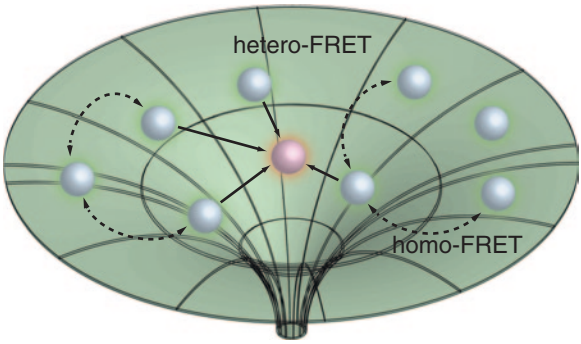

Fig. 5.6 Sketch of a FRET-based light harvesting system. The system functions as an energetic funnel, directing the excitation energy to the acceptor through hetero- and homo-FRET

for multi-chromophoric arrangements similar to those used to construct the photonic wires previously discussed. Additionally, I want to emphasize the connection between nanoscale photonic devices, such as the photonic hetero-FRET wire, DNA nanotechnology and light harvesting assemblies. The idea is that these light-harvesting applications could function in conjunction to other nanoscale devices, e.g. photonic wires, present within the DNA assemblage.

As in the case of the photonic wire, it is possible to find examples that have the properties of a light-harvesting device, although they might not have been branded as such. Armitage and co-workers have created a set of two- and three-dimensional DNA-based nanostructures which functions as hosts for the intercalating fluorophores oxazole yellow (YO-PRO-1) or its bis-intercalating dimer YOYO-1 [20, 21]. The intercalated YO or YOYO dyes act as FRET donors to an acceptor fluorophore, which is either covalently bound to the DNA structure or intercalated between the base pairs. The assemblies effectively work as nanoscale fluorescent markers, organizing multiple fluorophores in a defined region of sub-diffraction size. Although the DNA-based assemblies are primarily designed as brightly fluorescent tags, they have properties that make them interesting as light-harvesting devices. In 2007 Armitage and co-workers published work on the creation of a two-dimensional DNA-based fluorescent nanotag [20]. The assembly consists of a DNA construct that functions as scaffold for the intercalating dyes having three-way junction (3WJ) geometry with "arms" that are 10 base pairs long. In total, three, 20-base pair long, single-stranded DNA molecules are used to construct the 3WJ. The 3WJ assembly was created in two versions, one with an intercalating acceptor (Fig. 5.7a) and one with covalently attached acceptor molecules (Fig. 5.7b). Another cyanine dye, TO-PRO-3, was used as the intercalating acceptor. As with the case of the inter calator-based photonic wire, there is no control of the positioning of the fluorophores when intercalating donor and acceptor dyes are used. Instead, the ratio between added donor and acceptor is used in order to achieve high efficiency both for the light gathering and energy transfer processes. A 37 % quenching of YO-PRO-1 is reported for donor–acceptor ratios of 14:1. By increasing the acceptor concentration to ratios 13:2 and 12:3 the donor is quenched to 53 and 67 %, respectively. However, although the donor quenching is

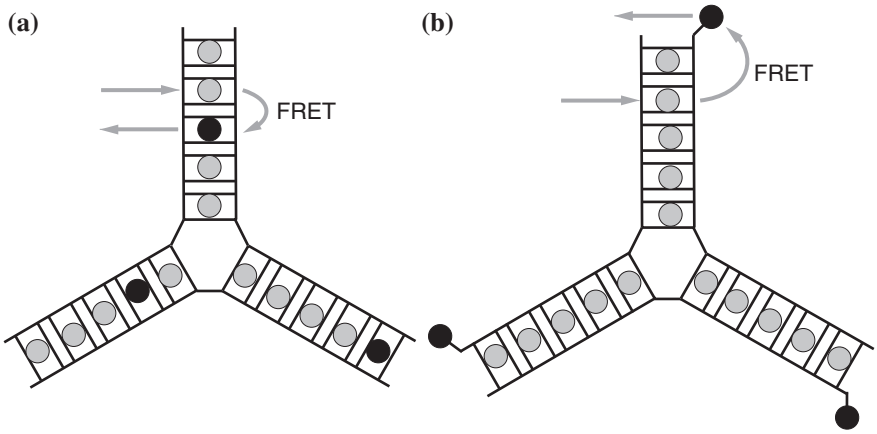

Fig. 5.7 Fluorescent nano tags based on DNA three-way junctions with intercalated donors and either intercalated (**a**) or covalently attached (**b**) acceptors. Adapted from Benvin et al. [20]

higher, there is no increase in the sensitized emission of the acceptor. A probable explanation for this is self-quenching of TO-PRO-3 due to the high loading, something that is supported by decreasing fluorescence intensity from directly excited TO-PRO-3 with increasing loading.

The alternative strategy, with covalently attached acceptors, involves YOYO-1 as donor and Cy3 as acceptor. Cy3 is attached to the terminus of the 3WJ assembly. An advantage with the covalent attachment is that the acceptor dyes do not compete with the donor dyes for the available binding sites in the DNA structure. The alternative assembly with covalently attached acceptors showed 95 % quenching of the YOYO-1 donor for a structure with two Cy3 acceptors. Using this as an example, it would appear as if covalent attachment of the acceptor is preferable over non-covalent binding. Certainly, if the assembly should function as a light-harvesting device with a focused output, there should only be one acceptor, placed in a well-defined position. With that in mind, the covalent option is more suitable. It is not as important to precisely control the positioning of the donors. As long as the binding sites are within energy transfer-distance to the acceptor, random binding of the donors will not hamper the light harvesting functions.

A further development of the DNA-based fluorescent nanotag is made possible using a DNA tetrahedron [21], designed by Turberfield and co-workers [37, 38] (Fig. 5.8). The same donor–acceptor pair as for the three-way junction, YOYO-1 and Cy3, is used for the tetrahedron (TH). Each side of the tetrahedron is 17 base pairs in length, connected with two-base TT hinges. This means that there are a total of 102 binding sites for YOYO-1 in the structure, compared to 30 for the 3WJ, this without a great increase in the size of the assembly. The increased compactness of the TH structure, and the concentration of donors that follows, is a distinct advantage associated with using three-dimensional assemblies over one-dimensional or two-dimensional ones. Using a YOYO-1 loading density of

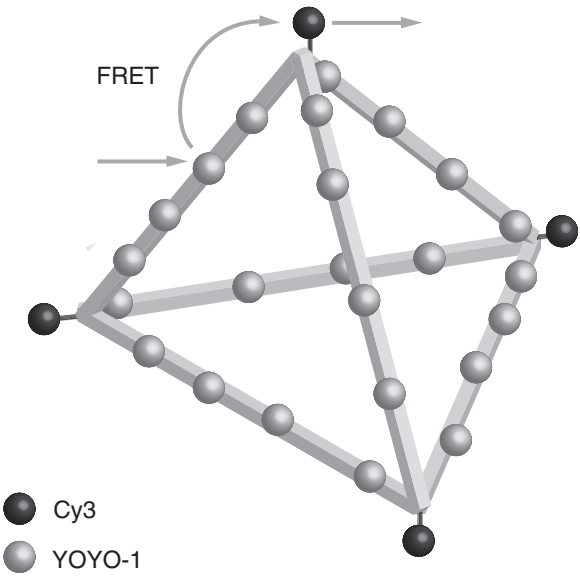

Fig. 5.8 Fluorescent nanotag based on a DNA tetrahedron. Adapted from Özhalıcı-Ünal et al. [21]

approximately 1:4 YOYO-1:base pair Armitage and co-workers obtain donor quenching efficiencies of 52, 74, 86 and 95 % for structures with 1,2,3 and 4 Cy3 acceptors, respectively [21].

A point that is not being discussed in either of the two papers is the effect of homo-FRET on the light-harvesting capacities of the assembled structure. Would a similar construct, built using donor fluorophores without homo-FRET capabilities, show substantially lower sensitized acceptor emission? Homo-FRET should, in principal, play an important role to direct excitation energy from donor dyes distal from the terminal acceptor towards the acceptor through diffusive energy migration. In paper III, were we assemble an antenna system with similar constitution as the YO and YOYO-based nanotegs, this issue is discussed.

The question of the importance of homo-FRET is, in part, addressed by Francis and co-workers in the creation of a protein-based, multi-chromophoric, antenna system [39]. Recombinant tobacco mosaic virus coat protein (TMVP) monomers are organized into either rods or disk shapes through self-assembly. The protein monomers are S123C mutants, i.e. a serine residue is substituted for cysteine. This provides a handle for attachment of thiol-reactive fluorophores. The overall design involves three different dyes, Oregon Green 488 (A), tetramethylrhodamine (B) and Alexa Fluor 594 (C). The fluorophores can be arranged into a FRET cascade, where A is the initial donor, B the intermediate donor and C the acceptor. Because of extensive overlap between the emission band of the donor and its own absorption band substantial donor–donor FRET (homo-FRET) is possible. Assembly of the TMVP monomers into the final structure is directed by pH; a low pH favors the formation of rods while high pH results in the formation of disks. Experiments with assemblies containing only fluorophores A and C showed that energy transfer

from donor fluorophores was the main contributor to acceptor emission at high donor-acceptor ratios. A comparison between a rod assembly carrying 33 donors for each acceptor with a similar assembly, but with equal amounts of donors and acceptors, showed that at least 20 donor fluorophores contributed to the acceptor emission. This is more than the maximum eight donors that can be positioned directly adjacent to the acceptor. Although it is possible that the contribution from non-adjacent donors comes from direct FRET, the multi-step, homo-FRET pathway presumably has an important contribution. To evaluate the light harvesting capabilities, Francis and co-workers measure the antenna effect of the system. The antenna effect, AE, was introduced by Fréchet and co-workers as a way to describe light-harvesting dendritic systems [40] and is defined here in Eq. 5.2

$$AE = I_{A(d\_ex)}/I_{A(a\_ex)} \tag{5.2}$$

In this expression I_A is the emission intensity of the acceptor and *d_ex* signifies donor excitation and *a_ex* direct acceptor excitation both excited at the respective absorption maximum. In the example mentioned above, the antenna effect increases with increasing donor: acceptor ratios from $AE = 0.3$ at 1:1 ratio to a four-fold amplification ($AE = 4$) at 16:1 ratio. A further increase in the donor: acceptor ratio to 33:1 and 101:1 results in and eight-fold and eleven-fold increase, respectively. Although a high antenna effect is observed, the overall efficiency of the system is fairly low, ranging from 34 % to a maximum of 47 %. This is explained by the poor spectral overlap between the donor emission and the acceptor absorption. Including the intermediate donor greatly increases the overall efficiency. By first constructing disk structures that contains either fluorophores B and C or only fluorophore A, and letting these self assemble to a rod structure, it is possible to position the intermediate donor in-between A and C, thereby obtaining a fluorophore organization promoting end-to-end FRET. At fluorophore ratio 8:4:1 the overall efficiency was 90 % and an antenna effect of 4.6.

Another way to spatially organize donor and acceptor fluorophores in order to promote light-gathering is presented by Liu and co-workers who construct an artificial light-harvesting antenna from a seven-helix DNA bundle [41]. The design is based on the seven-helix bundle (7HB) created by Seeman and co-workers [42]. In the light-harvesting assembly, donor fluorophores are positioned in six helices surrounding a central helix which houses the terminal acceptor fluorophore, schematically illustrated in Fig. 5.9a. Three different fluorophores are used in the assembled structure: ethynylpyrene (Py), Cy3 and Alexa Fluor 647 (AF). Pyrene functions as a primary donor to the intermediate fluorophore Cy3, which in turn functions as a donor for the acceptor fluorophore Alxea Fluor 647. The circular arrangement of donors around the acceptor creates an effective funnel for the excitation energy directing into to the acceptor. This circular organization resembles the organization of the bacterial light harvesting complex LH-I around the reaction center.

Four different assemblages with different chromophoric conformations were constructed. The chromophore assemblies, or triads, have the following dye ratios (donor intermediate donor-acceptor): 6:6:1, 6:3:1, 3:6:1 and 1:1:1 for the triads T1–T4, respectively (Fig. 5.9b). The chromophores (with the exception of

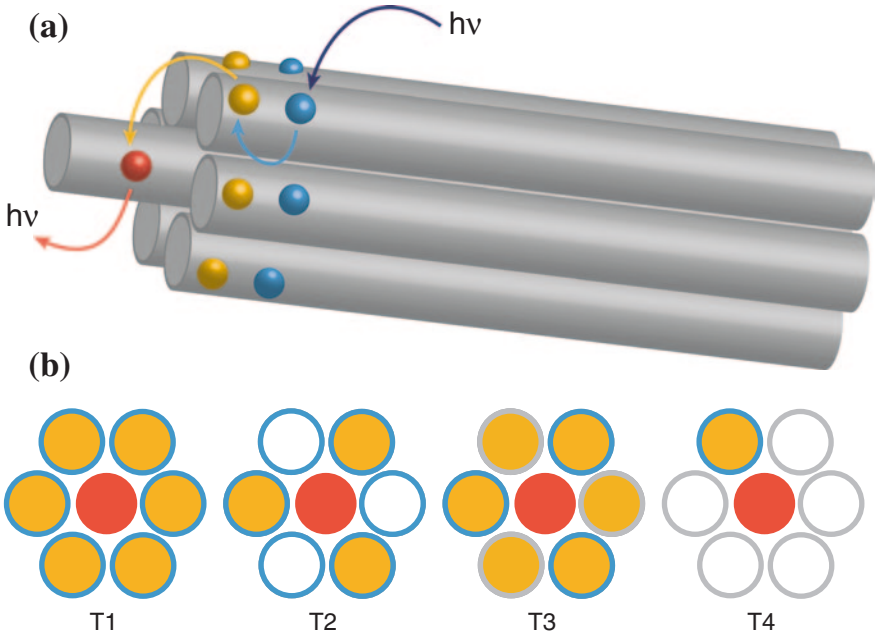

Fig. 5.9 **a** *Seven*-helix bundle with associated *three*-chromophoric array. **b** The different investigated triads T1–T4. Coloration indicated which dyes are present in the array. Adapted from Dutta et al. [41]

the central AF acceptor) are held rigidly close the DNA helix with a relatively well-defined orientation. Because of this, the assumption of random orientation ($k^2 = 2/3$) does not hold. It also means that donor-acceptor distances are relatively well defined (especially for the Py-Cy3 pair). For the T1 assembly (6:6:1), Py-Cy3 distances range between 2.1 and 2.7 nm. The Cy3-AF distance varies slightly more than the Py-Cy3 with a minimum distance at 1.8 nm to a maximum distance at 4.5 nm.

When the assemblies are excited at 380 nm there is a quenching of the donor fluorophore Py for all the triads, T1–T4, compared to an assembly without any of the two acceptors Cy3 and AF. The T1 (6:6:1) and T3 (3:6:1) show a 90 % quenching of Py while T2 (6:3:1) and T4 (1:1:1) show 30 and 70 % quenching, respectively. Comparing the results from the T1 and T2 triads it is clear that a high ratio of intermediate donors is required to achieve an effective donor quenching. However, increasing the amount of intermediate donors beyond a 1:1 ratio does not lead to further quenching of the primary donor (T1 and T3). Finally the difference in donor quenching between T1 and T4 shows that there is an effect of multiple energy transfer paths directing the excitation energy away from the Py donor.

As was the case with the photonic wire, it is not sufficient to just study the quenching of the primary donor to fully characterize the performance of the antenna system. Using the antenna effect measure introduced by Francis and co-workers [39] the efficiency of energy transfer to the terminal acceptor AF is estimated. The reported antenna effects for the T1–T4 triads are 0.85, 0.43, 0.47 and 0.16, respectively. It is interesting to note that the antenna effect of the T2 and T3 triads is approximately half that of T1. T2 has the same number of primary donors as T1 but only half the number of intermediate donors. Th us, T2 absorbs the same amount of light as T1, but the relaying is more inefficient. This is also reflected in the lack of quenching of the primary donor. T3 relays the excitation energy with the same efficiency as T1, but absorbs only half the amount of light that T1 does.

Using the antenna effect measure can be an effective way to characterize the light-harvesting capabilities of an antenna system. However, this measure is highly system specific. Since acceptor emission due to FRET is compared with direct excitation of the donor at the wavelength of maximum absorption, the obtained antenna effect will depend on the quality of the acceptor. The FRET efficiency, which contributes to AE is proportional to the sixth-root of the overlap between the donor emission and acceptor absorption. However, AE is proportional to ε_D^{-1}. High absorption coefficient will therefore have a negative contribution to the antenna effect. For this reason, poor acceptors will more easily result in a high antenna effect. To give a more generally comparable measure of the quality of the antenna system, the antenna effect can be multiplied with the absorption coefficient of the acceptor to give an effective absorption coefficient to the light-harvesting assembly.

Garo and Häner have created a DNA-based antenna system which design that is conceptually different from the ones previously discussed [43]. Instead of having fluorophores that are externally linked or non-covalently associated to DNA, Garo and Häner have constructed a system where the constituting dyes replace the DNA bases creating an arrangement of p-stacked chrompores inside the DNA duplex. The light harvesting assembly consists of the dyes phenanthrenes and pyrene. Assemblies containing 2, 4 or 8 phenanthrenes were created. When the assembled system is excited, emission is observed from the phenanthrene-pyrene exiplex that is formed. The exiplex is formed both if phenanthrene and if pyrene is excited. The emission from the exiplex increases in proportion to the number of phenanthrene units in the assembly.

One important question that remains to be addressed, both for the photonic wires and for the light-harvesting complexes, is that of photostability. From a device perspective, having systems that are durable and that can withstand repeated use is imperative. The natural systems rely on a huge abundance of donor dyes and ability for self-repair. Designed systems need to be built so that incorporated dyes do not photo-destruct or so that loss of a fraction of the dyes does not lead to substantial performance losses. This, or some kind of self-repair function needs to be incorporated. The fluoromodules with replaceable dyes designed Armitage and co-workers hint to something along this line [44].

References

1. Hu XC, Schulten K (1997) How nature harvests sunlight. Phys Today 50:28–34
2. Hu XC, Damjanovic A, Ritz T, Schulten K (1998) Architecture and mechanism of the light-harvesting apparatus of purple bacteria. Proc Natl Acad Sci USA 95:5935–5941
3. Koepke J, Hu XC, Muenke C, Schulten K, Michel H (1996) The crystal structure of the light-harvesting complex Ii (B800–850) from Rhodospirillum Molischianum. Structure 4:58–597
4. Wagner RW, Lindsey JS (1994) A molecular photonic wire. J Am Chem Soc 116:9759–9760
5. Ambroise A, Kirmaier C, Wagner RW, Loewe RS, Bocian DF, Holten D, Lindsey JS (2002) Weakly coupled molecular photonic wires: synthesis and excited-state energy-transfer dynamics. J Org Chem 67:3811–3826
6. Wagner RW, Lindsey JS, Seth J, Palaniappan V, Bocian DF (1996) Molecular optoelectronic gates. J Am Chem Soc 118:3996–3997
7. Lammi RK, Ambroise A, Balasubramanian T, Wagner RW, Bocian DF, Holten D, Lindsey JS (2000) Structural control of photoinduced energy transfer between adjacent and distant sites in multiporphyrin arrays. J Am Chem Soc 122:7579–7591
8. Hernando J, Hoogenboom JP, van Dijk E, Garcia-Lopez JJ, Crego-Calama M, Reinhoudt DN, van Hulst NF, Garcia-Parajo MF (2004) Single molecule photo bleaching probes the exciton wave function in a multichromophoric system. Phys Rev Lett, 93
9. Tong AK, Jockusch S, Li ZM, Zhu HR, Akins DL, Turro NJ, Ju JY (2001) Triple fluorescence energy transfer in covalently trichromophore-labeled DNA. J Am Chem Soc 123:12923–12924
10. Kawahara S-i, Uchimaru T, Murata S (1999) Sequential multistep energy transfer: enhancement of efficiency of long-range fluorescence resonance energy transfer. Chem Comm 563–564
11. Heilemann M, Tinnefeld P, Sanchez Mosteiro G, Garcia Parajo M, Van Hulst NF, Sauer M (2004) Multistep energy transfer in single molecular photonic wires. J Am Chem Soc 126:6514–6515
12. Tinnefeld P, Heilemann M, Sauer M (2005) Design of molecular photonic wires based on multistep electronic excitation transfer. Chem Phys Chem 6:217–222
13. Ohya Y, Yabuki K, Hashimoto M, Nakajima A, Ouchi T (2003) Multistep fluorescence resonance energy transfer in sequential chromophore array constructed on oligo-DNA assemblies. Bioconjugate Chem 14:1057–1066
14. Heilemann M, Kasper R, Tinnefeld P, Sauer M (2006) Dissecting and reducing the heterogeneity of excited-state energy transport in DNA-based photonic wires. J Am Chem Soc 128:16864–16875
15. Sanchez-Mosteiro G, van Dijk EM, Hernando J, Heilemann M, Tinnefeld P, Sauer M, Koberlin F, Patting M, Wahl M, Erdmann R, van Hulst NF, Garcia-Parajo MF (2006) DNA-based molecular wires: multiple emission pathways of individual constructs. J Phys Chem B 110:26349–26353
16. Uemura A, Kimura S, Imanishi Y (1983) Investigation on the interactions of peptides in the assembly of liposome and peptide by fluorescence. Biochim Biophys Acta 729:28–34
17. Vyawahare S, Eyal S, Mathews KD, Quake SR (2004) Nanometer-scale fluorescence resonance optical waveguides. Nano Lett 4:1035–1039
18. Stein IH, Steinhauer C, Tinnefeld P (2011) Single-molecule four-color fret visualizes energy-transfer paths on DNA origami. J Am Chem Soc 133:4193–4195
19. Ruiz-Carretero A, Janssen PGA, Stevens AL, Surin M, Herz LM, Schenning A (2011) Directing energy transfer in discrete one-dimensional oligonucleotide-template assemblies. Chem Commun 47:884–886
20. Benvin AL, Creeger Y, Fisher GW, Ballou B, Waggoner AS, Armitage BA (2007) Fluorescent DNA nano tags: supramolecular fluorescent labels based on intercalating dye arrays assembled on nanostructure DNA templates. J Am Chem Soc 129:2025–2034

21. Özhalıcı-Ünal H, Armitage BA (2009) Fluorescent DNA nano tags based on a self-assembled DNA tetrahedron. ACS Nano 3:425–433
22. Jullien L, Canceill J, Valeur B, Bardez E, Lefèvre J-P, Lehn JM, Marchi-Artzner V, Pansu R (1996) Multichromophoric cyclodextrins 4 light conversion by antenna effect. J Am Chem Soc 118:5432–5442
23. Choi M-S, Aida T, Yamazaki T, Yamazaki I (2002) Dendritic multiporphyrin arrays as light-harvesting antennae: effects of generation number and morphology on intramolecular energy transfer. Chem–Eur J, 8, 2667–2678
24. Choi M-S, Yamazaki T, Yamazaki I, Aida T (2004) Bioinspired molecular design of light-harvesting multiporphyrin arrays. Angew Chem Int Ed 43:150–158
25. Nakamura Y, Aratani N, Osuka A (2007) Cyclic porphyrin arrays as artificial photosynthetic antenna: synthesis and excitation energy transfer. Chem Soc Rev 36:831–845
26. Aratani N, Kim D, Osuka A (2009) Discrete cyclic porphyrin arrays as artificial light-harvesting antenna. Acc Chem Res 42:1922–1934
27. Yang J, Park M, Yoon ZS, Hori T, Peng XB, Aratani N, Dedecker P, Hotta JI, Uji-I H, Sliwa M, Hofkens J, Osuka A, Kim D (2008) Excitation energy migration processes in cyclic porphyrin arrays probed by single molecule spectroscopy. J Am Chem Soc 130:1879–1884
28. Schenning APHJ, Benneker FBG, Geurts HPM, Liu XY, Nolte RJM (1996) Porphyrin wheels. J Am Chem Soc 118:8549–8552
29. Hoffmann M, Karnbratt J, Chang MH, Herz LM, Albinsson B, Anderson HL (2008) Enhanced pi conjugation around a porphyrin [6] Nano ring. Angew Chem Int Ed 47:4993–4996
30. Wurthner F, Sautter A (2003) Energy transfer in multichromophoric self-assembled molecular squares. Org Biomol Chem 1:240–243
31. Sautter A, Kaletaş BK, Schmid DG, Dobrawa R, Zimine M, Jung G, van Stokkum IHM, De Cola L, Williams R, Würthner F (2005) Ultrafast energy-electron transfer cascade in a multichromophoric light-harvesting molecular square. J Am Chem Soc 127:6719–6729
32. Moore TA, Gust D, Mathis P, Mialocq JC, Chachaty C, Bensasson RV, Land EJ, Doizi D, Liddell PA, Lehman WR, Nemeth GA, Moore AL (1984) Photo driven charge separation in a carotenoporphyrin quinone triad. Nature 307:630–632
33. Gust D, Moore TA, Moore AL (1993) Molecular mimicry of photosynthetic energy and electron transfer. Acc Chem Res 26:198–205
34. SteinbergYfrach G, Liddell PA, Hung SC, Moore AL, Gust D, Moore TA (1997) Conversion of light energy to proton potential in liposomes by artificial photosynthetic reaction centres. Nature 385:239–241
35. Kuciauskas D, Liddell PA, Lin S, Johnson TE, Weghorn SJ, Lindsey JS, Moore AL, Moore TA, Gust D (1999) An artificial photosynthetic antenna-reaction center complex. J Am Chem Soc 121:8604–8614
36. Gust D, Moore TA, Moore AL (2001) Mimicking photosynthetic solar energy transduction. Acc Chem Res 34:40–48
37. Goodman RP, Berry RM, Turberfield AJ (2004) The single-step synthesis of a DNA tetrahedron. Chem Comm 1372–1373
38. Goodman RP, Schaap IAT, Tardin CF, Erben CM, Berry RM, Schmidt CF, Turberfield AJ (2005) Rapid chiral assembly of rigid DNA building blocks for molecular nanofabrication. Science 310:1661–1665
39. Miller RA, Presley AD, Francis MB (2007) Self-assembling light-harvesting systems from synthetically modified tobacco mosaic virus coat proteins. J Am Chem Soc 129:3104–3109
40. Brousmiche DW, Serin JM, Frechet JMJ, He GS, Lin TC, Chung SJ, Prasad PN, Kannan R, Tan LS (2004) Fluorescence resonance energy transfer in novel multiphoton absorbing dendritic structures. J Phys Chem B 108:8592–8600
41. Dutta PK, Varghese R, Nangreave J, Lin S, Yan H, Liu Y (2011) DNA-directed artificial light-harvesting antenna. J Am Chem Soc 133:11985–11993

42. Wang R, Liu W, Seeman NC (2009) Prototyping nano rod control: a DNA double helix sheathed within a DNA six-helix bundle. Chem Biol 16:862–867
43. Garo F, Häner R (2012) A DNA-based light-harvesting antenna. Angew Chem Int Ed 51:916–919
44. Shank NI, Zanotti KJ, Lanni F, Berget PB, Armitage BA (2009) Enhanced photostability of genetically encodable fluoro modules based on fluoro genic cyanine dyes and a promiscuous protein partner. J Am Chem Soc 131:12960–12969

Chapter 6
Lipids: Soft, Dynamic Containers

An important criterion in all definitions of life is the requirement for enclosure. There must be a boundary that separates the living systems from its surroundings, that prevents dissociation of genetic information and that enables an autopoietic metabolic system to be upheld. On the fundamental level of the single cell, enclosure is created by a doubled-layered membrane which encapsulates the cellular components, effectively isolating them from the cell exterior. The cell membrane is a highly dynamic system relying of self-assembly and self-organization. From a nanotechnological point of view these properties, which can be traced down to the properties of the individual building blocks, are highly interesting. In paper IV and V, bio-inspired membrane systems are utilized to facilitate reactions between molecules confined to a surface.

Cell membranes are primarily composed of a class of amphiphilic molecules called lipids comprising cholesterol, phospholipids, triglycerides and fatty acids. Lipids are characterized by having a hydrophilic, water-loving, "head" and a hydrophobic, water-hating, "tail". In solution lipids can spontaneously assemble into a plethora of different superstructures shielding either its hydrophobic or hydrophilic part from unfavorable interactions. When individual lipid molecules are present in water solution, the surrounding water is forced into a highly ordered cage-like structure around the hydrophobic tail of the lipid. When the lipids assemble into larger supramolecular structures, water is released and thus becomes less ordered. This release also increases the number of hydrogen bonds that the water molecules can partake in. It is this combined effect of the water that drives the formation of the highly ordered lipid assemblies. The exact nature of the assembled structure depends both on the properties of the lipid molecules and the nature of the surrounding media. Examples include micelles, inverted micelles or cubic phase structures. In the case of biological cells, it is the ability of certain lipids to spontaneously assemble into doubled layered membranes that is important. In water, the double-layer will fold to form a spherical volume shielding the hydrophobic membrane edges from interactions with the water. The result of this is an enclosed water volume on the interior of the membrane bubble, or vesicle,

J. Hannestad, *Fluorescence in Bio-inspired Nanotechnology*, Springer Theses,
DOI: 10.1007/978-3-319-01068-7_6,

that is shielded from the exterior by the hydrophobic barrier that is the membrane double-layer.

As previously stated, the topology of the assembled structure is governed, to a large extent, by the chemical properties of the constituent amphiphilic molecules. A useful way to describe the relationship between the structure of the individual lipid molecule and the topology of the final assembly is through the critical packing parameter *CPP* [1]. The critical packing parameter describes the relative size of the two functional domains of the lipid molecules: the hydrophilic head and the hydrophobic tail. The two dimensions compared is the effective volume of the lipid molecule (v) and the product of the length of the tail domain (l) and the effective area (a) of the head domain ($CPP = v/la$). Lipids can be divided into three different classes with respect to the packing parameter. Lipids with comparatively large head groups ($CPP < 1$) are cone-shaped and form micelles, single layer structures with high curvature. Here, the fatty tails face the interior of the micelle while the hydrophilic head-group is exposed to the exterior. The opposite case is true for lipids with $CPP > 1$. These lipids form high curvature structures similar to the conical lipids previously mentioned. However, in this case, the hydrophilic head group faces the interior and the fatty tail faces the exterior. Cylindrical lipids, having a $CPP \approx 1$ form the lamellar structures found in biological cell membranes. The relationship between lipid structure, packing parameter and assembly type is presented in Fig. 6.1. The main constituent in biological lipid membranes is phospholipids. Phospholipids have a polar head group containing a phosphate, usually together with some other small organic unit, and almost exclusively belong to the group of lipids forming bilayer structures. The properties of the head group vary both in size and in charge depending on the nature of the moiety linked to the phosphate. Moreover, the fatty tail, usually a diglycerid, also varies in length and saturation affecting the properties of the phospholipid. Aside from the structure of the lipid monomer, the topology of the assembled structure is also determined by factors such as lipid concentration and solvent polarity.

6.1 Lipid Layers on Surfaces

Apart from forming complex three-dimensional structures in solution, lipids are also capable of coating a wide variety of surfaces. Depending on the surface properties, the lipids will form either monolayer [2] or bilayer [3] structures. Additional bilayers can also form on top of the coating layer creating multilayered lipid structures. Supported lipid bilayers have been extensively studied [4–7]. They are highly interesting e.g. as model systems for cell membranes. However, as the work presented in this thesis involves lipid monolayers, I will mostly focus the discussion on those. The surface-coating lipid monolayer can form on hydrophobic surfaces with material from a solution reservoir, such as a multi-lamellar vesicle. When the multilamellar vesicle, which is a stable aggregate in water solution, lands upon a hydrophobic surface, the integrity of the cell membrane is

compromised. The membrane rupture then allows the lipid monolayer to form. The subsequent spreading of the lipid monolayer film is driven by the decrease in surface tension that occurs when the water that surrounds the hydrophobic surface is released. In order for lipid spreading to occur, the energetic gain associated with replacing the water around the hydrophobic surface with the hydrophobic tails of the lipids must be larger than the surface tension of the lipid vesicle. The spreading power S can be written according to Eq. 6.1

$$S = \sigma_{SL} - \sigma_{SA} - \sigma_v \tag{6.1}$$

where σ_{SL} and σ_{SA} are the surface tensions when the surface is wetted by the lipid film and by the aqueous solution, respectively. Further, σ_V is the surface tension of the lipid vesicle. Additionally, there is also a tension gradient across the lipid monolayer film. Close to the lipid reservoir, i.e. the multilamellar vesicle, there is an excess of lipid material resulting in a low surface tension. Close to the spreading front, there is instead a lack of lipid material. On a homogeneous surface, the lipid film spreads concentrically from the position of the lipid reservoir (Fig. 6.2a). This means that, since the circumference of the wetted patch grows as the lipids move further away from the reservoir, there will be a thinning of the lipid film when the same number of lipid molecules has to cover a larger area. This results in an increased surface tension. The tension difference between the vesicle and the spreading film results in a transport of lipid material from the vesicle to the spreading front. This type of tension-driven mass transport is called Marangoni flow. Czolkos et al. have demonstrated lipid monolayer spreading on several different hydrophobic surface materials such as SU-8 [2] and EPON 1002F [8] as

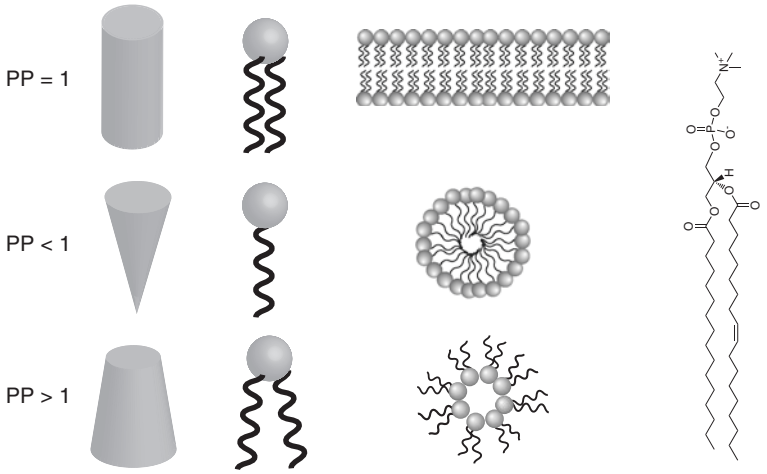

Fig. 6.1 Three examples of different type of lipid structures yielding different types of assemblies. Lipids with packing parameters PP = 1, PP < 1 and PP > 1 give lamellar, micellar or inverted micellar structures, respectively. Shown also is the phospholipid phosphatidyl choline (PC), which is one of the lipids used in the work presented in this thesis

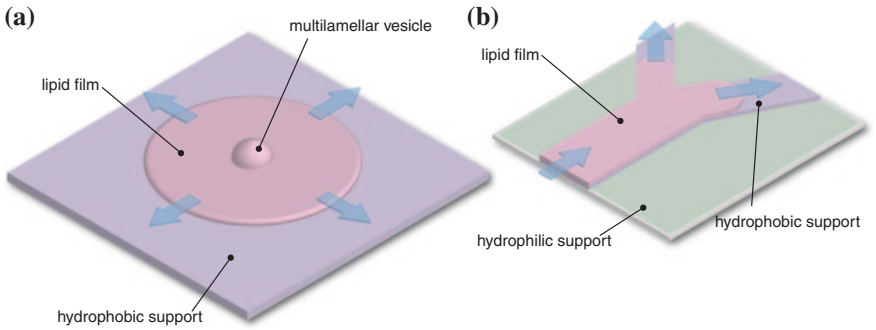

Fig. 6.2 **a** Concentric spreading of lipid monolayer fi lm from a multilamellar vesicle. **b** Spreading lipid monolayer fi lm, following the contours of the patterned hydrophobic surface. The *arrows* indicate the direction of the flow of the lipid film

well as on Teflon AF [9, 10]. Here, lipid film formation is observed using fluorescence microscopy detecting emission from fluorescently labeled lipids. The individual lipid molecules move in the formed lipid film by means of diffusion. For a lipid monolayer on SU-8 and Teflon AF, the experimentally determined diffusion coefficients are 0.3 and 0.8 $\mu m^2 s^{-1}$, respectively. In this work, they also show how the lipid film can be confined to a defined shape by having both hydrophobic and hydrophilic regions (Fig. 6.2b). This is discussed more in detail in Sect. 6.3.

6.2 Diffusion and Lipid Dynamics

As previously discussed, lipid membranes are not static structures with their components locked into a defined place or shape. On the contrary, lipid membranes are highly dynamic. Vesicles are capable of both shape and size changes and individual lipid molecules readily diffuse in the plane of the membrane creating a two-dimensional liquid. Here, I would like to focus on the phenomenon of diffusion itself. Diffusion is the process of particle motion along a concentration gradient. The particles move from a region of high concentration to a region of low concentration. These particles can for instance be molecules, but the phenomenon extends to anything that shows thermal motion and that can be ordered in space. Following this reasoning a diffusion coefficient D can be defined according to Fick's first law (Eq. 6.2)

$$J = -D\nabla c \tag{6.2}$$

where J is the particle flux through a cross section in space and ∇c is the concentration gradient in that cross section. The diffusion coefficient, D, then becomes a proportionality constant relating the flux to the concentration profile. The size of D, i.e. the diffusivity of a particle, is a property of the diffusing particle as well as its surroundings. We will get back to this more in detail later in the chapter.

The observed flux from high to low concentration is a macroscopic effect. When looking at the motion of the individual particle there is no directionality. In a system characterized by diffusion there is no force exerted on the diffusing particles providing directional motion. Instead, directionality is a purely statistical effect. The individual particles move by random Brownian motion. With this at hand we can consider the migration of an individual diffusing particle. As the particle flux depends on the diffusivity, D, of the particle, so does the traveled distance of each particle over time. We can express the root mean distance travelled as a function of time, t, according to

$$\left\langle x^2 \right\rangle^{1/2} = (2dDt)^{1/2} \tag{6.3}$$

where $\langle x^2 \rangle^{1/2}$ is the root mean square displacement and d is the Euclidian dimension in which diffusion is taking place ($d = 1, 2, 3$ for 1, 2 and 3 dimensions, respectively). The weak time dependence of the traveled distance means that diffusion is an inefficient means of transport over large distances. It would take an average diffusing particle roughly a day to travel 1 cm. However, for μm-scale distances (and shorter) diffusion is rapid. This means that diffusion is an efficient means of transport on the length scale of many biological systems and could be of potential use in nanotechnological applications.

It can be difficult to comprehend the actual diffusional mechanisms by just looking at the provided equations. A more intuitive way to understand diffusion is to look at is as a series of consecutive jumps. particle is capable of jumping a distance λ over a time τ. From the new position the particle can now make the same jump again travelling in any direction independently of all previous jumps. Inserting the discrete step length and rate into the diffusion equations we obtain the (one-dimensional) Einstein–Smoluchowski equation:

$$D = \frac{\lambda^2}{2\tau} \tag{6.4}$$

Now is the time to return to the diffusional constant D. As previously stated, D depends on the properties of both the diffusing particle and its surroundings. In the Stokes–Einstein relation, the diffusion coefficient is expressed as a function of the thermal energy (k_BT, where k_B is the Boltzmann constant and T the absolute temperature) and frictional force f.

$$D = \frac{k_BT}{f} \tag{6.5}$$

This expression is derived from the relationship between ionic mobility and frictional force together with the relationship between ionic mobility and the diffusion coefficient. However, the expression in Eq. 6.5 is valid for neutral molecules as well as for ions. The frictional force is a relation between the diffusing particle and the surrounding medium and depends on the hydrodynamic radius of the particle, a, and the viscosity, h of the medium. For a sphere the expression in Eq. 6.5 becomes:

$$D = \frac{k_B T}{6\pi \eta a} \tag{6.6}$$

Modeling diffusing particles as spheres is a valid assumption for actual spherical particles as well as for many small molecules or globular proteins. However, for molecules such as short DNA duplexes or other linear polymers this assumption does not hold. For many complex supramolecular assemblies, prolate or oblate shapes might be better approximations.

In a system where diffusion is the dominant mode of mass transport it is possible to calculate a characteristic mixing time for the system. The mixing time depends on both the diffusion coefficient of the component that is being mixed and the size of the system. Using the diffusion coefficient, D, and the linear size of the container where equilibration occurs, L, the equilibration time can be defined as in Eq. 6.7 [11].

$$\tau_{eq} = \frac{L^2}{D} \tag{6.7}$$

Again, from the equation, it is apparent that size plays an important role in systems dominated by diffusion. By decreasing the system size it is possible to dramatically decrease the time needed to equilibrate the system.

6.2.1 Anomalous Diffusion and its Implications

Biological cells are far from the homogenous, perfectly mixed environment found in a test tube. Instead, cells are crowded, inhomogeneous and filled with various obstacles. This means that mass transport will not be equal everywhere in the cell, and certain parts of the cell might be completely inaccessible. The perhaps most striking example of this type of substructuring of the cell environment are perhaps the membrane structures commonly known as lipid rafts [12–15]. These are domains in the cell membrane with a composition that differs from the overall cell membrane and that moves in the membrane as a single structure. Because of theses microenvironments, diffusing molecules are not free to probe the entire three-dimensional space inside the cell or the two-dimensional space in the cell membrane. This effect, which is called anomalous diffusion, can be understood as reduction in the dimensionality of the diffusional motion [16, 17]. rewriting Eq. 6.8 to accommodate for anomalous diffusion gives

$$\left\langle x^2 \right\rangle^{1/2} = (2dDt)^{\alpha/2} \tag{6.8}$$

where a < 1. What we obtain here is a dimensionality that is not purely one-, two- or three-dimensional. Diffusion in complex systems can many times be inhomogeneous and it is therefore important to consider the possibility of anomalous diffusion. Furthermore, anomalous diffusion might also influence other properties

of the studied system. For instance, if reactants in a second order reaction have restricted mobility this might change the actual reaction order giving rise to fractal reaction kinetics [16].

6.3 The Importance of Compartmentalization

Modern biological cells are highly structured entities. We have already mentioned the structured, mosaic exterior cell membrane. The plasma membrane of cells acts as a barrier regulating the flow of materials in and out of the cell [18–20]. Further, the cell membrane also acts as a host for numerous receptors responsible for the communication between the cell and its environments [21, 22]. In eukaryotes in particular, the cell has a high degree of interior structuring. Different functionalities are divided into separate dedicated compartments, enclosed by lipid membranes [23, 24]. This phenomenon is termed compartmentalization and is important, not only for biological system, but also within nanotechnology. Here, I will first investigate the biological relevance of compartmentalization. Moreover I will discuss mechanisms behind the phenomenon that are relevant also outside biology before finally describing how all this translates into nanotechnology.

The reasons behind compartmentalization in biology are many. We have touched upon one of them already. As much of the mass transport in cells is diffusion-driven, many cellular processes will rapidly become inefficient when cells grow to incorporate more complex functions.[1] To maintain high efficiency, reactants involved in related processes are located in the same intracellular compartments. This way, it is possible to have short diffusion time inside even the largest cells. Further, in modern cells, the intracellular conditions required for one chemical reaction may not be compatible with another one. In order for the cell to host both these two processes simultaneously, they need to be localized in separate compartments.

So far, we have dealt with compartmentalization in eukaryotic cells, which are large with many complex internalized functions. However, compartmentalization is of more fundamental importance for life in general. We can consider some of the most basic prerequisites for life, one being an information polymer capable of Darwinian evolution and a second one being a vessel to house the polymer in. In fact, encapsulation in vesicle-like containers has most likely played an important role in the actual emergence of life through strictly non-biological mechanisms. Here, I will describe how compartmentalization may have played an important role in the emergence of life. This might seem somewhat outside the scope of the thesis. However, the point that I want to make is that compartmentalization is not a passive process, but something that can be utilized, both in biology and in nanotechnology. I will base this discussion largely on the work by Jack W. Szostak focusing on prebiotic evolution and the effect of fatty acid containers [25].

[1] See discussion on mixing time and container size in Sect. 6.2.

First, let us focus on the vesicles alone. Szostak argues that the earliest and most primitive cell could not have had complex protein-based system for transport of molecular building blocks. Therefore, the first cell membranes must have been built from something that is more permeable to small molecules than the phospholipids of modern cells [26]. Bilayer membrane vesicles built from fatty acids have previously been shown to be able to trap macromolecules but to be permeable to small polar molecules [27]. Compared to phospholipid vesicles, fatty acid supramolecular structures are highly dynamic, rapidly exchanging material between vesicles and the surrounding solution [28]. Further, fatty acid vesicles spontaneously form in solution from micelles in an autocatalytic process where vesicles grow and divide resulting in an enrichment of vesicles over time [29]. Aside from their rapid exchange of material with the surrounding solution, fatty acid vesicles also show a high flip-flop rate. This property is a requirement for their ability to grow by absorbing free fatty acids from solution as these molecules first enter the outer leaflet of the bilayer [28]. Zhu et al. [30] suggests that vesicle division is initiated in large multilamellar vesicles that are fed with fatty acids from micelles. If material transport to the underlying membrane structures is slow, the outer membrane will grow by creating protrusions. The protrusion will then form a long threadlike vesicle that subsequently divides into multiple smaller ones.

What happens when we start adding other molecules to the fatty acid vesicle system? Chen et al. [31] has shown that osmotically swollen vesicles grow more rapidly than non-swollen ones. One cause for such osmotic stress can be incorporation of a high concentration of some kind of polymer, not capable of passing through the bilayer membrane. A polymer that could facilitate vesicle growth could for instance be RNA. Furthermore, RNA can form ribozymes capable of self-replication. This combination of a self-replicating vesicle with a self-replicating information polymer could constitute a simple one-gene cell capable of Darwinian evolution. Indeed, Chen et al. [31] observe an increased growth rate for vesicles that contain RNA compared to vesicle that do not. Another point of interest relates to the environment where the first primitive cells might have emerged. The clay montmorillonite has previously been shown to catalyze the polymerization of RNA from individual ribonucleotides [32–34]. Hanczyc et al. [35] show that the same clay is also capable of facilitating the transition from micelles to fatty acid vesicles. In addition, in some cases clay particles are observed to incorporate inside the newly formed vesicles. These encapsulated particles are speculated to act as catalysts for RNA polymerization inside the vesicles. This way, clay particles could simultaneously stimulate vesicle growth and RNA polymerization.

We see here how prebiotic evolution is an emergent property arising from the interaction of a geological, physical and chemical actors. What are the principle mechanisms behind such systems? In “A thousand years of nonlinear history” Manuel De Landa discusses Deleuze and Guattari’s concept of meshworks [36]. He states that meshworks are characterized not only by self-stimulation, but also by self-maintenance; that is, a meshwork combines a series of mutually stimulating processes to function as a whole. In our previous example, the meshwork is the assemblage of fatty acids, RNA and clay particles. Based on work by

Humberto Maturana and Fracisco Varelo on autocatalysis, De Landa introduces the concept of growth by drift. Growth by drift means that new functions are introduced in meshworks from previously unused raw material—or even waste products from already internalized processes—in a way that maintains the self-sustaining nature of the meshwork. From here, it is a very small step to Darwinian evolution. Returning to Deleuze and Guattari, De Landa proposes three aspects characterizing the emergence of meshworks. The first step is termed *articulation of superposition*. Here, interacting elements are brought together. In our case the elements brought together are the self-replicating fatty acid vesicles and the self-replicating RNA. To this, *intercalary elements* are added. Intercalary elements are objects that are able to facilitate the interaction of the superpositioned objects.[2] In the development of the fatty acid-RNA assemblage, both clay particles and osmotic pressure act as intercalary elements. Finally, meshworks are *self-consistent aggregates*, that is, they are capable of generating stable states. Again, we return to Szostak's primitive protocell. Here, however the system changes, the combination of a membrane-enclosed compartment and a self-replicating polymer remains stable. The exact constitution of these two elements might change, but their principal functionality is retained.

Why do we need this added level of abstraction? The point that I want to make, using the reasoning of De Landa, is that these mechanisms are not limited to chemical or basic biological systems, but instead are general phenomena, applicable to a wide range of systems of different nature. I will present two simplified cases in order to illustrate the general applicability of the meshwork concept. Being a biological system on a much larger scale than single cells, ecosystems can be considered as meshworks. An ecosystem is an interlocking of a large number of heterogeneous elements (different species of animals, plants, bacteria, etc.). These elements interact in numerous ways, where especially symbiotic relations build the meshwork and create stable states. An example of a cultural meshwork provided by De Landa is the small-town market. The market brings together people with heterogeneous needs. In the ideal case, interlocking of these needs and demands occurs automatically through the price mechanism. Money acts as an intercalary item increasing the probability that matching demands meet than what would be the case with pure barter.

Finally, what is then the conclusion of all this? One important notion is the fact that compartmentalization is not a passive process where the assembled compartments act as non-functional scaffolds for functional molecules. Instead, compartmentalization plays an active role in any process where it is found, influencing all other processes. For instance, the evolution of cellular life must be understood as an assemblage of a series of complex systems (e.g. information polymers, compartmentalization, metabolism) all interacting and affecting each other.

[2] Here, the word object refers to any material entity or process that is able to interact with the system.

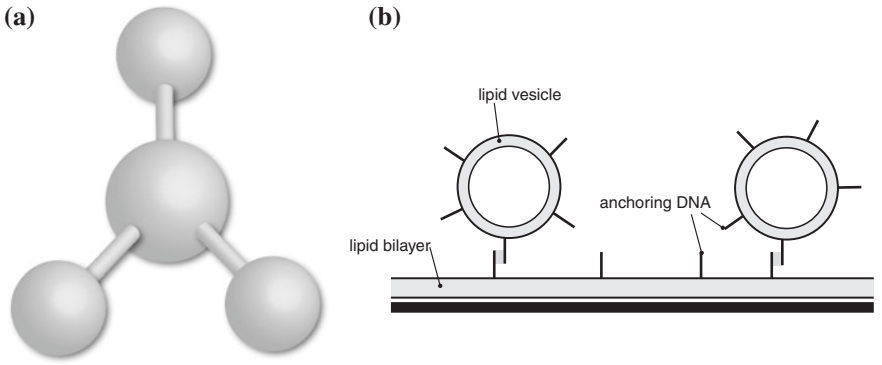

Fig. 6.3 **a** Lipid vesicle network as designed by Orwar and co-workers. The vesicles are connected by lipid nanotubes allowing transport of molecules between the vesicles. **b** Lipid vesicles decorated with DNA tethering them to a supported lipid bilayer, similar to systems designed by Höök and co-workers and Boxer and co-workers

Since the underlying mechanisms behind compartmentalization are essentially non-biological it is of interest to apply it in a technological context. Here, compartmentalization can be found in wide variety of applications. Compartmentalization is incorporated in (nano)technology in a wide variety of ways. Often, the context is within micro- or nanofluidics and the reasons for creating spatial restrictions vary. Several examples exist where molecules are captured inside femtoliter droplets [37–39]. Many of the constructed systems are inspired by biology and just as in the case of biological cells, lipid material is usually used to create the compartments [40]. Analogous the microdroplets, lipid vesicles have been created to capture individual molecules in order to allow studies of e.g. fast kinetics in small geometries [41].

Individual vesicles could be seen as a model system for biological cells, albeit on a very simplified level. Orwar and co-workers present a more complex model system where liposome networks, connected through lipid nanotubes, are created in two [42] and three dimensions [43, 44] (schematically represented in Fig. 6.3a). The different vesicles in the network are manually deposited and connected by nanotubes in a way that reflects the sequential order in which they were created. When formed, the liposome networks self-assemble into a structure that minimizes system energy, creating a shortest mean path nanotube grid connecting the vesicles. The networks allow material transport between the vesicles going through the nanotubes and can therefore be used to investigate chemical reactions that combine transport and confinement. Biological membrane compartments are dynamic entities with changing dimensions and topology. Sott et al. [45] showed that such geometrical changes affect the reactive behavior of enzymes enclosed in the network. The results show that enzymatic reactions inside multiple-liposome networks follow wavelike kinetic behavior. This phenomenon is explained by the transport barriers created by nanotube entrances. The reactions are also influenced

by factors such as the relative positioning of vesicles, connectivity and vesicle size. Furthermore, reaction kinetics can also be dynamically altered by e.g. changes in vesicle size or connectivity during the reaction procedure [46]. Lipid nanotubes networks cannot only be used to mimic cellular membrane and compartment systems; they can also be used to create nanoscale analytical devices. If an electric potential is applied over a lipid nanotube, the assembly can be utilized for electrophoretic transport of polyelectrolytes such as DNA [47].

Lipid vesicles cannot only be used to host molecules in the interior aqueous solution. Also the lipid bilayer itself constitutes a compartment to which various molecules can be tethered. Examples of this come from e.g. the work by Höök et al. [48–51] and Boxer et al. [52–54]. A representation of the principal design is shown in Fig. 6.3b. Both groups tether DNA molecules to the lipid vesicles, thereby creating functional handles enabling the vesicles to be functionally and spatially directed. Using sequential DNA hybridization Granéli et al. are able to create three-dimensional networks of small unilamellar vesicles (SUV). The vesicles are labeled with single stranded DNA molecules, modified in one end with a cholesterol moiety. The hybridization of complementary sequences allows for the controlled formation of a multi-layer matrix of SUVs on a gold substrate. The point of creating such a matrix is to e.g. facilitate the study of membrane proteins. Yoshina-Ishii et al. [52].have constructed a similar, albeit single-layer, system of surface tethered vesicles. An important difference however, is that the vesicles are anchored to supported lipid bilayers. The bilayers display single stranded DNA molecules that are complementary to the ones of the vesicles. Since the lipid bilayer is a two-dimensional fluid, the tethered vesicles are able to diffuse across the surface with an average diffusion coefficient of 0.9 $\mu m^2 s^{-1}$. As tethered liposomes are able to diffuse when attached to a lipid bilayer, it is also possible for them to interact with each other. Using a microfluidic device, Chan et al. [53] allowed two populations of membrane anchored vesicles flow into a common mixing chamber and interact. Aside from the tethering DNA, the vesicles were also decorated with complementary "docking" DNA strands making it possible for a vesicle from one population to combine with one from the other population through hybridization of the docking strands. This way, the two vesicles are able to move in tandem. Chan et al. show that the rate of this docking event depends strongly on the length of the DNA. For sequences requiring full overlap (i.e. complete hybridization), the rate is proportional to l^4, where l is the length of the docking DNA.

If brought close enough together, two separate lipid vesicle are capable of fusing together forming a single compartment. In nature, this process is often facilitated by SNARE[3] proteins [55]. Complementary pairs of proteins on separate vesicles are able to force the vesicles together by forming a complex, thereby catalyzing vesicle fusion. Stengel et al. [49] have presented an artificial mimic of the SNARE system using complementary DNA strands to bring the vesicles in close

[3] SNARE is an acronym derived from "Soluble NSF Attachment Protein (SNAP) receptor".

proximity. In the case of the lipid vesicle matrix, all DNA molecules were tethered to the vesicles in the 3′ end. This means that, when the strands hybridize, the formed duplex acts as a spacer keeping the two vesicles apart. In the SNARE-mimicking case, the situation is the opposite. Here, one strand is attached in the 3′ and the complementary strand in the 5′ end. Thus, for the DNA strands to fully hybridize, the vesicles must be in very close proximity. For this to happen, the energetic gain from duplex formation must outcompete the repulsive hydration forces between the lipid head groups. It is not only possible to fuse vesicles together; vesicles can also be fused with supported lipid bilayers, this way delivering their cargo to the underlying substrate [50, 54]. Finally, vesicles can also be used as probes, in a way similar to quantum dots or nanoparticles [51].

Compartmentalization does not have to be restricted to three-dimensional containers like lipid vesicles. Already when we are considering the vesicle bilayer as a container rather than enclosed aqueous volume we no longer deal with a fully three-dimensional compartment. The vesicular membrane could be treated as a curved two-dimensional compartment rather than as a three-dimensional one. The supported lipid bilayer used to tether the vesicles is also in a sense a two dimensional container. What happens when we move from three to two dimensions? A particle or molecule residing in solution has total translational and orientation freedom. When confined to a liquid surface such as a lipid membrane, the molecule can no longer move in every direction. It is restricted to the plane of the surface. This, of course, is trivial since this translational restriction is what is meant by two-dimensional confinement by definition. However, the confinement to a surface has other implications as well. Molecules in a surface are not only restricted to lateral in plane mobility, they also have an imposed orientational order. This is a consequence of the fact that the molecules need to be attached to the surface in some way. Because of the attachment, molecules at surfaces are not free to rotate. This effect can be utilized in reaction design. By locking reactants in an orientation that favors interaction, the probability of reactive encounters increases. The magnitude of the orientational confinement depends on how the molecule is attached. If the tether is stiff, the orientational restriction will be larger than if a flexible tether is used.

The two-dimensional container is not limited to a continuous surface. A surface can also be divided into sub-compartments, analogous to how a lipid vesicle is a sub-compartment to the entire three-dimensional space (or rather to the water volume in which it is situated). Boxer et al. [3, 56] have created compartmentalized systems by patterning supported lipid bilyers. Patterned substrates for supported lipid bilayers, where each bilayer patch was confined to a 200 × 200 μm square, was created using photolithographic techniques [3]. The barriers preventing the different lipid patches to mix are not mechanical. Instead, it is the differences in the surface electrostatic and chemical properties that drive the partitioning. Other methods to create membrane microarrays are e.g. microprinting or microfluidic flow patterning.

Another way to create two-dimensional lipid-based containers is to use the lipid monolayer films created by Czolkos et al. that were introduced in Sect. 6.1. The lipid monolayer films provide a means to position components such as reactants

giving them an orientational order while retaining a dynamic system capable of undergoing chemical reactions. This property is utilized in paper IV and V in this thesis, where hybridization of membrane anchored DNA molecules is studied. In addition to creating homogeneous hydrophobic surfaces enabling lipid monolayer formation, it is also possible to create mosaic surfaces with defied patterns that are hydrophobic. This has been shown at nanometer scale for SU-8 [2, 57, 58] and EPON 1002F [8] and at micrometer scale for Teflon AF [10]. As in the case with the compartmentalized bilayers, it is not a mechanical barrier that prevents the lipid monolayers from spreading outside the structures. The patterned surface that confines the lipid monolayer film, effectively creating a two-dimensional compartmentalization offering control over material mixing and thus also reaction control.

A property that is common to most two- and three-dimensional compartmentalization techniques is that they rely on top-down methods to produce that pattern that directs the compartmentalization process. In the case of the liposome networks, vesicles are created and positioned manually. For the two-dimensional compartmentalization techniques, the patterns directing the lipid films are created using methods such as photolithography. This way, these systems are characterized by a combination of top-down pattern creation and a bottom-up self-assembly of the final lipid structure.

References

1. Holmberg K, Jönsson B, Kronberg B, Lindman B (2003) Surfaces and polymers in aqueous solution, 2nd edn. Wiley, Chichester, p 545
2. Czolkos I, Erkan Y, Dommersnes P, Jesorka A, Orwar O (2007) Controlled formation and mixing of two-dimensional fluids. Nano Lett 7:1980–1984
3. Groves JT, Ulman N, Boxer SG (1997) Micropatterning fluid lipid bilayers on solid supports. Science 275:651–653
4. Evans E, Needham D (1987) Physical-properties of surfactant bilayer-membranes—thermal transitions, elasticity, rigidity, cohesion, and colloidal interactions. J Phys Chem 91:4219–4228
5. Evans E, Yeung A (1994) Hidden dynamics in rapid changes of bilayer shape. Chem Phys Lipids 73:39–56
6. Sackmann E (1996) Supported membranes: scientific and practical applications. Science 271:43–48
7. Nissen J, Gritsch S, Wiegand G, Radler JO (1999) Wetting of phospholipid membranes on hydrophilic surfaces—concepts towards self-healing membranes. Eur Phys J B 10:335–344
8. Czolkos I, Hannestad JK, Jesorka A, Kumar R, Brown T, Albinsson B, Orwar O (2009) Platform for controlled supramolecular nanoassembly. Nano Lett 9:2482–2486
9. Czolkos I, Guan J, Orwar O, Jesorka A (2011) Flow control of thermotropic lipid monolayers. Soft Matter 7:6926–6933
10. Czolkos I, Hakonen B, Orwar O, Jesorka A (2012) High-resolution micropatterned teflon AF substrates for biocompatible nanofluidic devices. Langmuir 28:3200–3205
11. Berg OG, Vonhippel PH (1985) Diffusion-controlled macromolecular interactions. Ann Rev Biophys Biophys Chem 14:131–160
12. Jacobson K, Mouritsen OG, Anderson RGW (2007) Lipid rafts: at a crossroad between cell biology and physics. Nat Cell Biol 9:7–14
13. Simons K, Ikonen E (1997) Functional rafts in cell membranes. Nature 387:569–572

14. Yoon TY, Jeong C, Lee SW, Kim JH, Choi MC, Kim SJ, Kim MW, Lee SD (2006) Topographic control of lipid-raft reconstitution in model membranes. Nat Mater 5:281–285
15. Ursell TS, Klug WS, Phillips R (2009) Morphology and interaction between lipid domains. Proc Natl Acad Sci USA 106:13301–13306
16. Berry H (2002) Monte Carlo simulations of enzyme reactions in two dimensions: fractal kinetics and spatial segregation. Biophys J 83:1891–1901
17. de Gennes PG (1982) Kinetics of diffusion-controlled processes in dense polymer systems. 1. non-entangled regimes. J Chem Phys 76:3316–3321
18. Conner SD, Schmid SL (2003) Regulated portals of entry into the cell. Nature 422:37–44
19. Munro S (2003) Lipid rafts: elusive or illusive? Cell 115:377–388
20. Ellgaard L, Molinari M, Helenius A (1999) Setting the standards: quality control in the secretory pathway. Science 286:1882–1888
21. Berridge MJ (1993) Inositol trisphosphate and calcium signaling. Nature 361:315–325
22. Artavanis-Tsakonas S, Rand MD, Lake RJ (1999) Notch signaling: cell fate control and signal integration in development. Science 284:770–776
23. Zerial M, McBride H (2001) Rab proteins as membrane organizers. Nat Rev Mol Cell Biol 2:107–117
24. Rothman JE, Wieland FT (1996) Protein sorting by transport vesicles. Science 272:227–234
25. Schrum JP, Zhu TF, Szostak JW (2010) The origins of cellular life. Cold Spring Harb Perspect Biol 2:a002212
26. Szostak JW, Bartel DP, Luisi PL (2001) Synthesizing life. Nature 409:387–390
27. Walde P, Goto A, Monnard PA, Wessicken M, Luisi PL (1994) Oparins reactions revisited—enzymatic-synthesis of poly(adenylic acid) in micelles and self-reproducing vesicles. J Am Chem Soc 116:7541–7547
28. Chen IA, Szostak JW (2004) A kinetic study of the growth of fatty acid vesicles. Biophys J 87:988–998
29. Walde P, Wick R, Fresta M, Mangone A, Luisi PL (1994) Autopoietic self-reproduction of fatty-acid vesicles. J Am Chem Soc 116:11649–11654
30. Zhu TF, Szostak JW (2009) Coupled growth and division of model protocell membranes. J Am Chem Soc 131:5705–5713
31. Chen IA, Roberts RW, Szostak JW (2004) The emergence of competition between model protocells. Science 305:1474–1476
32. Ferris JP, Ertem G (1993) Montmorillonite catalysis of RNA oligomer formation in aqueous solution. A model for the prebiotic formation of RNA. J Am Chem Soc 115:12270–12275
33. Ertem G, Ferris JP (1996) Synthesis of RNA oligomers on heterogeneous templates. Nature 379:238–240
34. Ertem G, Ferris JP (1997) Template-directed synthesis using the heterogeneous templates produced by montmorillonite catalysis. A possible bridge between the prebiotic and RNA worlds. J Am Chem Soc 119:7197–7201
35. Hanczyc MM, Fujikawa SM, Szostak JW (2003) Experimental models of primitive cellular compartments: encapsulation, growth, and division. Science 302:618–622
36. De Landa M (1997) A thousand years of nonlinear history. Zone Books, Brooklyn
37. Teh S-Y, Lin R, Hung L-H, Lee AP (2008) Droplet microfluidics. Lab Chip 8:198–220
38. He MY, Edgar JS, Jeffries GDM, Lorenz RM, Shelby JP, Chiu DT (2005) Selective encapsulation of single cells and subcellular organelles into picoliter- and femtoliter-volume droplets. Anal Chem 77:1539–1544
39. Edgar JS, Milne G, Zhao Y, Pabbati CP, Lim DSW, Chiu DT (2009) Compartmentalization of chemically separated components into droplets. Angew Chem Int Ed 48:2719–2722
40. Chan YHM, Boxer SG (2007) Model membrane systems and their applications. Curr Opin Chem Biol 11:581–587
41. Chiu DT, Wilson CF, Ryttsen F, Stromberg A, Farre C, Karlsson A, Nordholm S, Gaggar A, Modi BP, Moscho A, Garza-Lopez RA, Orwar O, Zare RN (1999) Chemical transformations in individual ultrasmall biomimetic containers. Science 283:1892–1895

42. Karlsson A, Karlsson R, Karlsson M, Cans AS, Stromberg A, Ryttsen F, Orwar O (2001) Molecular engineering—networks of nanotubes and containers. Nature 409:150–152
43. Karlsson M, Sott K, Davidson M, Cans AS, Linderholm P, Chiu D, Orwar O (2002) Formation of geometrically complex lipid nanotube-vesicle networks of higher-order topologies. Proc Natl Acad Sci USA 99:11573–11578
44. Karlsson M, Davidson M, Karlsson R, Karlsson A, Bergenholtz J, Konkoli Z, Jesorka A, Lobovkina T, Hurtig J, Voinova M, Orwar O (2004) Biomimetic nanoscale reactors and networks. Annu Rev Phys Chem 55:613–649
45. Sott K, Lobovkina T, Lizana L, Tokarz M, Bauer B, Konkoli Z, Orwar O (2006) Controlling enzymatic reactions by geometry in a biomimetic nanoscale network. Nano Lett 6:209–214
46. Lizana L, Bauer B, Orwar O (2008) Controlling the rates of biochemical reactions and signaling networks by shape and volume changes. Proc Natl Acad Sci USA 105:4099–4104
47. Tokarz M, Akerman B, Olofsson J, Joanny JF, Dommersnes P, Orwar O (2005) Single-file electrophoretic transport and counting of individual dna molecules in surfactant nanotubes. Proc Natl Acad Sci USA 102:9127–9132
48. Granéli A, Edvardsson M, Höök F (2004) DNA-based formation of a supported, three-dimensional lipid vesicle matrix probed by QCM-D and SPR. ChemPhysChem 5:729–733
49. Stengel G, Zahn R, Höök F (2007) DNA-induced programmable fusion of phospholipid vesicles. J Am Chem Soc 129:9584
50. Simonsson L, Jönsson P, Stengel G, Höök F (2010) Site-specific DNA-controlled fusion of single lipid vesicles to supported lipid bilayers. ChemPhysChem 11:1011–1017
51. Gunnarsson A, Sjövall P, Höök F (2010) Liposome-based chemical barcodes for single molecule DNA detection using imaging mass spectrometry. Nano Lett 10:732–737
52. Yoshina-Ishii C, Boxer SG (2003) Arrays of mobile tethered vesicles on supported lipid bilayers. J Am Chem Soc 125:3696–3697
53. Chan YHM, Lenz P, Boxer SG (2007) Kinetics of DNA-mediated docking reactions between vesicles tethered to supported lipid bilayers. Proc Natl Acad Sci USA 104:18913–18918
54. Rawle RJ, van Lengerich B, Chung M, Bendix PM, Boxer SG (2011) Vesicle fusion observed by content transfer across a tethered lipid bilayer. Biophys J 101:L37–L39
55. Jahn R, Lang T, Südhof TC (2003) Membrane fusion. Cell 112:519–533
56. Groves JT, Boxer SG (2002) Micropattern formation in supported lipid membranes. Acc Chem Res 35:149–157
57. Erkan Y, Czolkos I, Jesorka A, Wilhelmsson LM, Orwar O (2007) Direct immobilization of cholesteryl-TEG-modified oligonucleotides onto hydrophobic SU-8 surfaces. Langmuir 23:5259–5263
58. Erkan Y, Halma K, Czolkos I, Jesorka A, Dommersnes P, Kumar R, Brown T, Orwar O (2008) Controlled release of Chol-TEG-DNA from nano- and micropatterned SU-8 surfaces by a spreading lipid film. Nano Lett 8:227–231

Chapter 7
Methodology

In this chapter I will give a general presentation of the experimental techniques used in the work presented in this thesis. A more detailed description can be found in the materials and methods sections of the amended papers. The chapter covers different varieties of optical spectroscopy, i.e., analytical techniques based on interaction between light and matter. For a discussion on the underlying principles behind this, see Chap. 4 on photophysics.

7.1 Absorption Spectroscopy

Absorption spectroscopy is in a sense the most fundamental of the different spectroscopic techniques since it only measures the investigated sample's interaction with light. Molecules that absorb light are commonly called chromophores. In absorption spectroscopy monochromatic light is passed through the sample. By measuring the difference in light intensity before and after the sample the absorbance can be determined according to Eq. 7.1, known as the Beer-Lambert law.

$$A(\lambda) = \log\frac{I_0}{I} = \varepsilon(\lambda)cl \tag{7.1}$$

Here $A(\lambda)$ i the absorbance, I_0 and I the intensity of the incident and transmitted light respectively, $\varepsilon(\lambda)$ the molar absorptivity, c the sample concentration and l the length of the sample cell. For a schematic overview of the experimental layout, see Fig. 7.1. Since the absorption is proportional to the concentration this method is a convenient way to determine the chromophore concentration in a sample. The molar absorptivity is related to the transition dipole moment of the absorbing part of the molecule as is normally expressed in $M^{-1}cm^{-1}$. As many physical and chemical interactions can affect the transition dipole moments of a chromophore, so do they also affect the molar absorptivity. Because of this, absorption measurements can be used, not only to detect the presence of the studied molecule, but

J. Hannestad, *Fluorescence in Bio-inspired Nanotechnology*, Springer Theses,
DOI: 10.1007/978-3-319-01068-7_7,

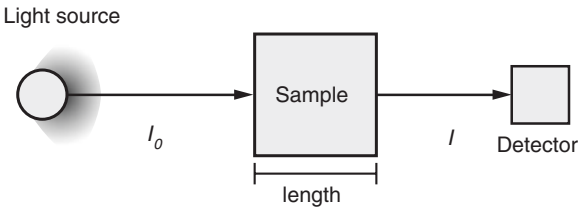

Fig. 7.1 Experimental setup for absorption spectroscopy consisting of *light source*, *sample* and *detector*. Transmitted light is measured by the detector

also to gain information on the properties of the molecule. In the work presented in the thesis, absorption spectroscopy in primarily used to verify the presence and to measure the concentration of the different active components is in the studied multi-chromophoric systems.

7.2 Fluorescence Spectroscopy

Fluorescence spectroscopy is a group name for a wide variety of techniques that relies on detection of emission from electronically excited molecules. Often, molecules are excited using light with a wavelength that corresponds to the energy of the first electronically excited state of the molecules. This basic principle is shared by most fluorescence-based experimental techniques. However, the similarities more or less end there. For convenience, I have divided the different techniques into three separate categories, each highlighting a different aspect of fluorescence spectroscopy. In the first category, steady state fluorescence, I describe the most fundamental way to perform a fluorescence measurement: a recording of the emission intensity from a bulk sample under continuous illumination. The second category focuses on time resolved fluorescence techniques, where samples are excited by pulsed light rather than continuous. In the third and final category, different aspects of fluorescence microscopy are discussed. This is by no means a guide to every possible way to detect fluorescence. Rather, it serves as an overview of the different techniques used in the work presented in this thesis.

7.2.1 Steady-State Fluorescence

In steady state fluorescence spectroscopy the molecules in a sample are excited using a continuous light source, conceptually similar to absorption spectroscopy. However, instead of measuring transmitted light, the light emitted from the sample is recorded. In the experimental setup, light source and detector are usually positioned so that emission is recorded perpendicular to the incident light (Fig. 7.2), this in order to minimize the amount of excitation light that reaches the detector. Using this arrangement, the steady state fluorescence intensity of the sample can

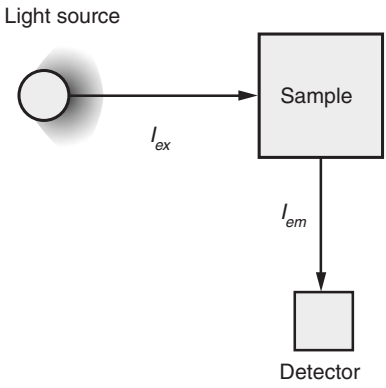

Fig. 7.2 Experimental setup for fluorescence spectroscopy. Emission is often detected perpendicular to the incident light

be recorded. The steady state intensity can be written as a function of the fluorescence lifetime according to Eq. 7.2.

$$I_{ss} = \int_0^\infty I_0 e^{-t/\tau} dt = I_0 \tau \tag{7.2}$$

where the factor I_0 depends on both the sample concentration and on instrumental parameters and τ is the fluorescence lifetime of the fluorophore. Since the equation involves a term that groups together a number of instrumental and environmental factors, it is of little practical use. In general, fluorescence measurements require more calibration than absorption measurements in order for them to be comparable with each other.

The molecular properties that determine the fluorescence intensity are the molar absorptivity and the fluorescence quantum yield. We discussed molar absorptivity in the previous section and its relation to fluorescence intensity is fairly simple: the more photons a fluorophore absorbs, the more fluorescent photons can be emitted. The fluorescence quantum yield (ϕ_f) is a measure of the fraction of the absorbed photons that are emitted as fluorescence.

It is possible to obtain structural information from fluorescence measurements. By illuminating the sample using polarized light, it is possible to exclusively excite molecules which absorption transition dipole moments are oriented in line with the polarization direction. If the fluorophores have unhindered rotational movement, the fluorescence will be depolarized since the rotational diffusion movement will randomize the direction in which fluorescence is emitted. However, if the rotational motion of the fluorophore is hindered in some way so that the orientational changes of the molecule are small during the fluorescence lifetime, the directional information will be retained. This is called fluorescence anisotropy and is a useful technique to investigate e.g., whether a ligand binds to a macromolecule or not. It is possible to measure fluorescence anisotropy using a steady-state set-up. However, the information revealed is fairly limited and can sometimes be misleading. I will therefore discuss fluorescence anisotropy more in detail when describing the time-resolved fluorescence techniques.

7.2.2 Time Correlated Single Photon Counting

Emission from fluorophores contains more information than the mere intensity provided by steady state measurement. By recording the fluorescence decay of a sample it is possible to measure e.g., sample heterogeneities or conformational changes during the excited state lifetime. Time Correlated Single Photon Counting (TCSPC) is one technique that enables the acquisition of time resolved fluorescence data. There are other similar but different techniques the does more or less the same thing such as e.g., streak camera systems. However, TCSPC is the technique that has been used in work presented in here. I will therefore limit the discussion to it.

Time correlated single photon counting works by recording the temporal difference between the laser pulse used to excite the sample and the detection of a single photon emitted by the sample. The timing in the TCSPC setup works in a start-stop fashion. When a laser pulse is detected, either directly through the laser driver electronics or through the use of a photodiode, a time-to-amplitude converter, TAC, is started. The TAC is then stopped when a photon is recorded by the detector. Using a suitable delay of the trigger signal, the same pulse can be used both for the start and stop signal eliminating effects from pulse period jitter. The voltage from the TAC is sent to an analog to digital converter, ADC, converting the voltage to a time stamp. The output is stored in one of a multichannel photon counting module. The signal from the ADC corresponds to the separation in time between the start and the stop photons. The number of detected photons in a time channel is proportional to the fluorescence intensity at that time. By creating a histogram over the number of photons in each time channel a representation of the actual fluorescence decay is obtained. This principle is illustrated in Fig. 7.3.

Time correlated single photon counting relies on the fact that only one photon at a time is detected for each signal period. At high light intensities there is a slight probability for two photons to be recorded. This will cause so called “pile-up” effect which favors the detection of early photons resulting in a distorted waveform. To avoid this, the intensity of light that reaches the detector is set so that the count rate is no more than approximately 1 % of the repetition rate.

When measuring the fluorescence decay of a sample two data sets are generally recorded, each with 10,000 counts in the top channel to get sufficient statistical quality. One of the sets is of the fluorescence decay of the sample, i.e., the actual measurement. The other is the instrument response function (IRF), i.e., the shape of the exciting pulse as seen by the detector. The IRF is measured by directing the excitation light to the detector, usually by using a scattering solution. The temporal resolution of TCSPC is primarily determined by the detector and the width of the time channels (witch in turn, is the width of the time window divided by the number of channels used). When measuring the sample decay what is actually seen is the convolution of the fluorescence decay of the excited molecule and the IRF, as described in Eq. 7.3,

$$N(t) = \int_0^t I(t-u)IRF(\mu)d\mu \tag{7.3}$$

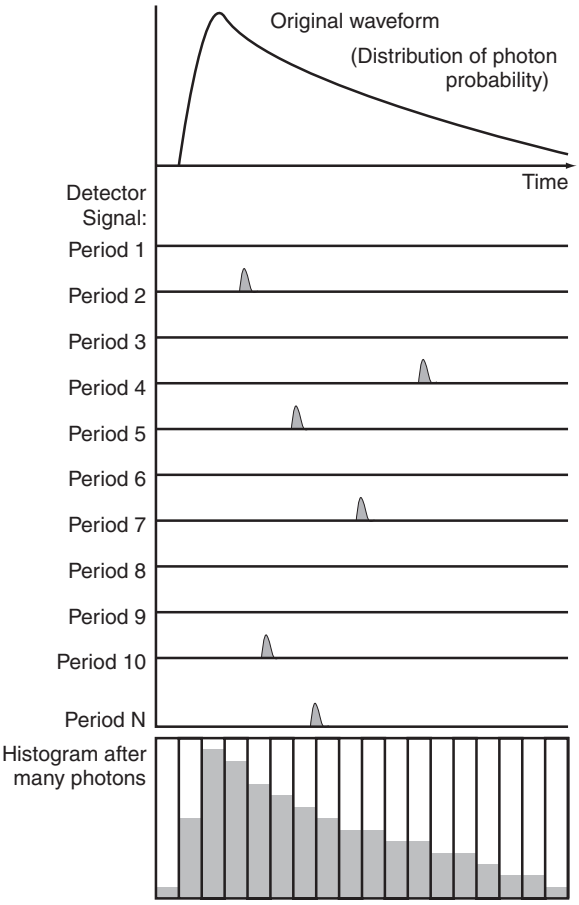

Fig. 7.3 Working principle for time correlated single photon counting. A statistical representation of the actual decay is obtained from the summation of individual photon counts

where N is the measured decay, I is the actual fluorescence decay and *IRF* is the instrument response function. Using the recorded IRF the measured data can be deconvoluted and the actual decay can be obtained. If the excited state lifetime is much longer than the FWHM of the IRF, the pulse shape has little influence on the sample decay, which can then be fitted directly without deconvolution. The fluorescence decay is usually fitted to a sum of exponentials as in Eq. 7.4.

$$I(t) = I_0 \sum_i \alpha_i \exp(-t/\tau_i) \tag{7.4}$$

Here, $I(t)$ is the fitted fluorescence decay, I_0 the intensity at time 0, a_i the fractional amplitude and t_i the corresponding excited state lifetime.

It is now time to return to the discussion on fluorescence anisotropy that was initiated in the previous section. Just as the population of the excited state decays exponentially, so does the sample anisotropy. Starting at a maximum anisotropy

directly following excitation, the directional information decays down to a completely isotropic state. In Eq. 7.5, the anisotropy decay law is presented.

$$r(t) = r_0 \sum_j g_j \exp(-t/\theta_j) \tag{7.5}$$

In this expression *r(t)* is the sample anisotropy, r_0 the fundamental anisotropy, g_j fractional amplitudes and θ_j rotational correlation times, Note that is possible for a sample to have multiple rotational correlation times, hence the sum of exponentials.

Fluorescence anisotropy is recorded by measuring the fluorescence intensity while varying the polarization of both the excitation and emission according to Eq. 7.6,

$$r_m(t) = \frac{I_{VV}(t) - GI_{VH}(t)}{I_{VV}(t) + 2GI_{VH}(t)} \tag{7.6}$$

where *V* and *H* denote vertical and horizontal polarization direction, respectively, written excitation direction first. The G-factor is the ratio I_{HV}/I_{HH} and compensates for inequalities in detection efficiencies with respect to polarization direction. Note that the intensities in Eq. 7.6 are the experimentally recorded intensity decays. The calculated anisotropy must therefore be subject to deconvolution analysis.

There are several important differences between the time resolved anisotropy analysis and the steady state one. The steady state anisotropy value does not reveal any sample heterogeneities. Therefore, the system anisotropy determined through steady state measurements might not actually represent the true correlation times. Further, it is important that the fluorescence decay and anisotropy decay occur on the same time scale. If the fluorescence decay is much faster than the anisotropy decay, the steady state anisotropy will be high. On the other hand, if the fluorescence decay is slow, the steady state anisotropy will be low. The actual rotational correlation time might be exactly the same in these two cases even though they have completely different steady state anisotropies.

7.2.3 Fluorescence Microscopy

In papers IV and V we use fluorescence microscopy to detect the hybridization of DNA strands anchored to lipid monolayer films. Fluorescence microscopy is a convenient tool to study molecules confined to a surface or to a defined region in space such as a cell or vesicle. Using bright fluorophores and sensitive detectors fluorescence from single molecules can be detected. The basic fluorescence microscopy is comprised of a light source for excitation, an objective to focus the light on the sample and a detector to measure the fluorescence form the sample. The microscope objective is not only used to focus the excitation light on the sample, but also to collect the fluorescence from the sample. Depending on the setup in use, a number of auxiliary components such as filters, pinholes and dichroic mirrors are also used.

When light is focused through the microscope objective a Gaussian circular pattern known as Airy disk is formed at the focal spot. Concentric circles of lower intensity surround the central bright intensity region. Together, they form a so-called, Airy pattern. The size of the Airy disk is determined by the diffraction of light caused by the microscope objective. In optical microscopy the obtained resolution is governed the size of the Airy disk, which depends on the numerical aperture, *NA*, of the objective in use and the wavelength of the diffracted light. This relationship can be expressed using Abbe's law, given in Eq. 7.7.

$$d = 0.61\frac{\lambda}{NA} \tag{7.7}$$

In this expression, d is the minimum resolvable distance, λ is the wavelength of the incident light and *NA* is the numerical aperture of the microscope objective. During the last 10 years, several techniques have emerged that overcome this resolution limit. We will return this subject later in the section.

Two principally different microscopy techniques are wide field and confocal microscopy. In a confocal microscope the excitation light is focused at diffraction limited spot of the sample. The fluorescence is collected through the objective and a pinhole is used to reject the out of focus light. The light is then focused at a point detector such as an avalanche photo diode (APD). Using a motorized stage the sample can be scanned and a composite image can be created. However, a confocal microscope can also be used just to collect fluorescence intensity from a single spot without generating an image. Figure 7.4 shows a general instrumental setup. The benefits of confocal microscopy are the possibility to generate images with contrast since only light from the focal plane is recorded. A drawback is that, when imaging, the temporal resolution is limited to the scanning speed. This makes it difficult to image fast processes occurring over larger areas.

In the other method, wide field microscopy, the laser light is not focused in a diffraction-limited spot of the sample, but instead used to illuminate a larger area containing multiple fluorophores. The wide-field illumination is obtained by focusing the laser light used for excitation at the back focal plane of the microscope objective using a pre-focusing lens. An array detector such as a CCD camera is used for detection. Figure 7.5 shows the schematic setup of a wide field fluorescence microscope. The advantage of using wide field detection is that sample dynamics can easily be followed in the illuminated field. In wide-field techniques, temporal resolution is set by the frame rate of the detector rather than by the scanning speed, as is the case in a scanning confocal setup. A drawback is that, since there is no pinhole rejecting the out of focus light, the contrast is lower compared to a scanning confocal microscope. The contrast in wide field microscopy can be improved by working in total internal reflection (TIR) mode. In TIR laser light used for excitation is not passed through the microscope objective at the objective normal. Instead, it is directed so that the angle of incidence exceeds the critical angle for going from a medium with higher (e.g., glass) refractive index to one with lower (e.g., water). This will cause the light to be completely reflected at the interface. However, light can still interact with the sample at the interface

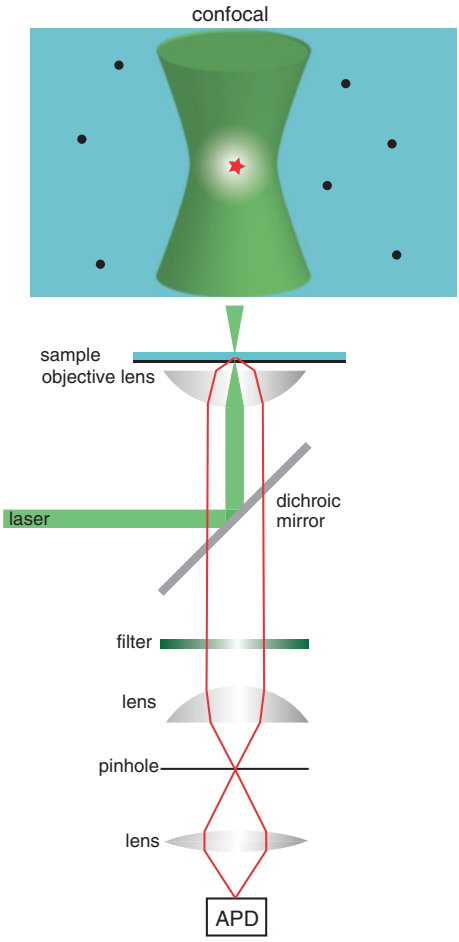

Fig. 7.4 Confocal fluorescence microscope. Excitation light is focused to a diffraction-limited spot and collected fluorescence is passed through a pinhole to filter out out-of-focus light before being focused at a point detector

through an evanescent wave that penetrates a short distance (typically sub-wavelength) into the sample. Since, excitation light only reaches a few hundred nanometers into the sample, there is no background emission from the complete, out of focus, sample volume, which greatly enhances the contrast. However, the total internal reflection fluorescence technique can only be applied when the studied molecules are positioned close to the cover slide surface.

With the development of new high performance detectors and bright and photostable dyes, the boundaries of fluorescence microscopy has been pushed down to the detection of single emitters. Single molecule fluorescence microscopy is a powerful technique to study heterogeneities in an ensemble of molecules that are averaged out in bulk measurements and to detect rare events. This is especially important when creating devices designed to function at a single molecule level. The field of single molecule fluorescence spectroscopy has grown immensely

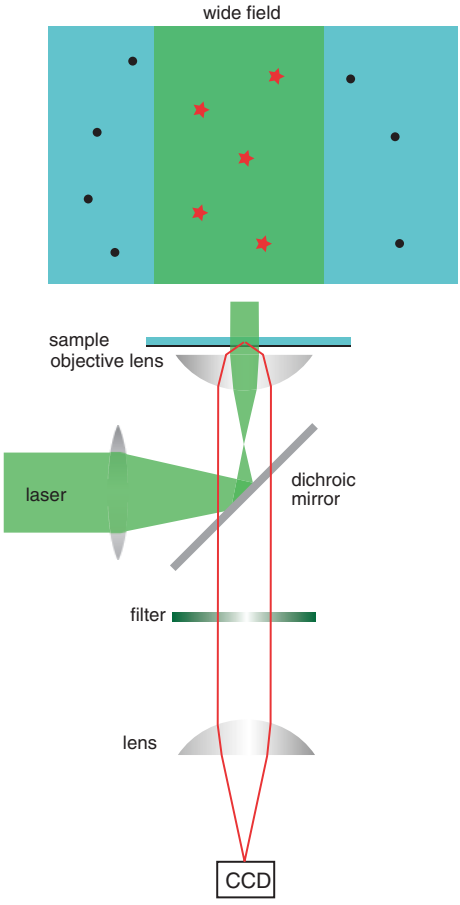

Fig. 7.5 Wide field fluorescence microscope. An expanded laser beam is focused at the back focal plane of the objective using a pre-focusing lens. Fluorescence is collected through the objective and focused at a CCD chip

since the initial demonstrations of single molecule detection in solution by Keller and co-workers in 1990 [1]. I will not try to give an overview of the wide variety of techniques that exists, but rather outline the underlying principles. For those interested of a more in-depth coverage of the research field, there are several comprehensible reviews published on the subject [2, 3].

In principle, single molecule techniques do not differ from ensemble microscopy techniques. The microscope set-ups look the same and consist of the same basic components. However, detection of individual emitters put high performance requirements on all parts of the system. High quality lasers and objectives with high numerical aperture are required to obtain high spatial resolution. Samples need to be free from impurities contributing to background emission. High quality filters that effectively remove scattered light while transmitting as much of the fluorescence as possible are also needed. Further, detectors need to have a low noise and high quantum efficiency, i.e., the need to have an efficient photon to current conversion.

Fluorophores to be used for single molecule detection need to be both bright (i.e., have high molar absorptivity and quantum yield) and photostable. In single molecule fluorescence experiments, the imaged fluorophores need to undergo many excitation and de-excitation cycles in order to generate enough fluorescence photons to enable detection. Even with a moderately low quantum yield for excited state reactions, photobleaching, i.e., irreversible photochemical destruction of the dye, will be an issue. Another issue that needs attention is inter-system crossing to a triplet state. Since triplets are generally long-lived compared to singlets and often non-emissive, this is equivalent to turning off the fluorescence. This process is generally referred to as blinking as fluorescence can be recovered, in contrast to the irreversible process of photobleaching. In order to combat these effects, additives that minimize both blinking and photobleaching have been developed [4, 5].

One of the more important advances in fluorescence microscopy during the last 10 years has been the development of super-resolution techniques. Since many intracellular components have dimensions that are smaller than the minimum resolvable distance offered by optical microscopy there has been a need in e.g., bio-imaging for techniques that enables imaging of smaller structures. Although super-resolution techniques are not used for any of the papers presented in the thesis, they are likely to be used in future work in many of the projects and are therefore worth mentioning.

Two principally different super-resolution techniques that have been widely used are STED [6, 7], developed by Stefan Hell, and the stochastic techniques PALM [8] and STORM [9, 10]. STED, which is an acronym for stimulated emission depletion microscopy, is based on the combination of two different laser lines of different wavelength. The first laser line is used to excite the molecules in the sample while the second induce stimulated emission. The second laser line is passed through a wave-plate creating a donut-shaped beam. When the two beams are overlapped, only the central hole-region of the combined beam will contribute to excitation of fluorophores in the sample. By varying the intensity of the donut beam, the size of the hole can be controlled enabling the creation of an excitations spot considerably smaller that the diffraction limit.

PALM and STORM are acronyms for two, more or less identical techniques, relying on stochastic activation of fluorophores in a sample. Since the Airy disk has an essentially Gaussian profile, it is fairly straightforward to find the center of emission of the recorded fluorescence from single emitters. By making the assumption that the center of emission corresponds to the position of fluorophore, it is possible to determine its position with a precision that is higher than the diffraction limit. This procedure relies on the fact that it is possible to isolate the emission from single fluorophores. However, if one wants to image something like an intracellular structure, labeling with multiple fluorophores is needed. By working under conditions that lead to stochastic activation of only a few fluorophores at a time, it is possible to combine dense labeling with single molecule positioning. There are several ways to achieve stochastic activation of fluorescence, one way is to use photoswitchable dyes. Buffer conditions can also be set to stimulate blinking. Much work is being put into the design of novel dyes suitable for super-resolution imaging e.g., by enabling controlled switching between bright and dark states [11–13].

References

1. Shera EB, Seitzinger NK, Davis LM, Keller RA, Soper SA (1990) Detection of single fluorescent molecules. Chem Phys Lett 174:553–557
2. Tinnefeld P, Sauer M (2005) Branching out of single-molecule fluorescence spectroscopy: challenges for chemistry and influence on biology. Angew Chem Int Ed 44:2642–2671
3. Weiss S (1999) Fluorescence spectroscopy of single biomolecules. Science 283:1676–1683
4. Vogelsang J, Kasper R, Steinhauer C, Person B, Heilemann M, Sauer M, Tinnefeld P (2008) A Reducing and oxidizing system minimizes photobleaching and blinking of fluorescent dyes. Angew Chem Int Ed 47:5465–5469
5. Rasnik I, McKinney SA, Ha T (2006) Nonblinking and longlasting single-molecule fluorescence imaging. Nat Methods 3:891–893
6. Hell SW, Wichmann J (1994) Breaking the diffraction resolution limit by stimulated-emission—stimulated-emission-depletion fluorescence microscopy. Opt Lett 19:780–782
7. Klar TA, Jakobs S, Dyba M, Egner A, Hell SW (2000) Fluorescence microscopy with diffraction resolution barrier broken by stimulated emission. Proc Natl Acad Sci USA 97:8206–8210
8. Betzig E, Patterson GH, Sougrat R, Lindwasser OW, Olenych S, Bonifacino JS, Davidson MW, Lippincott-Schwartz J, Hess HF (2006) Imaging intracellular fluorescent proteins at nanometer resolution. Science 313:1642–1645
9. Rust MJ, Bates M, Zhuang XW (2006) Sub-diffraction-limit imaging by stochastic optical reconstruction microscopy (storm). Nat Methods 3:793–795
10. Heilemann M, van de Linde S, Schuttpelz M, Kasper R, Seefeldt B, Mukherjee A, Tinnefeld P, Sauer M (2008) Subdiffraction-resolution fluorescence imaging with conventional fluorescent probes. Angew Chem Int Ed 47:6172–6176
11. Dempsey GT, Vaughan JC, Chen KH, Bates M, Zhuang X (2011) Evaluation of fluorophores for optimal performance in localization-based super-resolution imaging. Nat Meth 8:1027–1036
12. Grotjohann T, Testa I, Leutenegger M, Bock H, Urban NT, Lavoie-Cardinal F, Willig KI, Eggeling C, Jakobs S, Hell SW (2011) Diffraction-unlimited all-optical imaging and writing with a photochromic Gfp. Nature 478:204–208
13. Heilemann M, Dedecker P, Hofkens J, Sauer M (2009) Photoswitches: key molecules for sub diffraction-resolution fluorescence imaging and molecular quantification. Laser Photon Rev 3:180–202

Chapter 8
Summary of Publications

This chapter covers the papers which make up the foundation of this thesis. The papers can be found through the references on page III. Many of the themes have already been discussed in the previous chapters and I will refer back to these discussions and also try to bring in some new aspects. I have decided to divide the chapter into three parts covering three different themes. The first part covers the work presented in papers I and II. Here, focus is on creating DNA-based multi-chromophoric systems for directional, long-range energy transfer, either in the form of a wire or as a two-dimensional network. The second part describes the construction of a DNA-based light-harvesting device using intercalated YO-PRO-1 as donors and a membrane anchored porphyrin as acceptor. This part covers work presented in paper III. Finally, the third part presents work from papers IV and V. Here, investigations into duplex formation of complementary DNA molecules tethered to lipid monolayers are discussed. In papers IV and V, fluorescence is mainly used as an indirect probe. However, in papers I-III, fluorescence is an integral part of the studied systems. Here, fluorescence makes the transition from probe, to function.

8.1 Photonic Wires (Papers I and II)

How can we design a photonic wire with high end-to-end efficiency that does not suffer from incomplete assembly as described by Sauer and co-workers? [1]. In the previous discussion on photonic wires (Chap. 5.2), we only considered covalently linked fluorophores whose positions were well defined. However, photonic wires can also be created using fluorophores that interact non-covalently with a wire scaffold. In paper I we construct a wire where the mediating part of the wire bind non-covalently to DNA with the aim of creating a system with reduced complexity and increased degree of self-assembly [2].

For a DNA-based wire there are two principal ways in which a fluorophore can associate with the DNA strand to assemble the wire, either through intercalation or by binding to the major or minor groove. In the cases where the dyes are

J. Hannestad, *Fluorescence in Bio-inspired Nanotechnology*, Springer Theses,
DOI: 10.1007/978-3-319-01068-7_8,

not covalently bound to specific positions in the DNA strand, there is no control of fluorophore distribution; it is therefore only possible to create a photonic wire based on this approach with dyes capable of homo-FRET.

In our wire construct, we use the fluorophore combination of Pacific Blue, YO-PRO-1 (YO) and Cy3 to assemble a photonic wire capable of long range, directional energy transfer. The wire consists of a linear DNA duplex, either a 20-mer or a 50-mer, with an injector fluorophore in one end and a detector fluorophore Cy3 in the other end. The intercalator YO mediates energy transfer from Pacific Blue to Cy3 by means of homo-FRET. A schematic image of the assembled wire is presented in Fig. 8.1. Because the intercalation of YO is not sequence specific there is no control of the positioning of the mediating units. However, it also enables the wire to be loaded with a large number of fluorophores creating a strong connection due to short fluorophore–fluorophore distances.

Figure 8.2 shows emission spectra for different conformations of the wires following excitation of the injector fluorophore Pacific Blue. Without added YO, the emission is dominated by Pacific Blue. For the 20-mer wire, there is a slight effect of direct Pacific Blue to Cy3 energy transfer as can be seen from the hint at a peak around 570 nm. When YO is added to the wires two things happened. One effect is that we observe a quenching of Pacific Blue together with the appearance of a peak at approximately 510 nm corresponding to YO emission. This shows that there is energy transfer from Pacific Blue to the YO-part of the wire. The second effect is that there is an increase in the Cy3 emission. This effect is seen for both the 20- and 50-mer wire. However, it is more pronounced for the 20-mer wire. The emission from Cy3 also increases with increased YO concentration. These effects in combination tell us that there is end-to-end energy transfer going from Pacific Blue to Cy3 via the mediator YO. In order to make sure that the observed Cy3 emission is not an effect of direct excitation, we performed the same experiments with wires lacking the injector fluorophore Pacific Blue. In the 20-mer case, the

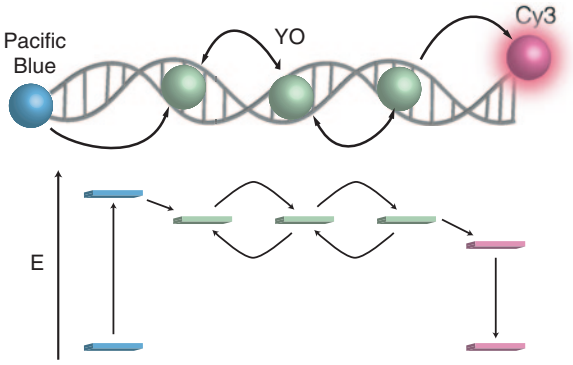

Fig. 8.1 Photonic wire with *Pacific Blue* as primary donor and Cy3 as final acceptor. The intercalator YO-PRO-1 (YO) acts as mediator. Energy transfer between individual mediators is non-directional

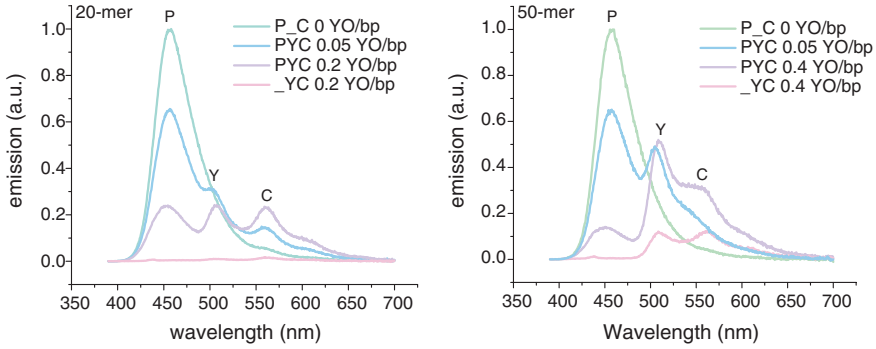

Fig. 8.2 Emission spectra for 20-mer and 50-mer wire following 380 nm excitation. The letters *P*, *Y* and *C* denote peaks corresponding to emission from *Pacific Blue*, YO and Cy3, respectively. The legend shows which dyes are present in each sample. PYC, P_C and _YC indicate samples where all dyes are present, YO is lacking and *Pacific Blue* is lacking, respectively

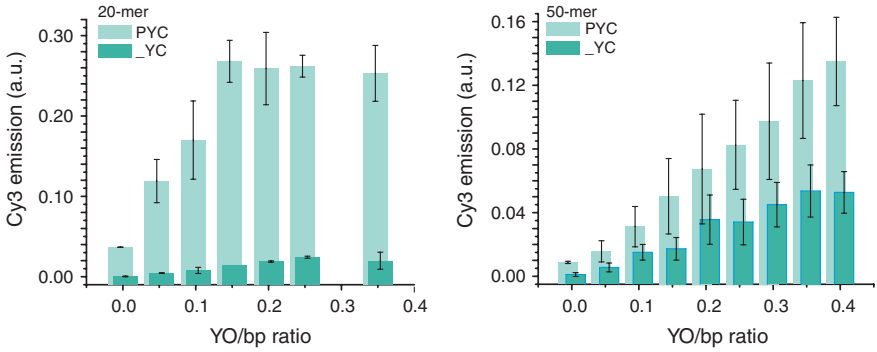

Fig. 8.3 Average extracted Cy3 emission following 380 nm excitation for 20 and 50-mer wire with and without *Pacific Blue*. The legend shows which dyes are present in each sample. PYC indicate samples where all dyes are present and _YC indicate samples where *Pacific Blue* is lacking. The *error bars* represent the standard deviation

wires showed virtually no Cy3 emission at any of the tested loading ratios. For the 50-mer wires, an increased Cy3 emission with increasing YO concentration was observed. However, the levels were lower than for the corresponding wire with Pacific Blue. Extracted Cy3 emission for wire with and without Pacific Blue at different YO concentration is shown in Fig. 8.3.

In addition to performing fluorescence measurements, we also simulated wire performance using a Markov chain model. The model was developed by Albinsson and co-workers to describe fluorescence depolarization due to homo-FRET is systems of DNA-associated fluorophores [3]. A brief description of the model is provided in Sect. 4.3.2. Simulation results for 20-mer and 50-mer wires are shown

together with experimentally determined energy transfer efficiencies. The energy transfer efficiency is determined from experiments by comparing the amount of excitation energy arriving at Cy3 with the amount of excitation energy that was used to excite Pacific Blue according to Eq. 8.1

$$E = \frac{(F_{CP} - F_C)/Q}{F_P/Q_P} \tag{8.1}$$

where F_{CP} and F_C are the emission intensities from Cy3 in the presence and absence of Pacific Blue, respectively. Q_C is the Cy3 quantum yield and Q_P is the Pacific Blue quantum yield. Finally, F_P is the Pacific Blue fluorescence intensity.

In this kind of wire, the end-to-end efficiency as a function of intercalator density follows approximately a sigmoidal function (Fig. 8.4). For shorter wires, the initial lag-phase is non-existent, as energy transfer between Pacific Blue and Cy3 exists to some extent even without mediators. As intercalators are added to the system the end-to-end energy transfer efficiency immediately starts to increase to finally level out at higher mediator densities. For a 20-mer wire this plateau level is reached at approximately 0.15 YO-PRO/base pair giving a 90 % end-to-end energy transfer efficiency. Ideally, the maximum efficiency would be 100 %. However, this would require a high loading of mediators with almost perfect delocalization of the excitation across the whole wire. Assuming nearest neighbor exclusion there is a finite limit to how dense the mediating units can be packed in the DNA-based photonic wires. In a short wire, this might be sufficient to obtain end-to-end transfer of excitation energy with 100 % efficiency. However, as more and more intercalator dyes are added to the system the influence

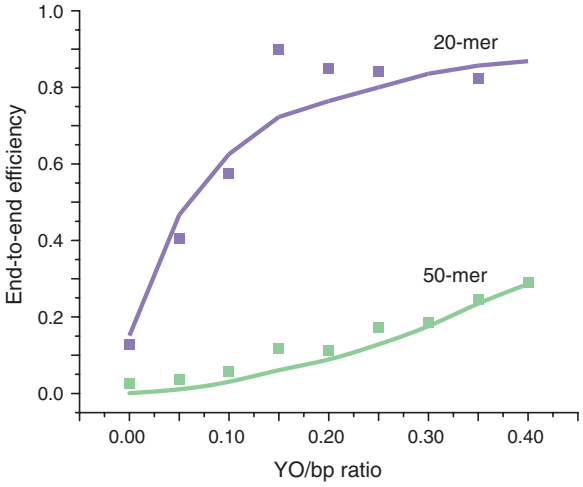

Fig. 8.4 Experimental (*squares*) and simulated (*lines*) end to-end energy transfer efficiencies for 20-mer (*purple*) and 50-mer (*green*) photonic wires

of alternative binding modes, other than intercalation, become important [3]. With higher mediator loading there is also an increased probability that two intercalating molecules that are in close proximity form energetic sinks that hinder the propagation of excitation energy. These trap states prevents 100 % efficiency from being practically obtainable. For a longer wire (e.g., 50-mer), a low number of mediators is not sufficient to achieve connection between input and output dyes. Therefore, an initial lag phase is observed with no increase in end-to-end transfer efficiency with increasing mediator density. In the case of the 50-mer wire, the connection between input and output of the wire is not strong enough to obtain a limit where the increase in transfer efficiency levels off with increasing mediator density, even when the intercalator concentration approaches the maximum value of 0.5 YO-PRO/base pair. For the 50-mer wire, a maximum of 30 % end-to-end energy transfer efficiency is obtained at 0.4 YO per base pair. The perhaps most important result from this paper is that we show that, using our wire design, it is possible to obtain end-to-end excitation energy transfer over distances above 20 nm. This is well above the limit for single-step FRET and cover a wide range of nanostructures.

As for the photonic wire created by Quake and coworkers [4], the homo-FRET nature of the wire depends on the length of the DNA strands. In the case of the short 20-mer wire, end-to-end transfer is essentially a two-step process combining Pactific Blue to YO FRET and YO to Cy3 FRET. This is reflected by the rapid increase in efficiency observed for the 20-mer wire. However, as the mediator inserts randomly into the DNA strand there is no controllable way to obtain wires showing strict two-step FRET. For the longer wire, the separation between Pacific Blue and Cy3 is too large for one intercalated YO to bridge the input and detector fluorophores. Instead, excitation energy has to hop between multiple mediator molecules in a diffusive fashion.

The non-covalent approach brings up other important aspects that need to be considered in the case of nanoscale technology: self-assembly and bottom-up design. Non-covalent association of the constituting fluorophores means that the creation of the wire requires fewer controlled linkage steps forcing the fluorophores into their correct positions. For more complex systems, extensive modifications are a limitation.

In an effort to tackle the uncertainties associated with the non-specific binding of YO-PRO to DNA and to create a more programmable photonic wire Burley and co-workers have constructed system where the YO-PRO mediator binds to a specific base pair sequence. This is achieved by tethering the fluorophore to pyrrole-imidazole polyamides (PA) [5]. The polyamides were initially constructed in by the Dervan group and bind to the minor groove specifically targeting the sequence 5′-WWGGWCW-3′, where W is either adenine or thymine [6, 7]. Through the specific binding of the PAs to DNA the intercalation of YO-PRO can be directed to a certain binding site.

A downside with this method to obtain sequence specificity is that it involves a reduction in the possible mediator density. As the binding motif for the polyamide moiety responsible for the sequence specificity is larger than the base pair

occupancy of one YO-PRO molecule, it is not possible to pack the intercalators as closely as if they were binding randomly to the DNA strand. Thus, the major advantage of the sequence specific binding mainly appears at low mediator concentrations when it is possible to achieve a much more favorable intercalator distribution by controlling their positions in the wire. Burley and co-workers constructed three different wire lengths, one 21-mer, one 55-mer and one 80-mer having one, four and six binding sites, respectively. An asymmetric core polyamide, recognizing the sequence 5′-ATGGACA-3′ was selected, both for its high binding affinity to DNA as well as for its directional binding. The YO intercalator is attached to the PA by a tether with a length corresponding to two base pairs. This means the total binding site size is 9 base pairs, in addition to the space occupied by the intercalator itself. The photonic wire was assembled using Pacific Blue as donor, YO as mediator and Cy3 as acceptor, similar to the self-assembled wire we constructed. The effect of the sequence specific mediator binding was investigated by comparing the enhanced emission of Cy3 upon Pacific Blue excitation with YO added to the system, both for wires with and without sequence specific mediator binding. Adding one equivalent of the sequence specific YO assembly to the 21-mer DNA-wire results in a threefold increase of Cy3 emission, compared to when a randomly binding YO assembly is added. Because the emission intensities from Pacific Blue and YO were comparable in both cases, the Cy3 enhancement is attributed to increased efficiency for the transfer of excitation energy from YO to Cy3. The increase in energy transfer efficiency for the 21-mer wire that is associated with directed mediator binding is not surprising. Since a distance of 10–11 base pairs is well within single-step FRET distance, there is only need for a single, correctly placed, mediator molecule to enable the two-step end-to-end energy transfer (i.e., Pacific Blue-YO-Cy3). When mediators bind randomly, many, less efficient, conformations are enabled. Thus, a higher loading is required when the mediators bind randomly to achieve efficient end-to-end transfer. Increasing the concentration of randomly binding YO to 3 equivalents resulted in Cy3 emission levels comparable to those of the sample with sequence specific binding. However, this also resulted in a fourfold enhancement of the YO emission, indicating that many of the YO molecules bind in positions not favoring end-to-end FRET. For the longer wire lengths (55-mer and 80-mer), there is a substantial influence of YO to YO homo-FRET in the end-to-end energy transfer process. For the 55-mer, and intercalator concentration of four equivalents (i.e., one intercalator per binding site) results in a two-fold increase in the Cy3 emission for the sequence specific YO-PA-sample compared to the sample with non-specific binding of YO. Compared to the 21-mer, a substantial amount of excitation energy is trapped in the YO part of the 55-mer wire, both for the sample with and without sequence specific binding of YO. This effect is reflected in the efficiency of the YO-PA wires, which is 49 and 26 % for the 21-mer and the 55-mer wires, respectively. For an 80-mer wire (with 6 equivalents of YO-PA) the enhancement decreases further to 1.5 and the resulting end-to-end efficiency is 14 %. Thus the advantage of sequence specific binding decreases with increasing wire length. Instead, the footprint of the polyamide unit becomes disadvantageous since it prevents dense

packing of mediator dyes. However, it is clear that programmable binding of mediator molecules substantially enhances energy migration at low binding densities.

Besides sequence specific binding, there is another way that the arrangement of the communicating fluorophores can be controlled to achieve higher FRET efficiency. The relative orientation of donor and acceptor dyes strongly influences the energy transfer efficiency. In DNA, the orientation will depend on the turning of the DNA helix, and thus of the number of base pairs separating the donor and acceptor molecules. The effect of this has been shown both for a FRET pair based on nucleic acid base analogs [8] and also for the FRET pair Cy3 and Cy5 [9]. In both cases the decrease in FRET efficiency due to donor–acceptor separation along the DNA axis is modulated by the orientation effect emanating from the turn of the DNA helix. A similar effect was observed in single molecule studies of fluorophores bound to DNA origami structures [10]. Because most covalently bound fluorophores utilizes flexible linkers to attach the fluorophore to the DNA, the orientation effect is not as apparent for all DNA-based FRET systems. However, achieving a controlled orientation of the mediating fluorophores that favors FRET can greatly enhance the efficiency of the wire construct. To illustrate, a change from randomly oriented donor and acceptors ($k^2 = 2/3$) to donor and acceptor with head-to-tail orientation ($k^2 = 4$) corresponds to a 35 % increase in R_0.

An important practical consideration in the case of wires based on the homo-FRET principle with a large number of mediator units connecting injector and detector dyes is the probability for direct excitation of the mediating part of the wire. As wires grow in length, the number of mediator units needed to achieve end-to-end energy transfer increases. Thus, the collective absorptivity of the mediator part of the wire increases with increasing length. This means that, if there is any probability for directly exciting the mediator dye at the injector excitation wavelength, the effect of one-step transfer from the mediator to the detector dye will be more pronounced the longer the wire is.

After constructing a self-assembled photonic wire we decided in paper II to expand the concept by incorporating the wire design in a multi-dimensional assembly [11]. Here, fluorophores are attached to a hexagonal DNA assembly with arms extending from the nodes of the hexagon. The DNA hexagon was designed by Nordén and co-workers aiming at creating a nanoscale DNA structure with addressability on the single base pair level [12]. The features of this structure were discussed in greater detail in Sect. 3.1.1. The hexagonal structure is used to create a photonic device with one input fluorophore and two, spatially and spectrally separate, output fluorophores (Fig. 8.5a). The fluorophore composition is the same as for the photonic wire previously discussed, with the addition of fluorescein. Here, Pacific Blue functions as the input fluorophore while fluorescein and Cy3 are the two output fluorophores. All three fluorophores are added to the assembly through covalent attachment to 10-mer oligonucleotides that binds to the single stranded 10-mer extensions of the hexagon. Pacific Blue is an efficient FRET donor to Fluorescein but requires a mediating chromophore to donate excitation energy to the other output dye, Cy3. Just as with the wire, a mediating dye, in the form of YO, is utilized to make the Pacific Blue to Cy3 FRET efficient. This way

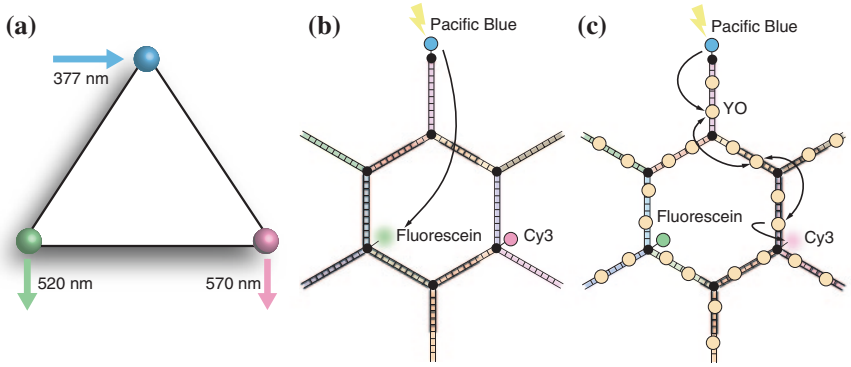

Fig. 8.5 **a** Photonic network with one input and two spatially and spectrally separate output. **b** Assembly without YO primarily directs excitation energy to Fluorescein. **c** When YO is added to the system, excitation energy is directed to Cy3

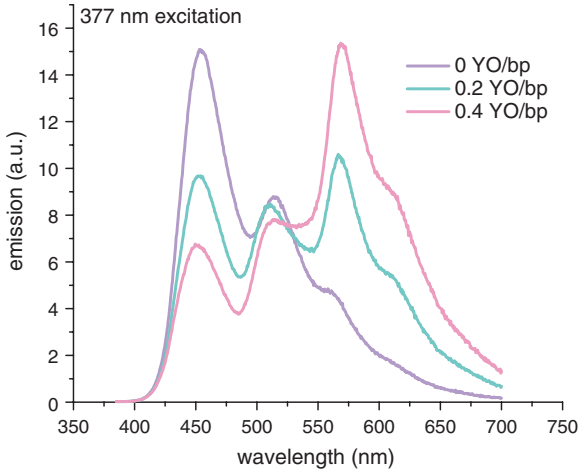

Fig. 8.6 Emission spectra for different network constructs. Without YO present, system emission comes from *Pacific Blue* and *fluorescein*. When YO is added, *Pacific Blue* is quenched and Cy3 emission is enhanced

it is possible to use mediator binding as a means to select which output in the multichromophoric system that will be active. In the absence of YO, excitation energy is transferred to fluorescein (Fig. 8.5b), while in the presence of YO the excitation energy is transferred to Cy3 (Fig. 8.5c).

Figure 8.6 shows emission spectra for different network constructs excited at 377 nm. When no YO is present, emission from fluorescein is observed. The energy transfer efficiency is approximately 0.57 and the system shows substantial remaining emission from Pacific Blue. There is also detectable Cy3 emission. This

is due to both direct Pacific Blue to Cy3 FRET and fluorescein to Cy3 FRET. As YO is added, Pacific Blue is further quenched and emission from Cy3 increases. Although YO is added to the system, there is no increase in the emission in the region around 510 nm which is shared between fluorescein and YO. This is indicates that the switching mechanism is effective.

By extracting fluorescein and Cy3 from the emission spectra, it is possible to estimate the relative intensity of the two fluorophores. The results show that emission from the system, following excitation of Pacific Blue, is dominated by fluorescein when no YO is present. As YO is added, Cy3 emission becomes dominant (Fig. 8.7a). The contrast between the state dominated by fluorescein and the state dominated by Cy3 emission is diminished to some extent because of two factors: direct energy transfer between Pacific Blue and Cy3, and energy transfer between fluorescein and Cy3. The emission from Cy3 also increases with increasing YO concentration, with approximately 0.35 and 0.5 end-to-end FRET efficiency at 0.2 and 0.4 YO per base pair, respectively (Fig. 8.7b). Just as in the case of the photonic wire comprising the fluorophores Pacific Blue, YO and Cy3 (vide supra), the excitation energy that is transferred between Pacific Blue and Cy3 is mediated by YO in a diffusive manner. The difference is that the fractal dimensionality of the hexagonal assembly contains more stray paths where excitation energy can be lost, than the one-dimensional wire, where the excitation energy only can travel along the path connecting the initial donor and the terminal acceptor. Therefore, there needs to be a strong connection, i.e., rapid diffusive energy migration, for end-to-end energy transfer to be efficient. Thus, compared to the wire, the hexagon requires high loading of mediators for successful Pacific Blue to Cy3.

In addition to the fluorescence measurements, the multi-chromophoric system was also investigated using the Markov chain model described above. As with the photonic wire, there is good agreement between experimentally determined energy transfer efficiencies and simulation results. The simulations show that the energy

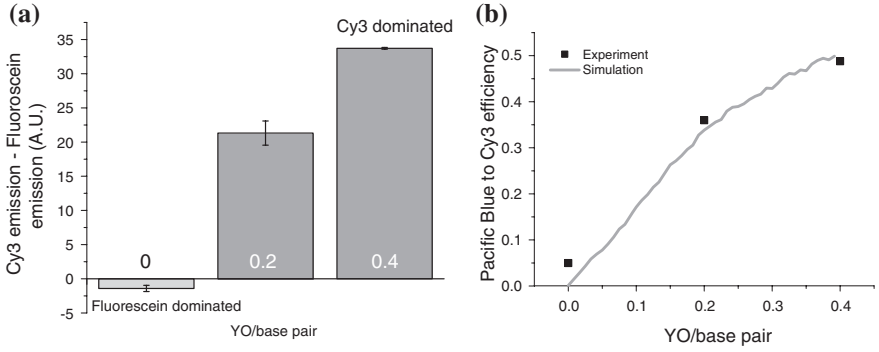

Fig. 8.7 **a** Difference between extracted fluorescein emission and extracted Cy3 emission. Without YO, fluorescein emission dominates. As YO is added, Cy3 emission increases and becomes dominant. **b** Experimental and simulated *Pacific Blue* to Cy3 energy transfer efficiency

transfer behavior of the system is distinctly different at different YO concentrations. The arrival rate of excitation energy at Cy3 shows a strong dependence on the mediator loading with almost immediate steep increase excitation energy at Cy3 at 0.4 YO per base pair. In contrast, at 0.1 loading ratio, there is a 1 ns lag time before excitation energy starts to arrive at Cy3. Furthermore, there is concentration dependence in the variance in energy migration kinetics. The difference between the slowest and most inefficient conformation and fastest and most efficient conformation is largest for the intermediate loading ratio (0.2 YO/bp). In order to explain this, we travel with the excitation energy migrating through the system. At low YO concentrations, excitation energy starting out at Pacific Blue is first transferred to a proximal mediator unit. Once there, the probability that there is another intercalator within energy transfer distance is low, especially if we want the next energy transfer step to take the excitation energy closer to Cy3. Here, escape from the system through emission from YO becomes probable. Contrastingly, at high YO concentrations, YO to YO energy transfer is efficient. That means that the excitation energy can travel around the network, probing the energetic landscape. Even if it migrates far away from Cy3, it has a non-negligible probability to find its way back. Here, the exact placement of the intercalators is not important, because they communicate efficiently anyway. It is in the intermediate regimes where we can find certain conformations that communicate the excitation energy efficiently towards Cy3 and others that do the same thing, but away from Cy3, hence the large variability in energy migration kinetics.

Our example shows how the concept of the photonic wire can be incorporated into more complex assemblies to introduce new functionalities. The photonic network is designed to control of directionality of the flow of excitation energy through the positioning of fluorophores in the DNA assembly. However, the added complexity can also be used to include functions that relate to the output and usage of the transferred excitation energy, as well as the design of systems for maximizing the influx of excitation energy to specific positions.

This photonic network also illustrates the drawback of using random positioning of mediator fluorophores. The random positioning entails that there is no direct path of intermediate fluorophores guiding the excitation from the initial donor to the terminal acceptor. Instead, systems based on random positioning have to rely on high mediator loading (implying efficient mediator–mediator communication) ensuring that there is little probability for the excitation to be lost before it reaches the terminal acceptor. It can be of interest to compare this system with the origami-based one presented by Tinnefeld and co-workers [13], which was discussed in Sect. 5.2. Compared to the 120 base pairs of the DNA hexagon, the DNA origami structure is much larger with its more than 7,000 base pairs. Incorporating the YO-based wire in such a system would simply not be possible. There are too many binding sites for YO, it would demand a much tighter packing of intercalators than is practically possible. However, it might also be argued is such a large and complex system as a DNA origami structure is actually needed. After all, the linear end-to-end distance is less than 10 nm and the rectangle is 70×100 nm [2].

8.2 DNA-Based Artificial Antenna (Paper III)

The designs of the different varieties of photonic wires were all inspired by how natural light harvesting complexes utilizes multi-step energy transfer to direct excitation energy to a specific target. However, as we discussed in Sect. 5.3 there are several examples of structure designs that go even further in mimicking natural light harvesting by arranging donor fluorophores around a single acceptor. In the work of Liu and co-workers, the ability of DNA to arrange fluorophores in an antenna-like fashion was highlighted [14]. Also drawing inspiration from photosynthetic systems, Börjesson et al. have constructed a supramolecular assembly for energy and electron transfer comprising a donor fluorophore and a porphyrin, both covalently linked to a DNA scaffold [15]. Here, the porphyrin does not only act as an excitation energy acceptor, but also as a functional group capable of performing photo-induced electron transfer. A drawback with these systems is that the covalent linking of donor fluorophores is difficult to combine with high donor concentrations.

In order to create an antenna system that overcomes the limitation associated with previously assembled systems, we look towards non-covalent means of donor association. Armitage and co-workers have shown how high excitation concentration can be achieved in a DNA-based system by using intercalating fluorophores such as YO-PRO-1 or YOYO-1 [16, 17]. Based on the DNA-porphyrin arrangement, we have designed an antenna system using YO-PRO-1 as donor. In the case of the photonic wires, we saw that the use of homo-FRET dyes comes with some inherent problems. One being the excitation scrambling caused by diffusive, non-directional, energy transfer through the wire limiting its applicability in larger systems. This effect is not nearly as detrimental in antenna systems where the homo-FRET dye is directly excited. As excitation energy does not travel from a defined point A to a defined point B, there is less of an optimum path in the same way as in the wire systems. Instead, homo-FRET can play an important role by allowing donor fluorophores that are distal from the acceptor to partake in the light gathering.

Our light harvesting system, presented in paper III, consists of a 39-mer DNA with a porphyrin moiety, connected through a phenyl-ethylene linker, attached at the central base pair position (Fig. 8.8). Aside from being an energy transfer acceptor, the porphyrin also anchors the assembly to a lipid membrane, positioning the porphyrin in the hydrophobic part of the bilayer. This way, the antenna assembly creates a system that facilitates phase transition and compartmentalization by shifting the excitation location from fluorophores in the aqueous phase to the porphyrin in the confined lipid phase. The linking moiety consists of either two or three phenyl-ethylene units. In the original work, a single unit was used to connect the porphyrin to DNA [15]. However, more recent work has shown that hybridization on liposome surfaces is more efficient using longer linkers, most probably because the short tinker positions the DNA strand too close the liposome surface [18]. Using QCM-D, Woller et al. have shown how porphyrin anchored duplexes can be melted and re-annealed without loss of the bilayer association [19].

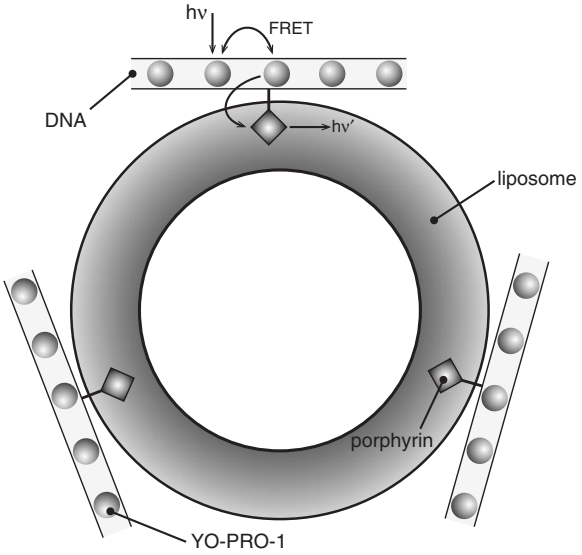

Fig. 8.8 Light harvesting system consisting of a DNA scaffold for intercalated donor fluorophores, anchored to a lipid bilayer through aporphyrin moiety. The porphyrin also act as FRET acceptor

We evaluate the system performance by probing the emission at 700 nm while varying the excitation wavelength for assemblies with different YO concentration. At 700 nm there is almost exclusively emission from the porphyrin. By varying the excitation wavelength we can compare the emission intensity due to energy transfer from YO with the one due to direct excitation of the porphyrin. From this it is possible to calculate an effective extinction coefficient. Using Eq. 5.2 we can also calculate the antenna effect. Figure 8.9a shows excitation spectra for different YO concentrations. Without added YO, we see a peak at 510 nm. This corresponds to emission from the porphyrin. As YO is added to the system, a peak around 480 nm appears and grows. This shows that it is not only possible to excite the porphyrin using FRET from YO, it is also more efficient than exciting the porphyrin directly at its absorption maximum. The inset shows the effective extinction coefficient. At the mixing ration of 20:1 YO:porphyrin, an extinction coefficient of 290,000 M^{-1} cm^{-1} is reached. This corresponds to an antenna effect of 12. The emission spectra presented in Fig. 8.9b show that there is hardly any fluorescence from YO at 700 nm. Further, no direct excitation of the porphyrin can be detected when exciting at 483 nm.

As previously mentioned, homo-FRET might have en important influence on the energy transfer behavior, and thereby also the efficiency of the antenna system. We investigate this both using energy transfer simulations and time resolved fluorescence measurements. To simulate energy transfer efficiency, we employ the same Markov chain simulations as for the photonic wires. Figure 8.10 shows the

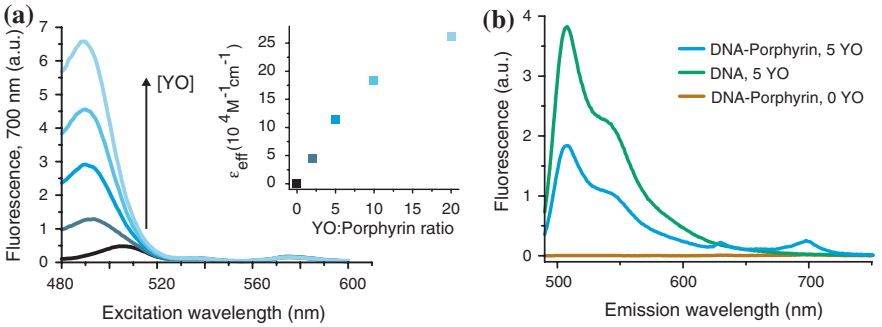

Fig. 8.9 **a** Excitation spectra for antenna system recorded at 700 nm where the porphyrin emits. As more YO is added, porpyrin emission increases due to excitation energy transfer from YO. The inset shows the effective extinction coefficient for the porphyrin as a function of YO concentration. **b** Emission spectra for excitation at 483 nm. The YO-porphyrin system (*green*) shows quenched YO emission compared to the YO only system (*blue*). Porphyrin emission can be detected as a peak around 700 nm

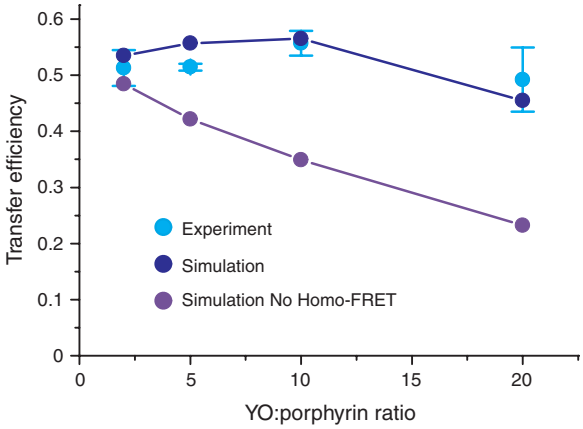

Fig. 8.10 Experimentally determined FRET efficiencies compared with simulation results with and without YO-to-YO FRET

experimentally determined YO to porphyrin energy transfer efficiency compared with energy transfer efficiencies obtained from simulations, with and without the presence of YO to YO FRET. Simulations show more or less constant energy transfer efficiency for all mixing ratios. This is in agreement with experimental results. The fact that the efficiency is constant, rather than increasing which would be the expected result when the YO-to-YO distance decreases, is due to increased self quenching as the YO monomers come closer together. In simulations not allowing homo-FRET, the transfer efficiency decreases, indicating that this process plays an important role in channeling excitation energy to the porphyrin acceptor.

Using TCSPC, we also investigate the impact of homo-FRET for the different linker lengths by measuring the fluorescence decay of YO at different concentrations for systems with and without acceptor. Because donor fluorophores insert randomly along the DNA strand, the system cannot be characterized by a single donor–acceptor distance. Instead, fluorescence decay curves have to be fitted using a distribution of distances using the expression in Eq. 8.2,

$$I_{DA}(t) = g(t) \otimes \int_{R\text{min}}^{R\text{max}} \sum_i P(R)\alpha_i \exp\left[(-t/\tau_i)\left(1 + \{R/R_0\}^6\right)\right] dR \quad (8.2)$$

here, $g(t)$ is the instrument response function, R_{min} and R_{max} are the minimum and maximum donor–acceptor separations respectively, $P(R)$ is the distance distribution function, α_i and τ_i are the intrinsic donor amplitudes and lifetimes respectively, R_0 is the Förster distance. To represent the donor–acceptor distance distribution we use a one-dimensional Lorentzian distribution, Eq. 8.3, with the linker length as the center distance,

$$P(R) = \frac{2I}{\pi}\left[\frac{[\gamma^2]}{4\,(R - R_L)^2 + \gamma^2}\right] \quad (8.3)$$

where I and g are the height and width of the distribution, respectively. The terms R and R_L denote the donor–acceptor distance and the linker length, respectively. In this example, R_L is inserted as R_{min} in Eq. 8.2.

Since there is no preferred binding site along the DNA strand, all possible donor–acceptor distances are equally probable (that does not mean that energy transfer efficiency is equal in all sites though) in a system where there is no homo-FRET. When this is the case, we expect a uniform distance distribution. In the results presented in Fig. 8.11, we see that this is the case at the lowest mixing ratio for both linker lengths. This means that, at this binding ratio, excitation energy is transferred to the porphyrin almost exclusively through direct, one-step FRET. When the mixing ratio increases we see a shift to distributions more dominated by the short donor–acceptor distances. This is an effect of increased importance for homo-FRET. Donors that are positioned far from the acceptor have a lower probability for direct FRET than the more proximal ones. Therefore, they have a proportionally higher probability for YO-to-YO FRET. This result in a shift in the excitation population favoring YO units positioned close to the acceptor, who then partakes in FRET with the acceptor. We see that this effect is more pronounced for the system with the long linker. This makes sense because with a short linker, more YO molecules are within direct FRET distance of the porphyrin, decreasing the need for multi-step FRET.

The closer the donors are positioned to the acceptor, the more efficient an antenna system is. In this respect, an antenna system built from a linear DNA strand

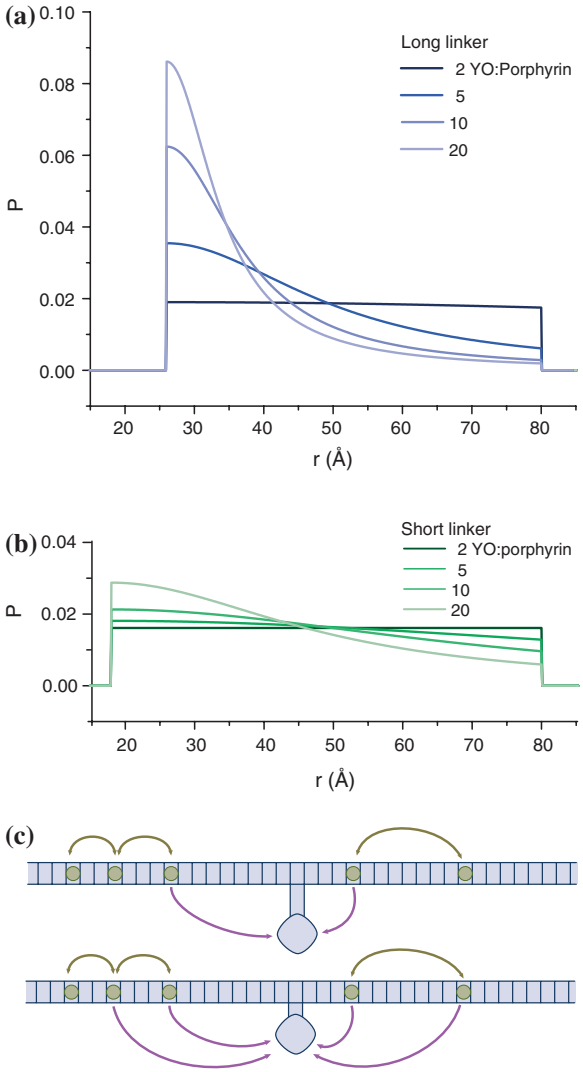

Fig. 8.11 Donor acceptor distribution obtained from TCSPC measurements for light harvesting assemblies having long (**a**) or short (**b**) linker between DNA and porphyrin. **c** The differences in distribution are explained by the fact that, for the short linker length, more donor fluorophores are within direct FRET distance of the porphyrin. Therefore, the system with the short linker relies less on homo-FRET than the system with the long linker

is far from ideal. Armitage and co-workers brings up this question by describing the increasing system compactness when creating assemblies with one, two or three-dimensional architecture using the same number of base pairs. Recently, Börjesson constructed a hexagonal DNA assembly, anchored to a liposome through one, two

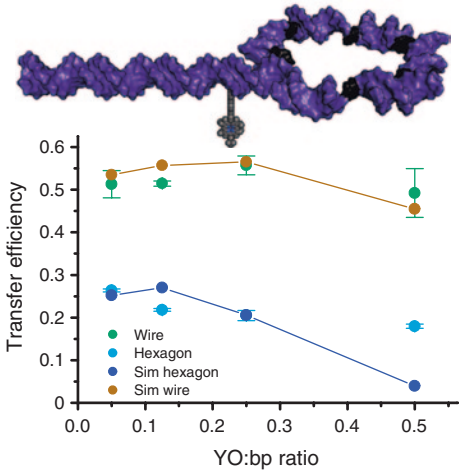

Fig. 8.12 Schematic structure of hexagonal DNA structure presented together with experimental and simulated FRET efficiencies

or three porphyrin moieties [20]. Based on this design, we created a more complex antenna system, consisting of the hexagonal assembly and one anchoring porphyrin unit. Experimental and simulation results from this structure are presented in Fig. 8.12. Because the hexagon is larger than the linear assembly (100 bp compared to 39), the overall energy transfer efficiency is lower. However, more base pairs also mean more donor fluorophores and a potentially higher antenna effect. This is the case for the hexagon which has an effective extinction coefficient of 395,000 $M^{-1}cm^{-1}$, which corresponds to an antenna effect of 18.

In their 2009 work, Börjesson and et al. also demonstrate another property of the porphyrin unit: its ability to partake in electron transfer reactions [15]. In their work sequential energy transfer and electron transfer experiments were performed using 2,6-di-t-butyl-p-benzoquinone (BQ) buried in the lipid bilayer quenching zink porphyrin (ZnP) emission through electron transfer. The quenching process was initially studied using direct excitation of the DNA-ZnP without any attached donor fluorophore. The benzoquinones were shown to effectively quench the ZnP fluorescence having a diffusion-controlled bi-molecular quenching constant of 1.8×10^9 $M^{-1}s^{-1}$. The complete system, where a fluorescein donor is excited instead of the porphyrin, showed approximately the quenching results as for the porphyrin-only experiments. Thus, the quenching of porphyrin fluorescence is independent of whether the excitation energy comes from FRET or from direct excitation. In a related work, a system consisting of two closely spaced anchors are shown to be able to coordinate a number of different electron accepting bidentate ligands showing that it is also possible to assemble porphyrins into binding pockets [21]. These last examples highlight the versatility of the porphyrin anchor. Being so much more than just an inert reporter unit, porphyrins enable the creation of functionalized structures on the nanoscale.

8.3 A Platform for Nanochemical Assembly (Paper IV and V)

Creating solutions for detection and control of molecules and molecular assemblies has led to a development of a large number of low volume techniques confining components into e.g., pico- or femtoliter volumes [22, 23], single droplets [24, 25] or lipid vesicles [26, 27]. These designed systems for compartmentalization all rely on enclosure in three-dimensional volumes.

In paper IV we want to explore the interactions between two reactants that are both confined to a two-dimensional liquid film. The system of micro- and nanofabricated hydrophobic structures developed by Czolkos et al. enables the controlled formation of lipid monolayers films by means of multilamellar vesicle deposition [28, 29]. This platform functions both as a model system for molecular interaction in biological membranes and as a "device" for controlled assembly of supramolecular structures.

In DNA nanotechnology, most of the created structures are studied either in solution or deposited onto mica surfaces for AFM detection. From a device perspective it is of interest to attach the constructed DNA assemblies to a surface that allows a wide range of functionalities. Surface incorporation in deposited lipid films instead enables the creation of dynamic systems allowing the different entities to interact and react. For these reasons, we decided to use our lipid monolayer platform to study DNA hybridization. However, the design is not limited to DNA. Other interesting study objects involve e.g., protein–protein interaction.

In order allow incorporation into the lipid film, we modify the DNA strands with a C16 lipophilic anchor. The DNA strand is separated from the lipid anchor and thus also the surrounding lipid film by a hexa-ethylene-glycol spacer (HEG). Figure 8.13a shows the structure of the modified DNA oligomers with the different components highlighted.

The hydrophobic substrates are constructed from the photoresist EPON 1002F. The material is fashioned into a shape consisting of a large central mixing domain with four auxiliary circular patches connected to the main body through narrow lanes. The structures rest on top of a gold layer that prevents the lipid film to spread outside the designed pattern (Fig. 8.13b).

Complementary strands of 10-mer DNA were incorporated in separate lipid vesicles which we place in separate ends of the EPON 1002F structure using capillary pipettes. When the vesicles are placed on the surface, they start to form a lipid monolayer film displacing the water proximal to the hydrophobic surface. As the wetted area increases, the two lipid films coalesce allowing their contents to mix (Fig. 8.13c). When the lipid films merge, a concentration gradient emerges, going in opposite direction for the two complementary DNA strands. This then allows mixing by diffusion to occur. From FRAP measurements (Fluorescence Recovery After Photobleaching) we estimate the diffusion coefficient for lipid-DNA molecules moving in the lipid film by diffusion to be 0.65 $\mu m^2\ s^{-1}$. In the mixing process, there is a chance that two complementary strands meet, enabling

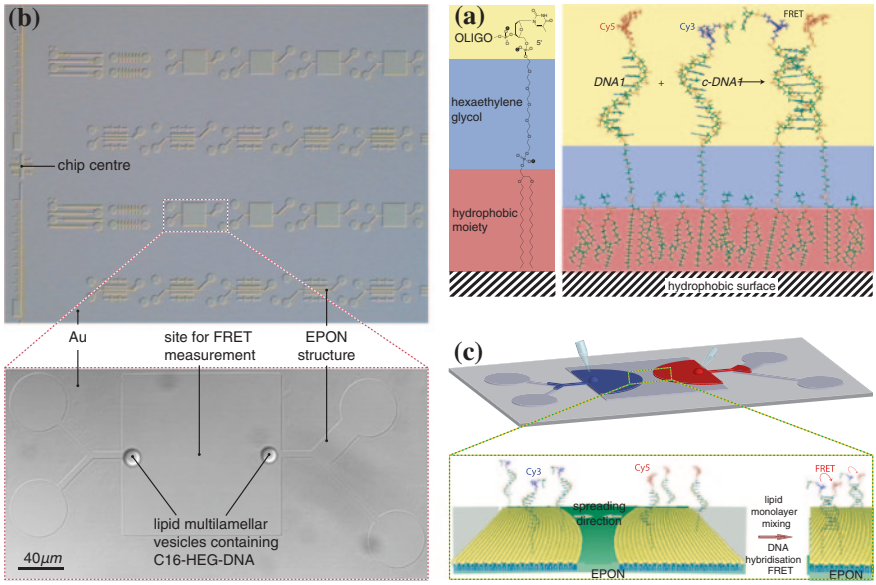

Fig. 8.13 **a** Modified DNA oligomer comprising a hydrophobic moiety enabling incorporation in lipid film and a hexaethylene glycol spacer. **b** Micropatterned EPON 1002F structures on gold substrate. **c** Deposition of multilamellar vesicles enables content mixing through lipid film formation. This process is monitored through FRET

duplex formation to occur. The probability for this to occur is highest in the completely mixed system.

Using energy transfer between Cy3 and Cy5 positioned on the different stands, we are able to follow the accumulation of formed duplexes. In order to make sure that emission from Cy5 is associated with duplex formation we perform the same experiments with the same energy transfer set-up using non-complementary strands. Moreover, we also investigate emission from samples containing only one of the single-stranded species. For all experiments, we prepared DNA-lipid mixtures with three different DNA:lipid ratios: 1:1500, 1:4610, 1:15000. Emission from the samples was detected in the centre of the structure where mixing of lipid film components was complete. Our results, presented in Fig. 8.14, show a significant increase in Cy5 emission for complementary strands compared to the other tested strand combinations. The emission from Cy5, which is proportional to the amount of formed product, increases with increasing concentration of DNA molecules. This result is of course not surprising since a higher concentration of reactants means a higher probability for them to encounter each other and react. Aside from the increased emission from Cy5, the fluorescence measurements also show substantial background fluorescence from the EPON 1002F substrate. The exact cause of this emission is not known. However, it is likely to be caused by residual processing chemical from the structure fabrication.

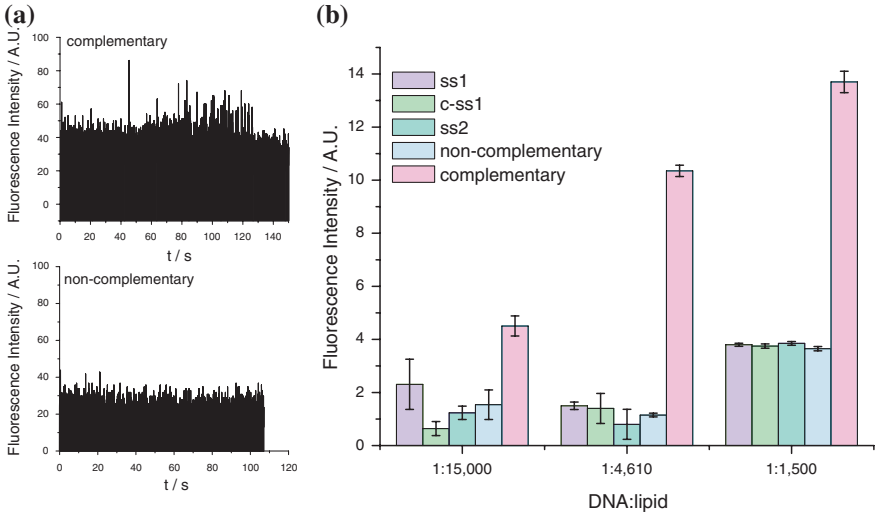

Fig. 8.14 **a** Sample acceptor emission traces for complementary and non-complementary strand combinations. **b** Average emission intensities for single stranded DNA (ss1, c-ss1, ss2) and DNA duplexes (non-complementary, complementary)

The micro- and nanofabrication techniques allow for a great variation in potential structure geometries and sizes. Lipid monolayer spreading has previously been shown possible in lanes constructed from SU-8 as narrow as 25 nm [29]. Assuming a lipid size of approximately 60 $Å^2$/molecule [30], this corresponds to a width of about 30 lipid molecules. By directing lipid flow through narrow lanes it is possible to obtain conditions suitable for single molecule detection even from high concentration samples. In a second structure design, two lipid deposition patches are joined in a mixing junction that extends into a tapered lane, with a width the decreases in discrete steps from 1,000 nm, through 500 nm and finally to 200 nm. When the DNA-containing lipid vesicles are deposited onto the two separate patches, the lipid films start to spread thereby flowing into the mixing junction where the complementary strands are allowed to meet and hybridize. The flow is then directed through the tapered lane where the emission is recorded. At these widths, the lanes contain approximately 1,200, 600 and 240 lipid molecules in one "row" of lipids for the 1,000, 500 and 200 lanes, respectively. The row thickness is approximately 10 Å. Using a DNA:lipid ratio of 1:1,500 DNA:lipid this results in 0.8, 0.4 and 0.16 DNA molecules per row. The results show similar emission intensities for all lanes 1000 and 500, with a lower intensity for the 200 lane. This is again not surprising as both the 1,000 and the 500 lanes are wider than the focal spot, while the 200 lane is smaller.

The work presented in paper IV shows that it is possible to use lipid film mixing to promote and control chemical reactions between molecules confined to a surface. This is a step towards a system where supramolecular structures can be

created not only in solution, but also in a dynamic surface environment where components can meet and assemble in the two-dimensional liquid crystal phase. However, the study only shows that reactions between surface associated DNA molecules are possible. It does not tell us anything about the mechanisms behind the process. In paper V we take a closer look at the actual hybridization event.

In order for two surface-associated molecules to react with each other, a number of criteria have to be fulfilled simultaneously.[1] First of all, the molecules have to come within a reactive distance of each other in order for any reaction to be possible. When they do so, they need enough thermal energy to overcome any energetic barriers. And finally, the formed product need to be stable enough so that external forces, e.g., convection, do not revert the process.

In paper V, we investigate the hybridization mechanism of the C16-HEG-DNA molecules using single molecule fluorescence spectroscopy. As in paper IV, complementary DNA strands are incorporated in separate multilamellar lipid vesicles. The vesicles are deposited onto a hydrophobic surface distal from each other allowing isolated lipid monolayers containing either of the two strands to form. In this work we use a glass slide coated with Teflon AF to facilitate lipid spreading. There are two main reasons for abandoning EPON 1002F for Teflon AF. The first reason is the monolayer spreading properties. Czolkos et al. report a spreading coefficient for lipid monolayer on Teflon AF of 12–20 $\mu m^2\ s^{-1}$ [31]. This value should be compared to a spreading coefficient of approximately 5 $\mu m^2\ s^{-1}$ for EPON 1002F [32]. Diffusion is also faster on Teflon AF than on EPON 1002F with diffusion coefficient for phospholipids of 0.8 $\mu m^2 s^{-1}$ and 0.65 $\mu m^2 s^{-1}$, respectively. Both these factors are relevant from a device perspective as they speed up the transport and mixing processes of the system, and thereby allow any process to occur more rapidly. The second reason has to do with fluorescence detection. As previously mentioned, EPON 1002F shows substantial background emission which makes it incompatible with single molecule detection. This motivates a shift to Teflon AF which does not suffer the same drawbacks due to radically different processing methods (for details on the structure fabrication, see work by Czolkos et al. on SU-8 [28], EPON 1002F [32] and Teflon AF [33]). For these experiments we used homogenous Teflon AF surface without any structuring.

As before, lipid monolayer spreading eventually leads to film coalescence and thereby content mixing by diffusion. In order to follow this process on the single molecule level we label the complementary strands with the fluorophores ATTO 488 and ATTO 647N. By simultaneous excitation of both fluorophores we are able to follow the diffusing DNA molecules either in their single-stranded variant (showing emission from either of the two fluorophores) or as duplexes (appearing as superimposed emission from both fluorophores moving in tandem). To accomplish this, we excite the samples with the laser lines 488 and 641 nm using wide field illumination. The emission is split into two images, each corresponding to one of the fluorophores, and was imaged simultaneously on a CCD chip. The

[1] Here I use the word "react" in a wide sense, including formation of both covalent and non-covalent interactions.

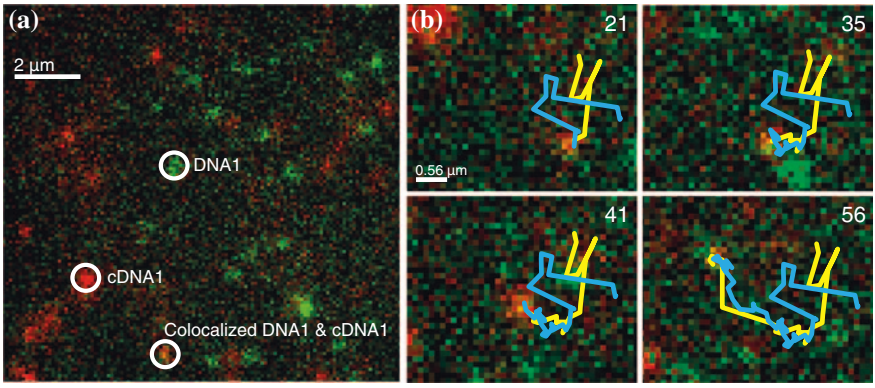

Fig. 8.15 **a** Fluorescence micrograph of DNA molecules anchored to lipid film. The image consists of two channels corresponding to emission form ATTO 488 (*green*) and ATTO 647N (*red*) that have been false-colored and overlaid. Single strands appear as *red* or *green dots* and duplexes as *yellow dots*. **b** Tandem motion of two complementary DNA strands as indicator for hybridization. The numbers show the current 30 ms time frame

images were later overlaid creating two-color image showing the different complementary strands in different color (Fig. 8.15a).

In order to obtain a notion of the reaction procedures we wanted to investigate whether the length of the DNA moiety has any influence on the hybridization rate, i.e., is the reaction procedure dictated by molecular affinity or does only depend on the diffusive encounter of the reactants? We therefore created two different C16-HEG-DNA constructs, one with a 20-mer DNA strand and one with a 40-mer DNA strand, both with mixed base compositions. When the lipid films containing complementary DNA strand had coalesced we traced the mixing process by tracking the diffusive migration of individual DNA molecules. We then analyzed the traces for instances of co-migration between the two channels and used that as a marker for hybridization (Fig. 8.15b). From this analysis, we indeed see higher hybridization rates for the 40-mer DNA than for the 20-mer. As the absolute number of formed duplexes with time depends on the number of DNA strands present in the measurement, direct comparison between experiments is not possible. We therefore performed lattice diffusion simulations using the distribution of DNA strands at the start of the corresponding measurement as input data. For these simulations, the probability for duplex formation following superposition of complementary strands was used as a variable parameter. This model is similar to the one used by Boxer and co-workers used to investigate docking of membrane tethered vesicles [34]. Figure 8.16 a shows an example measurement trace (black) together with simulation outcomes for different reaction probabilities.

Comparing experimental results with the simulations we find reaction probabilities of 0.03 and 0.09 for the 20-mer and 40-mer, respectively (Fig. 8.16b). From the simulation results it is evident that the same input parameters can generate large variations in outcome (accumulated duplexes). This means that we have a

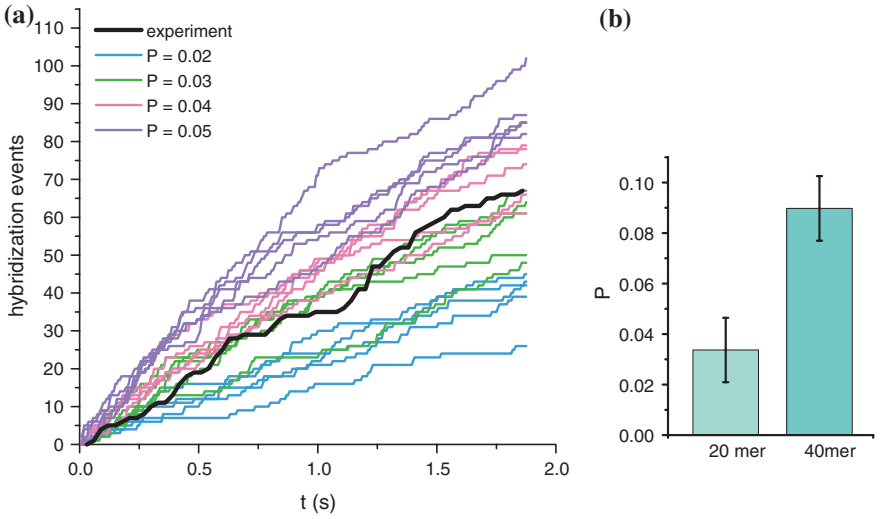

Fig. 8.16 **a** Accumulation of hybridization events. Experimental results (*black*) are displayed together with simulation outcomes for different reaction probabilities. **b** Average reaction probabilities for 20-mer and 40-mer DNA strands

variability that is not due to the reaction probability. This phenomenon can be seen as a combined effect of both the rate of diffusion (and hence the collision rate) and the reaction probability. Consider the case of a very fast diffusion rate. If that were the case, reactants would encounter each other often having many opportunities to react. Then, reaction rates would only be directed by the reaction probability. Consider then the case where the reaction probability is the same for both strand length, then of course, we would only see an effect of the diffusion rate on the system. Over time, the system will converge to an equilibrium rate showing no stochastic behavior. However, at the onset of the reaction, the total number of reactive events is few enough for this effect to be apparent. How fast the system converges depends both on the reaction probability and on the rate of diffusion. The higher they are, the faster the system converges.

What produces the differences in reaction probability that we see? To understand this, we need to take a closer look at the process of duplex formation. The first thing that forms is a nucleation site consisting of a two base pairs. Following this, the duplex can close in a zipper-like fashion. Before the second base pair has formed, the two strands can dissociate and associate rather freely. The time between the formation of the first and second base pair is on the order of 0.5 and 1 ns [35]. During this time, very little lateral strand movement is possible. This means, that when two strands have started to form base pairs, it is likely that they stay within base pairing distance giving a high probability for a stable duplex to form. Because the DNA moieties of our C16-HEG-DNA molecules protrude into the solution, they have a fairly large conformational freedom. This means that they are able to probe their surroundings in a hemispherical volume producing

a reactive space. As the size of this volume depends on the length of the DNA strand, the 40-mer has a larger reactive volume than the 20-mer explaining the higher reaction probability (see illustration in Fig. 8.17). The point here is that the reaction rate does not depend on the stability of the fully formed duplex, but on ability of the DNA strand to form nucleation base pairs.

In the presented work we only look at DNA molecules with mixed sequences. Boxer and co-workers report higher probabilities for duplex formation for poly (A/T) sequences [34]. In their case this is not surprising as they fuse two different bilayers together. When approaching from opposite directions, a mixed sequence would need (more or less) complete overlap for base pairs to form. The poly (A/T) sequence however, need very little overlap making duplex formation more probable (see graphical explanation in Fig. 8.18). For complementary strands confined to the same lipid layer, the benefit is not as apparent. However, this remains to be investigated. Furthermore, studies on the single molecule level on the effects of confinement to lanes might yield interesting mechanistic information.

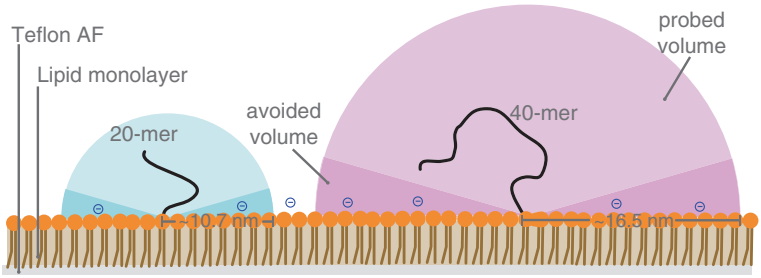

Fig. 8.17 Membrane-anchored DNA molecules probe hemispherical volumes in of the solution. The strand length determines the size of this reaction volume

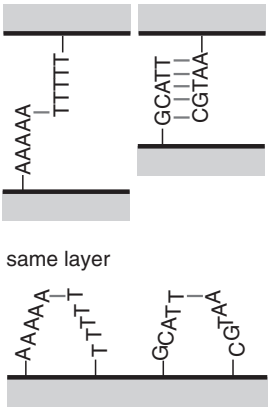

Fig. 8.18 Comparison between base-pairing opportunities for complementary strands positioned in separate and same lipid layers

References

1. Heilemann M, Kasper R, Tinnefeld P, Sauer M (2006) Dissecting and reducing the heterogeneity of excited-state energy transport in DNA-based photonic wires. J Am Chem Soc 128:16864–16875
2. Hannestad JK, Sandin P, Albinsson B (2008) Self-assembled DNA photonic wire for long-range energy transfer. J Am Chem Soc 130:15889–15895
3. Carlsson CLA, Björkman M, Jonsson M, Albinsson B (1997) Experimental and simulated fluorescence depolarization due to energy transfer as tools to study DNA-dye interactions. Biopolymers 41:481–494
4. Vyawahare S, Eyal S, Mathews KD, Quake SR (2004) Nanometer-scale fluorescence resonance optical waveguides. Nano Lett 4:1035–1039
5. Su W, Schuster M, Bagshaw CR, Rant U, Burley GA (2011) Site-specific assembly of DNA-based photonic wires by using programmable polyamides. Angew Chem Int Ed 50:2712–2715
6. Cohen JD, Sadowski JP, Dervan PB (2007) Addressing single molecules on DNA nanostructures. Angew Chem Int Ed 46:7956–7959
7. Cohen JD, Sadowski JP, Dervan PB (2008) Programming multiple protein patterns on a single DNA nanostructure. J Am Chem Soc 130:402
8. Börjesson K, Preus S, El-Sagheer AH, Brown T, Albinsson B, Wilhelmsson LM (2009) Nucleic acid base analog fret-pair facilitating detailed structural measurements in nucleic acid containing systems. J Am Chem Soc 131:4288–4293
9. Iqbal A, Arslan S, Okumus B, Wilson TJ, Giraud G, Norman DG, Ha T, Lilley DMJ (2008) Orientation Dependence in Fluorescent Energy Transfer between Cy3 and Cy5 Terminally Attached to Double-Stranded Nuclelic Acids. Proc Natl Acad Sci USA 105:11176–11181
10. Stein IH, Schüller V, Böhm P, Tinnefeld P, Liedl T (2011) Single-molecule fret ruler based on rigid DNA origami blocks. Chem Phys Chem 12:689–695
11. Hannestad JK, Gerrard SR, Brown T, Albinsson B (2011) Self-assembled DNA-based fluorescence waveguide with selectable output. Small 7:3178–3185
12. Tumpane J, Sandin P, Kumar R, Powers VEC, Lundberg EP, Gale N, Baglioni P, Lehn JM, Albinsson B, Lincoln P, Wilhelmsson LM, Brown T, Nordén B (2007) Addressable high-information-density DNA nanostructures. Chem Phys Lett 440:125–129
13. Stein IH, Steinhauer C, Tinnefeld P (2011) Single-molecule four-color fret visualizes energy-transfer paths on DNA origami. J Am Chem Soc 133:4193–4195
14. Dutta PK, Varghese R, Nangreave J, Lin S, Yan H, Liu Y (2011) DNA-directed artificial light-harvesting antenna. J Am Chem Soc 133:11985–11993
15. Börjesson K, Tumpane J, Ljungdahl T, Wilhelmsson LM, Nordén B, Brown T, Mårtensson J, Albinsson B (2009) Membrane-anchored DNA assembly for energy and electron transfer. J Am Chem Soc 131:2831–2839
16. Benvin AL, Creeger Y, Fisher GW, Ballou B, Waggoner AS, Armitage BA (2007) Fluorescent DNA nanotags: supramolecular fluorescent labels based on intercalating dye arrays assembled on nanostructured DNA templates. J Am Chem Soc 129:2025–2034
17. Özhalıcı-Ünal H, Armitage BA (2009) Fluorescent DNA nanotags based on a self-assembled DNA tetrahedron. ACS Nano 3:425–433
18. Börjesson K, Wiberg J, El-Sagheer AH, Ljungdahl T, Mårtensson J, Brown T, Nordén B, Albinsson B (2010) Functionalized nanostructures: redox-active porphyrin anchors for supramolecular DNA assemblies. ACS Nano 4:5037–5046
19. Woller JG, Börjesson K, Svedhem S, Albinsson B (2012) Reversible hybridization of DNA anchored to a lipid membrane via porphyrin. Langmuir 28:1944–1953
20. Börjesson K, Lundberg EP, Woller JG, Nordén B, Albinsson B (2011) Soft-surface DNA nanotechnology: DNA constructs anchored and aligned to lipid membrane. Angew Chem Int Ed 50:8312–8315

21. Börjesson K, Woller JG, Parsa E, Mårtensson J, Albinsson B (2012) A bioinspired self assembled dimeric porphyrin pocket that binds electron accepting ligands. Chem Commun 48:1793–1795
22. Martinez AW, Phillips ST, Whitesides GM (2008) Three-dimensional microfluidic devices fabricated in layered paper and tape. Proc Nat Acad Sci USA 105:19606–19611
23. Chen D, Du WB, Liu Y, Liu WS, Kuznetsov A, Mendez FE, Philipson LH, Ismagilov RF (2008) The chemistrode: a droplet-based microfluidic device for stimulation and recording with high temporal, spatial, and chemical resolution. Proc Nat Acad Sci USA 105:16843–16848
24. Edgar JS, Milne G, Zhao Y, Pabbati CP, Lim DSW, Chiu DT (2009) Compartmentalization of chemically separated components into droplets. Angew Chem Int Ed 48:2719–2722
25. Jeffries GDM, Kuo JS, Chiu DT (2007) Dynamic modulation of chemical concentration in an aqueous droplet. Angew Chem Int Ed 46:1326–1328
26. Sott K, Lobovkina T, Lizana L, Tokarz M, Bauer B, Konkoli Z, Orwar O (2006) Controlling enzymatic reactions by geometry in a biomimetic nanoscale network. Nano Lett 6:209–214
27. Bolinger PY, Stamou D, Vogel H (2008) An integrated self-assembled nanofluidic system for controlled biological chemistries. Angew Chem Int Ed 47:5544–5549
28. Czolkos I, Erkan Y, Dommersnes P, Jesorka A, Orwar O (2007) Controlled formation and mixing of two-dimensional fluids. Nano Lett 7:1980–1984
29. Erkan Y, Halma K, Czolkos I, Jesorka A, Dommersnes P, Kumar R, Brown T, Orwar O (2008) Controlled release of chol-teg-DNA from nano- and micropatterned su-8 surfaces by a spreading lipid film. Nano Lett 8:227–231
30. Nagle JF, Tristram-Nagle S (2000) Structure of lipid bilayers. Biochim Biophys Acta 1469:159–195
31. Czolkos I, Guan J, Orwar O, Jesorka A (2011) Flow control of thermotropic lipid monolayers. Soft Matter 7:6926–6933
32. Czolkos I, Hannestad JK, Jesorka A, Kumar R, Brown T, Albinsson B, Orwar O (2009) Platform for controlled supramolecular nanoassembly. Nano Lett 9:2482–2486
33. Czolkos I, Hakonen B, Orwar O, Jesorka A (2012) High-resolution micropatterned teflon af substrates for biocompatible nanofluidic devices. Langmuir 28:3200–3205
34. Chan YHM, Lenz P, Boxer SG (2007) Kinetics of DNA-mediated docking reactions between vesicles tethered to supported lipid bilayers. Proc Natl Acad Sci USA 104:18913–18918
35. Monti S, Cacelli I, Ferretti A, Prampolini G, Barone V (2010) Simulating DNA hybridization on an amine-functionalized silicon substrate. J Phys Chem B 114:8341–8349

Chapter 9
Concluding Remarks

In this thesis, I have presented a series of different self-assembled systems. The fundamental functionality of these assemblies is derived from three different biomolecular frameworks: DNA, light-harvesting complexes and lipid assemblies. In our constructed systems, aspects of all three parts are incorporated in the design, resulting in new functionalities. In the first paper, we construct a DNA-based self-assembling photonic wire capable of linear transfer of excitation energy over distances of more than 20 nm. Here, DNA was used as a scaffold for three different fluorophores, which assembled in a way that resulted in a downhill flow of excitation energy. Keeping the same basic constituents, the wire design was expanded in paper II to a more complex meshwork comprising one input and two output fluorophore. The different dyes were positioned in a DNA hexagon, creating a branched system where the directionality was determined by the presence of the mediator fluorophore YO-PRO-1. In paper III, the goal was different. Here, intercalated YO-PRO-1 molecules were used to harvest excitation energy, delivering it to a membrane-anchored porphyrin, covalently attached to the DNA scaffold. Using both a linear DNA and a larger hexagonal assembly, effective light-harvesting was obtain resulting in an enhancement of the absorption coefficient of the porphyrin by a factor of 12 and 18, respectively.

What can be done to expand the functionality of these systems? Currently, work is ongoing where the porphyrin anchors are incorporated in a rectangular DNA origami scaffold. It has previously been shown that it is possible to anchor DNA assemblies using multiple porphyrins [1] and that multi-porphyrin systems can introduce new functionalities [2]. Moving to a DNA origami scaffold, range of possible modification patterns is expanded to a two dimensional matrix. This has been shown already for fluorophores [3], gold nanoparticles [4] and reactive chemical modifications [5]. Combining the addressability of DNA origami with surface incorporation through membrane anchoring, this might be a seed for a platform for photo-induced molecular lithography. However, several important challenges remain. How can a staple pattern be formed in a dynamic lipid system? What kind of substrate should be used to create a permanent pattern with this

J. Hannestad, *Fluorescence in Bio-inspired Nanotechnology*, Springer Theses,
DOI: 10.1007/978-3-319-01068-7_9,

kind of system? The former question can perhaps be answered in part by lipids with phase transitions near room temperature [6]. The latter remains more open. Both the wire and the light-harvesting constructs rely on non-covalent association of homo-FRET dyes for their functionalities. Is this compatible with an origami-based system? We saw in case of the two different wire assemblies, that end-to-end efficiencies diminish with increasing size and complexity due to scrambling of excitation energy in the mediator part of the wire. It is likely that an origami substrate would not withstand the dye density that would be required for effective end-to-end transfer. Here, the approach taken by Stein et al. using a cascade of different fluorophores is better suited [3]. Sequence specific binding is another potential solution [7]. For an antenna system, the situation is different. For high acceptor enhancement, high donor–acceptor ratio is needed, with the donors preferably being in close vicinity of the acceptor. This is more readily achieved with non-covalent association. Especially in a multi-acceptor system, it is likely that any intercalated dye is within FRET distance of at least one acceptor. Still, it can be worthwhile to look at other, more compact solutions. The design principle based on the assembly of smaller origami-like tiles recently presented by Yin and co-workers represent an interesting alternative [8]. A further pathway for functionalization is the introduction of reversible switching of energy transfer. This is, I think, mostly relevant for photonic wires or similar systems. An attractive means of switching is phot isomerization [9], this because of the non-invasiveness of light. However other techniques such as toehold chemistry [10] or triplex binding [11] might also be of interest.

In papers IV and V we study the hybridization of membrane anchored complementary DNA strands. The duplex formation is driven by the mixing of separate lipid monolayer films formed on a hydrophobic support. Paper IV shows that duplex formation is possible in varied container geometry and that formed product can be detected in lanes approaching nanoscale width. In paper V duplex formation is followed in real time using single molecule tracking. Here, we show that the probability for duplex formation depends on the strand length, with the longer strand having higher probability. One development opportunity that appears is the possibility to, instead of just following duplex formation by dual excitation of both strands looking for co-migration, an ALEX scheme could be set up to monitor both this *and* the FRET efficiency. This way, it would be possible to know, not only if the strands move in tandem or not, but also to obtain an estimate of the linear separation of the two dyes. This could provide information on the strand structure, if they all are fully formed or if incomplete duplexes (having larger dye separation due to partly single-stranded) are capable of moving together. Furthermore, a natural question, since a large part of this thesis has dealt with complex DNA structures consisting of multiple DNA strands, is if it is possible to assemble structures more advanced than the single duplex using this method. The lithographic technique used to create the patterned hydrophobic support allows the creation of two-dimensional container networks with arbitrary mixing pattern. A substrate could be designed so that, in the first mixing zone, two strands are allowed to meet and hybridize. The lipid film containing the newly formed

duplex can than be directed towards a third strand which then would be added to the structure, and so on. However, for complex assemblies of DNA, having every strand anchored to a lipid layer is probably not feasible. Instead, it is likely that strands would have to be added from solution. Rather than allowing the formation of complex assembly through controlled mixing, I think that the most important property of this platform is the ability to increase the effective concentration (defined as average molecular separation) of a target molecule through transition from three to two dimensions. Molecules attached to a lipid film can be directed through a two-dimensional flow cell to interact with a potential detector, which does not have to be fluorescence-based. Finally, it would be interesting to see how this platform could be used together with molecular assemblies other than DNA. One molecular family that comes to mind is G-protein coupled receptors [12].

References

1. Börjesson K, Lundberg EP, Woller JG, Nordén B, Albinsson B (2011) Soft-surface DNA nanotechnology: DNA constructs anchored and aligned to lipid membrane. Angew Chem Int Ed 50:8312–8315
2. Börjesson K, Woller JG, Parsa E, Mårtensson J, Albinsson B (2012) A bioinspired self assembled dimeric porphyrin pocket that binds electron accepting ligands. Chem Commun 48:1793–1795
3. Stein IH, Steinhauer C, Tinnefeld P (2011) Single-molecule four-color fret visualizes energy-transfer paths on DNA origami. J Am Chem Soc 133:4193–4195
4. Kuzyk A, Schreiber R, Fan ZY, Pardatscher G, Roller EM, Hogele A, Simmel FC, Govorov AO, Liedl T (2012) DNA-based self-assembly of chiral plasmonic nanostructures with tailored optical response. Nature 483:311–314
5. Voigt NV, Torring T, Rotaru A, Jacobsen MF, Ravnsbaek JB, Subramani R, Mamdouh W, Kjems J, Mokhir A, Besenbacher F, Gothelf KV (2010) Single-molecule chemical reactions on DNA origami. Nat. Nanotechnol, 5, 200–203
6. Czolkos I, Guan J, Orwar O, Jesorka A (2011) Flow control of thermotropic lipid monolayers. Soft Matt 7:6926–6933
7. Su W, Schuster M, Bagshaw CR, Rant U, Burley GA (2011) Site-specific assembly of DNA-based photonic wires by using programmable polyamides. Angew Chem Int Ed 50:2712–2715
8. Wei B, Dai M, Yin P (2012) Complex shapes self-assembled from single-stranded DNA tiles. Nature 485:623–626
9. Andersson J, Li SM, Lincoln P, Andreasson J (2008) Photoswitched DNA-binding of a photochromic spiropyran. J Am Chem Soc 130:11836–11837
10. Graugnard E, Kellis DL, Bui H, Barnes S, Kuang W, Lee J, Hughes WL, Knowlton WB, Yurke B (2012) DNA-controlled excitonic switches. Nano Lett 12:2117–2122
11. Tumpane J, Kumar R, Lundberg EP, Sandin P, Gale N, Nandhakumar IS, Albinsson B, Lincoln P, Wilhelmsson LM, Brown T, Nordén B (2007) Triplex addressability as a basis for functional DNA nanostructures. Nano Lett 7:3832–3839
12. Gilman AG (1987) G-Proteins—transducers of receptor-generated signals. Annu Rev Biochem 56:615–649